DAMPING POWER SYSTEM OSCILLATIONS USING A PHASE IMBALANCED HYBRID SERIES CAPACITIVE COMPENSATION SCHEME

A Thesis

Submitted to the College of Graduate Studies and Research

in Partial Fulfillment of the Requirements

For the Degree of Master of Science

in the Department of Electrical and Computer Engineering

University of Saskatchewan

Saskatoon, Saskatchewan

By

Sushan Pan

PERMISSION TO USE

I agree that the Library, University of Saskatchewan, may make this thesis freely available for inspection. I further agree that permission for copying of this thesis for scholarly purpose may be granted to the professor or professors who supervised the thesis work recorded herein or, in their absence, by the Head of the Department or the Dean of the College in which the thesis work was done. It is understood that due recognition will be given to me and to the University of Saskatchewan in any use of the material in this thesis. Copying or publication or any other use of this thesis for financial gain without approval by the University of Saskatchewan and my written permission is prohibited.

Request for permission to copy or to make any other use of the material in this thesis in whole or part should be addressed to:

Head of the Department of Electrical and Computer Engineering
57 Campus Drive
University of Saskatchewan
Saskatoon, Saskatchewan
Canada S7N 5A9

ABSTRACT

Interconnection of electric power systems is becoming increasingly widespread as part of the power exchange between countries as well as regions within countries in many parts of the world. There are numerous examples of interconnection of remotely separated regions within one country. Such are found in the Nordic countries, Argentina, and Brazil. In cases of long distance AC transmission, as in interconnected power systems, care has to be taken for safeguarding of synchronism as well as stable system voltages, particularly in conjunction with system faults. With series compensation, bulk AC power transmission over very long distances (over 1000 km) is a reality today. These long distance power transfers cause, however, the system low-frequency oscillations to become more lightly damped. As a result, many power network operators are taking steps to add supplementary damping devices in their systems to improve the system security by damping these undesirable oscillations. With the advent of thyristor controlled series compensation, AC power system interconnections can be brought to their fullest benefit by optimizing their power transmission capability, safeguarding system stability under various operating conditions and optimizing the load sharing between parallel circuits at all times.

This thesis reports the results of digital time-domain simulation studies that are carried out to investigate the effectiveness of a phase imbalanced hybrid single-phase-Thyristor Controlled Series Capacitor (TCSC) compensation scheme in damping power system oscillations in multi-machine power systems. This scheme which is feasible, technically sound, and has an industrial application potential, is economically attractive when compared with the full three-phase TCSC which has been used for power oscillations damping.

Time-domain simulations are conducted on a benchmark model using the ElectroMagnetic Transients program (EMTP-RV). The results of the investigations have demonstrated that the hybrid single-phase-TCSC compensation scheme is very effective in damping power system oscillations at different loading profiles.

ACKNOWLEDGMENTS

My first, and most earnest, acknowledgment must go to my co-supervisor, Dr. S.O. Faried. Nearly two and half years ago, an unscheduled meeting with him for the first time started me on the path of electric power systems that I had no knowledge about it before that meeting. Dr. Faried has been instrumental in ensuring my academic, professional, financial, and moral wellbeing ever since. In every sense, none of this work would have been possible without him. I attribute the level of my Masters degree to his encouragement and effort and without him this thesis, too, would not have been completed. One simply could not wish for a better or friendlier supervisor.

I offer my sincerest gratitude to my co-supervisor, Dr R. Gokaraju, who has supported me throughout my thesis with his patience and knowledge. The financial support provided by Dr. Gokaraju is very much appreciated.

I also owe a huge debt of gratitude to my fellow graduate student, the gifted, Mr. Dipendra Rai for his invaluable help and for always being there when I needed his advice. Last but not least, I would like to express my gratitude to my parents, Mr. Pan Pan and Ms. Hong Ye.

TABLE OF CONTENTS

LIST OF FIGURES

LIST OF TABLES

LIST OF SYMBOLS

C	capacitor
C_{TCSC}	fixed capacitor of TCSC
C_s	capacitor of the RC snubber circuit
d	direct axis
E_{fd}	exciter output voltage
E_R	output voltage of the voltage regulator amplifier
E_{ref}	reference voltage of the excitation system
E_{SB}	feedback stabilizing signal of the excitation system
Fixed C	Transmission lines are series capacitor compensated
e_d, e_q	d- and q- axis stator voltages
e_{fd}	field voltage
$G_p(s)$	transfer function of a proportional type TCSC supplemental controller
$G_{L\text{-}L}(s)$	transfer function of a lead-lag type TCSC supplemental controller
Hybrid	Transmission lines are compensated with the hybrid single-phase-TCSC compensation scheme
i_d, i_q	d- and q- axis stator currents
i_{fd}	field winding current
i_{1d},	d-axis damper winding current
i_{1q}, i_{2q}	q-axis damper winding currents
IMG	imaginary part of a complex number
K_A	gain of the voltage regulator amplifier
K_E	exciter gain
K_{FE}	feedback stabilizing loop gain of the excitation system
K_G	supplemental controller gain
K_P	proportional controller gain
K_i	integral controller gain
L_{TCSC}	fixed inductor of TCSC
L_{ad}	d-axis magnetizing inductance
L_{aq}	q-axis magnetizing inductance

L_d, L_q	d- and q-axis synchronous inductances
L_{ffd}	self-inductance of the field winding
L_{11d}	self-inductance of the d-axis damper winding
L_{11q}, L_{22q}	self-inductances of the q-axis damper winding
P	real power
PI	proportional integral
P_{L1} and P_L1	real power flow in transmission line L_1
P_{L2} and P_L2	real power flow in transmission line L_2
P_m	mechanical power
Q	reactive power
q	quadrature axis
R_L	resistance of the series capacitor compensated transmission line
R_a	armature resistance
R_{fd}	field winding resistance
R_{1d}	d-axis damper winding resistance
R_{1q}, R_{2q}	q-axis damper winding resistances
r_s	resistance of the RC snubber circuit
s	Laplace transformation operator
T	superscript to denote matrix transpose
t	time
T_F	forward thyristor
T_R	reverse thyristor
T_A, T_E, T_{FE}	time constants in the excitation system
T_{ELEC}	air-gap torque
T_m	supplemental controller low-pass filter time constant
T_{MECH}	mechanical torque
T_1, T_2, T_3, T_4	lead-lag network time constants
T_w	washout filter time constant
V_C	voltage across the series capacitor of the compensated transmission line
V_{Cd}, V_{Cq}	voltages across the series capacitor in the d-q reference frame

V_L	voltage across the inductance of the series capacitor compensated transmission line
V_{Ld}, V_{Lq}	voltages across the inductance in the d-q reference frame
V_R	voltage across the resistance of the series capacitor compensated transmission line
V_{Rd}, V_{Rq}	voltages across the resistance in the d-q reference frame
V_{Rmax}, V_{Rmin}	maximum and minimum ceiling voltages of the excitation system respectively
V_b	infinite-bus voltage
V_t	generator terminal voltage
V_{td}, V_{tq}	d- and q- axis generator terminal voltages
X_C	series capacitor reactance
X_L	inductive reactance of the series capacitor compensated transmission line
X_{-max}, X_{-min}	maximum and minimum TCSC reactances respectively
X_{order}	dynamic reactance of TCSC
X_{TCSCo}	initial net reactance of TCSC
α	thyristor firing angle
Ψ_d, Ψ_q	d- and q- axis stator flux linkages
Ψ_{fd}	field winding flux linkage
Ψ_{1d}	d-axis damper winding flux linkage
Ψ_{1q}, Ψ_{2q}	q-axis damper winding flux linkages
δ	generator power (load) angle
δ_{21} *and d21*	generator 2 load angle measured with respect to generator 1 load angle
δ_{31} *and d31*	generator 3 load angle measured with respect to generator 1 load angle
ω	angular velocity
ω_0 (f_0)	synchronous frequency (377 rad/sec)
ω_{21}	generator 2 speed measured with respect to generator 1 speed
ω_{31}	generator 3 speed measured with respect to generator 1 speed
$_0$	suffix to denote the initial operating condition
$^{-1}$	superscript to denote matrix inversion

Chapter 1

INTROUDUCTION

1.1 General

Growth of electric power transmission facilities is restricted despite the fact that bulk power transfers and use of transmission systems by third parties are increasing. Transmission bottlenecks, non-uniform utilization of facilities and unwanted parallel-path or loop flows are not uncommon. Transmission system expansion is needed, but not easily accomplished. Factors that contribute to this situation include a variety of environmental, land-use and regulatory requirements. As a result, the utility industry is facing the challenge of the efficient utilization of the existing AC transmission lines. Thus, the transmission systems are being pushed to operate closer to their stability and thermal limits. Although electricity is a highly engineered product, it is increasingly being considered and handled as a commodity. Thus, the focus on the quality of power delivered is also greater than ever.

Series capacitive compensation of power transmission lines is an important and the most economical way to improve power transfer capability, especially when large amounts of power must be transmitted through long transmission lines. However, one of the impeding factors for the increased utilization of series capacitive compensation is the potential risk of Subsynchronous Resonance (SSR), where electrical energy is exchanged with turbine-generator shaft systems in a growing manner which can result in shaft damage [1]. Figure 1.1 shows a typical time response of a turbine-generator shaft torsional torque during and after clearing a fault on a series capacitive compensated transmission line in the presence of the SSR phenomenon. It is worth noting here that this shaft is designed to withstand a maximum torsional torque of 2 per unit. Another limitation of series capacitive compensation is its inability to provide adequate damping to power system oscillations after clearing system faults. Figure 1.2 shows a typical time response of a generator load angle, measured with respect to a reference generator load angle, during and after clearing a three-phase fault on a series capacitive compensated transmission line. As it can be seen from this figure, the oscillations are not

completely damped after the first few seconds from fault clearing which results in degrading the power quality of the system.

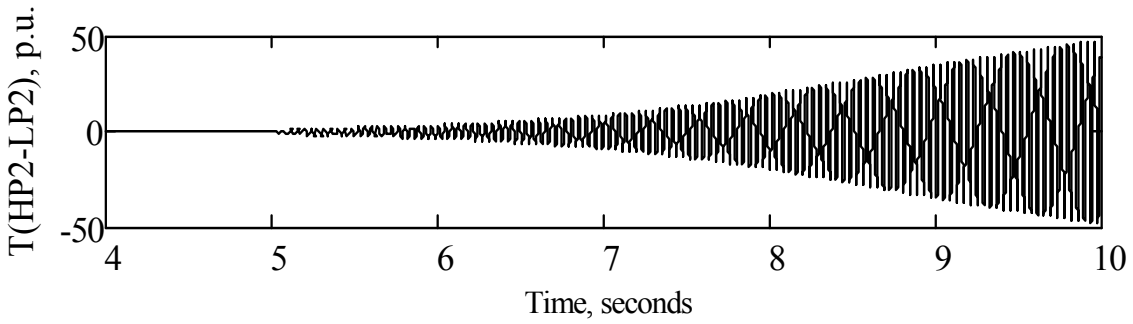

Figure 1.1: Transient time response of a turbine-generator shaft torsional torque during and after clearing a system fault on a series capacitive compensated transmission line.

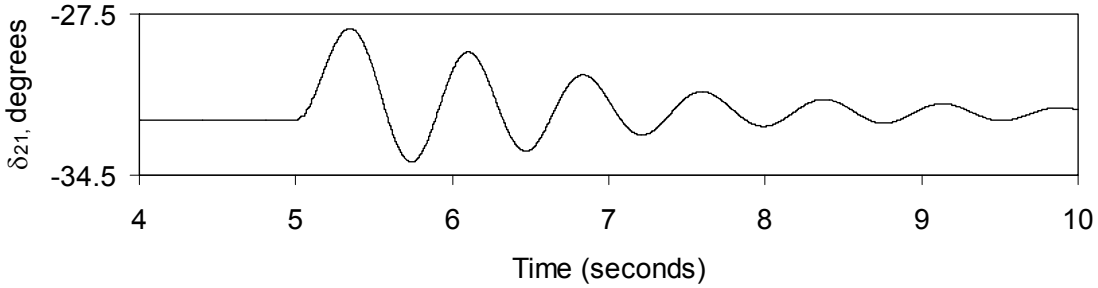

Figure 1.2: Transient time response of a generator load angle, measured with respect to a reference generator load angle, during and after clearing a system fault on a series capacitive compensated transmission line.

1.2 Transmission Line Series Compensation

The main purpose of series compensation in a power system is virtual reduction of line reactance in order to enhance power system stability and increase the loadability of transmission corridors [2]. The principle is based on the compensation of the distributed line reactance by the insertion of a series capacitor. The reactive power generated by the capacitor is continuously proportional to the square of the line current. This means that the series capacitor has a self-regulating effect. When the system loading increases, the reactive power generated by the series capacitor increases as well. The response of the series capacitor is automatic, instantaneous and continuous as long as the capacitor current remains within the specified operating limits. The following are some of the major benefits of incorporating series capacitors in transmission systems:

1.2.1 Steady-state voltage regulation

A series capacitor is capable of compensating the voltage drop of the series inductance of a transmission line. Referring to Figure 1.3, during light loading (Load L), the voltage drop on the series capacitor is low. When the load increases (Load H) and the voltage drop on the line becomes larger, the contribution of the series capacitor increases and, therefore, the system voltage at the receiving line end will be regulated as desired.

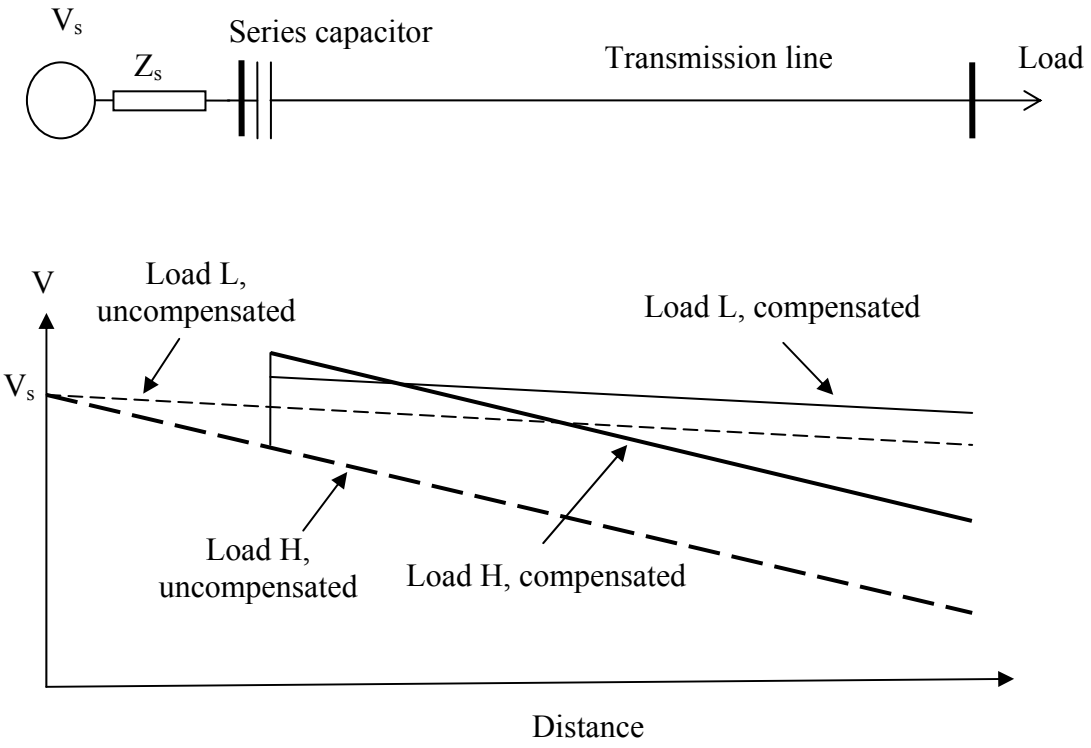

Figure 1.3: A simple radial power system and voltage drop compensation with a series capacitor.

1.2.2 Increase the power transfer capability by raising the first swing stability limit

A substantial increase in the stability margin is achieved by installing a series capacitor. The series compensation will improve the situation in two ways: it will decrease the initial generator load angle corresponding to a specific power transfer and it will also shift the power-load angle (P-δ) characteristic upwards. This will result in increasing the transient stability margin.

1.2.3 Increase in power transfer

The increase in the power transfer capability as a function of the degree of compensation for a transmission line can be illustrated using the circuit and the vector diagram shown in Figure 1.4. The power transfer on the transmission line is given by:

$$P = \frac{|V_s||V_R|}{X_{line} - X_c}\sin\delta = \frac{|V_s||V_R|}{X_{line}(1-k)}\sin\delta \qquad (1.1)$$

where k is the degree of compensation defined as

$$k = \frac{X_c}{X_{line}}$$

The effect on the power transfer when a constant load angle difference is assumed is shown in Figure 1.5. Practical compensation degree ranges from 20 to 70 percent. Transmission capability increases of more than two times can be obtained in practice.

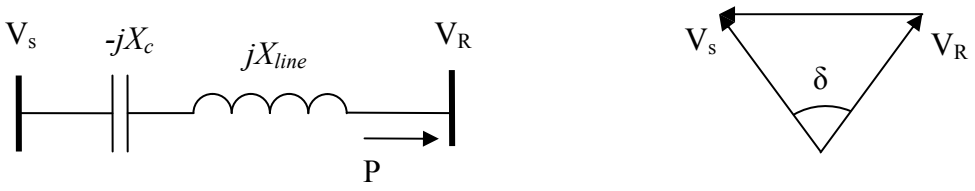

Figure 1.4: Transmission line with series capacitor.

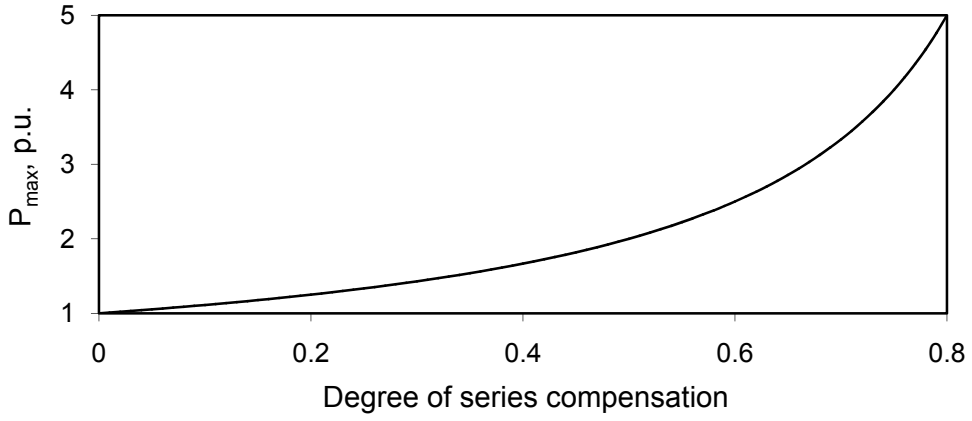

Figure 1.5: Maximum power transmitted over a transmission line as a function of the degree of series compensation ($|V_s| = |V_R| = 1\,p.u., X_{line} = 1\,p.u.$).

1.2.4 Active load sharing between parallel circuits

When two transmission lines are connected in parallel, the natural power sharing between them is dictated by their respective impedances. If the two lines are of different configurations (and consequently of different thermal ratings), their impedances could still be very close. Therefore, the power transmitted in each line will be similar. The voltage drop in both circuits is identical, and therefore, the relationship between the line currents I_{L1} and I_{L2} can be expressed as:

$$I_{L1}Z_{L1} = I_{L2}Z_{L2} \tag{1.2}$$

If overloading the lower thermal rating line, (L_2 , Figure 1.6) is to be avoided (i.e., $I_{L2} \le I_{L2\max}$), then the full power capacity of the other line, L_1, will never be reached (i.e. $I_{L1} < I_{L1\max}$). For example, consider the case when L_1 is a four conductor bundle (quad) circuit configuration, whereas L_2 has a two conductor bundle (twin) circuit configuration. If the conductors of the two bundles are identical, then L_1 has twice the rating of L_2. The inductive reactances of the two lines, however, are very close. If a series capacitor is installed in the higher thermal rating line, both transmission lines can operate at their maximum capacity when the appropriate degree of compensation is provided (50% in this case) [3].

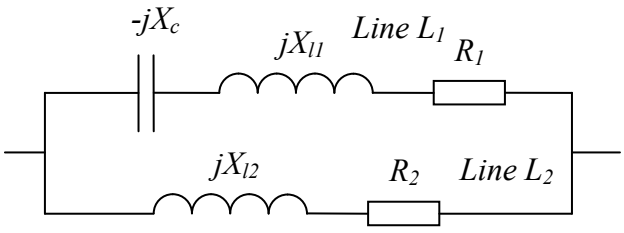

Figure 1.6: Adjusting the power sharing between two parallel lines using a series capacitor.

1.3. Series Capacitor Location

The optimum location for a single series capacitor bank, in terms of the most effective use of the series capacitive reactance, is at the middle of the transmission line [2]. The "effectiveness", which is based on the distributed parameter theory of transmission lines, is the figure of merit for the reduction of the series inductive reactance by a series capacitor. One Canadian installation that has the capacitors located at the middle of the transmission line is the

B.C. Hydro 500 kV system described in [4]. A number of utilities, especially in the U.S., have tended to utilize two series capacitor banks and locate them at the ends of the transmission lines, in order to take advantage of existing land and the availability of service personnel at the line terminals [2]. In some situations, there may be valid reasons (geographical restrictions or specific benefits) for selecting other locations. For example, B.C. Hydro has a 605 Mvar, 500 kV single capacitor bank installed at McLeese substation which is located "nearly" mid-line between Williston and Kelly Lake substations (180 km from Williston and 130 km from Kelly Lake) [5].

1.4. Power System Oscillations

Many electric utilities world-wide are experiencing increased loadings on portions of their transmission systems, which can, and sometimes do, lead to poorly damped, low-frequency oscillations (0.5 – 2 Hz). These oscillations can severely restrict system operations by requiring the curtailment of electric power transfers as an operational measure. They can also lead to widespread system disturbances if cascading outages of transmission lines occur due to oscillatory power swings, like during the blackout in Western North America on August 10, 1996 [6].

Damping is defined as the energy dissipation properties of a material or a system. Power system oscillations can be damped, when extra energy is injected into the system which is instantaneously decelerated, and/or when extra energy is consumed in the system which is instantaneously accelerated. The damping energy is obtained by the modulation of load or generation for a period of time, typically in the range of five to ten seconds. The damping energy must have the correct phase shift relative to the accelerated/decelerated system as incorrect phase angles can excite the oscillations. Figure 1.7 shows different possibilities to damp power system oscillations [7].

1.5. Flexible AC Transmission Systems

All of the above discussed advantages of series compensation can be achieved without the risks of SSR phenomenon if series Flexible AC Transmission Systems (FACTS) devices are used instead of series capacitors. These devices are also be able to provide adequate and fast damping to power system oscillations.

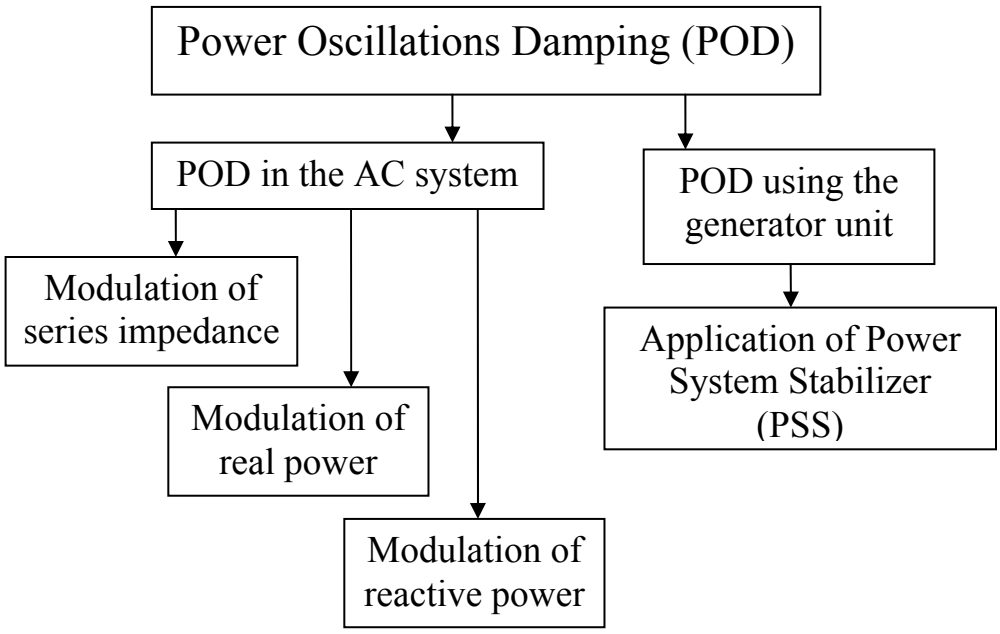

Figure 1.7: Strategies to damp power system oscillations.

FACTS controllers are power electronic based controllers which can influence transmission system voltages, currents, impedances and/or phase angles rapidly [8], [9]. These controllers have the flexibility of controlling both real and reactive power, which could provide an excellent capability for improving power system dynamics. FACTS technology provides an unprecedented way for controlling transmission grids and increasing transmission capacity.

FACTS controllers may be based on thyristor devices with no gate turn-off (only with gate turn-on), or with power devices with gate turn-off capability. In general, the principal controllers with gate turn-off devices are based on an dc to ac converters, which can exchange active and/or reactive power with the ac system. In the studies conducted in this thesis, only the series FACTS controller based on thyristor switches is considered. This controller, shown in Figure 1.8, is called a Thyristor Controlled Series Capacitor (TCSC). The TCSC, which will be discussed in detail in Chapter 3, has been installed and operated successfully by utilities in several countries. One example of these installations is the Brazilian North-South interconnection (a 500 kV, 1020 km transmission line with a rated transmitted power of 1300 MW), where a hybrid three-phase-TCSC connects the North and South systems [10], [11]. Such a hybrid three-phase-TCSC, shown in Figure 1.9, consists of five fixed capacitors (distributed equally along the line length) and two TCSC modules (located at the sending and receiving

ends). The degree of compensation of the interconnection is 66% (1100 Mvar capacitive), where the fixed capacitors provide 54% and each TCSC module provides 6%. The task of the TCSC modules is purely damping the low-frequency, inter-area power oscillations between the two systems. These oscillations would otherwise provide a hazard to the stability of the interconnected system.

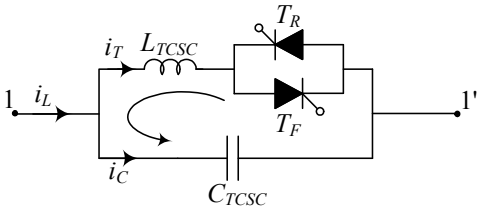

Figure 1.8: A schematic diagram of the TCSC.

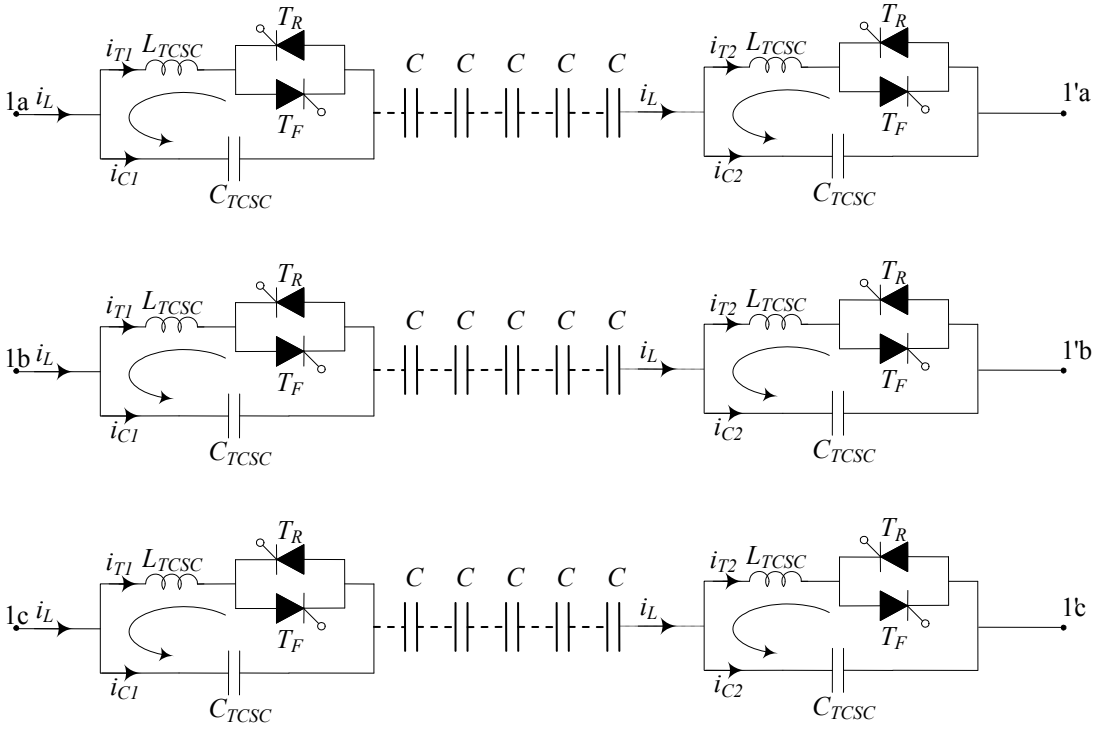

Figure 1.9: A single-line diagram of a hybrid three-phase-TCSC.

1.6. Research Objective and Scope of the Thesis

The TCSC and the hybrid three-phase-TCSC which are already employed by several utilities for power flow control and damping low-frequency and SSR oscillations have shown superior performance through field tests, analytical and simulation studies [12] – [26]. The main

objective of this research work is to investigate the possibility of damping power system oscillations resulting from large disturbances (mainly transmission line faults) in multi-machine power systems using the hybrid single-phase-TCSC scheme shown in Figure 1.10. This scheme which is feasible, technically sound, and has an industrial application potential would, definitely be economically attractive when compared with the full three phase TCSC, which has been used/proposed for power oscillations damping. Furthermore, reducing the number of thyristor valves to one third, will also have a positive impact on system reliability, when compared with the full three-phase-TCSC.

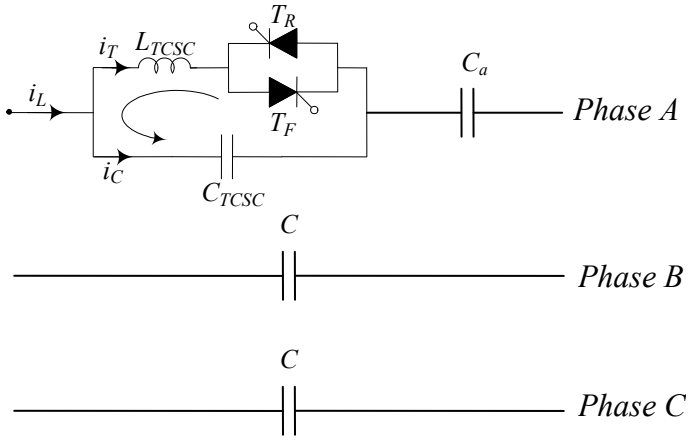

Figure 1.10: A three-line diagram of a hybrid single-phase-TCSC.

There are five chapters in this thesis. The main topics of each chapter are as follows:

Chapter 1 introduces the fundamental benefits of series compensation of transmission lines. Brief introductions to SSR, FACTS controllers and the TCSC are also presented. The objective of the research is also presented in this chapter.

In Chapter 2, the system used for the investigations conducted in this thesis is described and the detailed dynamic models of its individual components are also presented in this chapter. The results of the digital time-domain simulations of a case study for the system during a three-phase fault are presented at the end of this chapter.

Chapter 3 presents a comprehensive description of the TCSC, its three modes of operation and the analysis of its net reactance. The phase imbalanced hybrid single-phase-TCSC compensation scheme and its modeling in the ElectroMagnetic Transient Program (EMTP-RV) are also presented.

Chapter 4 demonstrates the effectiveness of the proposed hybrid single-phase- TCSC compensation scheme in damping power system oscillations through time-domain simulation studies. The performance of different supplementary controller structures and stabilizing signals are also investigated.

Chapter 5 summarizes the research described in this thesis and presents some conclusions.

Chapter 2

POWER SYSTEM MODELING FOR LARGE DISTURBANCE STUDIES

2.1 General

In this chapter, the system used for the studies reported in this thesis is described and the mathematical models of its various components are presented. A digital time-domain simulation of a case study of the system during a three-phase fault is presented at the end of this chapter.

2.2 System under Study

The system used in the investigations of this thesis is shown in Figure 2.1. It consists of three large generating stations (G_1, G_2 and G_3) supplying two load centers (S_1 and S_2) through five 500 kV transmission lines. The two double-circuit transmission lines L_1 and L_2 are series compensated with fixed capacitor banks located at the middle of the lines. The compensation degree of L_1 and L_2 is 50%. The total installed capacity and peak load of the system are 4500 MVA and 3833 MVA respectively. Shunt capacitors are installed at buses 4 and 5 to maintain their voltages within 1±0.05 p.u. The system data are given in Appendix A.

2.3 Power System Modeling

The nonlinear differential equations of the system under study are derived by developing individually the mathematical models which represent the various components of the system, namely the synchronous generator, the excitation system, the transmission line and the system load. Knowing the mutual interaction among these models, the whole system differential equations can be formed.

2.3.1 Modeling of the synchronous machine

In a conventional synchronous machine, the stator circuit consisting of a three-phase winding produces a sinusoidally space distributed magnetomotive force. The rotor of the machine carries the field (excitation) winding which is excited by a dc voltage. The electrical damping due to the eddy currents in the solid rotor and, if present, the damper winding is represented by three

equivalent damper circuits; one on the direct axis (d-axis) and the other two on the quadrature axis (q-axis). The performance of the synchronous machine can be described by the equations given below in the d-q reference frame [27]. In these equations, the convention adopted for the signs of the voltages and currents are that *v* is the impressed voltage at the terminals and that the direction of positive current *i* corresponds to generation. The sign of the currents in the equivalent damper windings is taken positive when they flow in a direction similar to that of the positive field current.

With time *t* expressed in seconds, the angular velocity ω expressed in rad/s($\omega_0 = 377 rad/\sec$) and the other quantities expressed in per unit, the stator equations become:

$$e_d = \frac{1}{\omega_0}\frac{d\Psi_d}{dt} - \frac{\omega}{\omega_0}\Psi_q - R_a i_d \tag{2.1}$$

$$e_q = \frac{1}{\omega_0}\frac{d\Psi_q}{dt} + \frac{\omega}{\omega_0}\Psi_d - R_a i_q \tag{2.2}$$

The rotor equations:

$$e_{fd} = \frac{1}{\omega_0}\frac{d\Psi_{fd}}{dt} + R_{fd} i_{fd} \tag{2.3}$$

$$0 = \frac{1}{\omega_0}\frac{d\Psi_{1d}}{dt} + R_{1d} i_{1d} \tag{2.4}$$

$$0 = \frac{1}{\omega_0}\frac{d\Psi_{1q}}{dt} + R_{1q} i_{1q} \tag{2.5}$$

$$0 = \frac{1}{\omega_0}\frac{d\Psi_{2q}}{dt} + R_{2q} i_{2q} \tag{2.6}$$

The stator flux linkage equations:

$$\Psi_d = -L_d i_d + L_{ad} i_{fd} + L_{ad} i_{1d} \tag{2.7}$$

$$\Psi_q = -L_q i_q + L_{aq} i_{1q} + L_{aq} i_{2q} \tag{2.8}$$

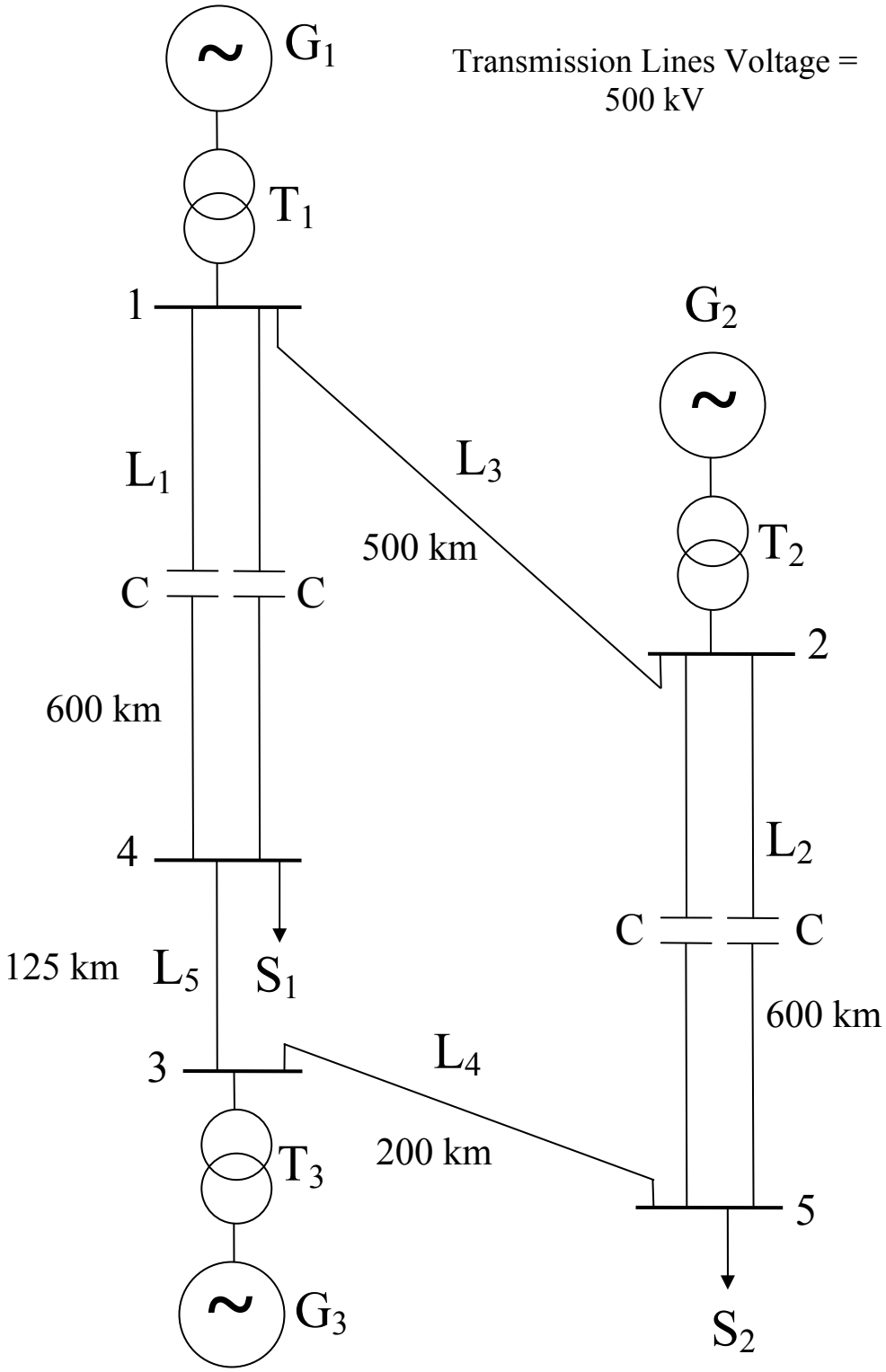

Figure 2.1: System under study.

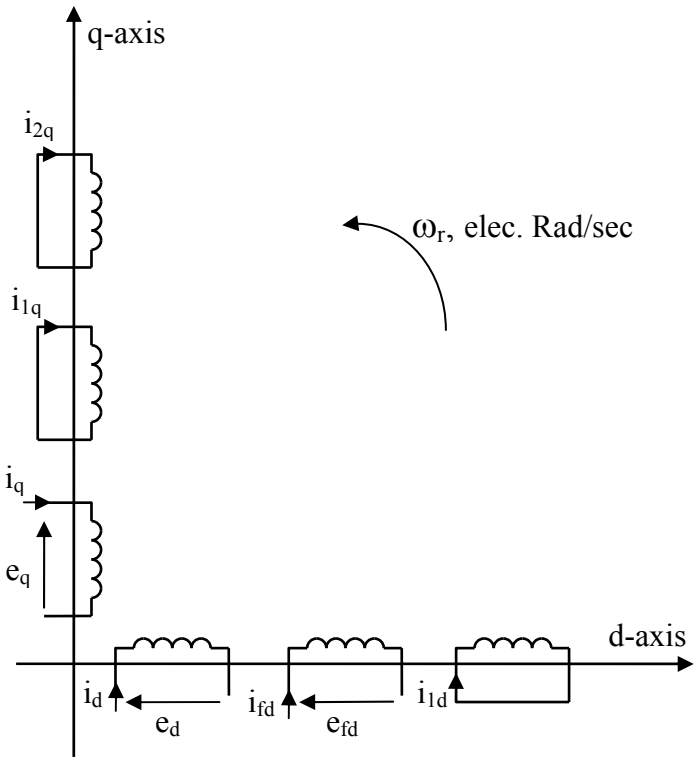

Figure 2.2: Modeling of the synchronous machine in the d-q reference frame.

The rotor flux linkage equations:

$$\Psi_{fd} = L_{ffd} i_{fd} + L_{ad} i_{1d} - L_{ad} i_d \tag{2.9}$$

$$\Psi_{1d} = L_{ad} i_{fd} + L_{11d} i_{1d} - L_{ad} i_d \tag{2.10}$$

$$\Psi_{1q} = L_{11q} i_{1q} + L_{aq} i_{2q} - L_{aq} i_q \tag{2.11}$$

$$\Psi_{2q} = L_{aq} i_{1q} + L_{22q} i_{2q} - L_{aq} i_q \tag{2.12}$$

The air-gap torque equation:

$$T_{ELEC} = \Psi_d i_q - \Psi_q i_d \tag{2.13}$$

The overall differential equations which describe the transient performance of the synchronous machine are given by the following matrix equation:

$$\left[\frac{dX_{syn}}{dt}\right] = \left[At_{syn}\right]\left[X_{syn}\right] + \left[Bt_{syn}\right]\begin{bmatrix} V_{td} \\ V_{tq} \\ e_{fd} \end{bmatrix} \tag{2.14}$$

where

$$[X_{syn}] = [i_d \quad i_q \quad i_{fd} \quad i_{1q} \quad i_{1d} \quad i_{2q}]^T$$

$$[At_{syn}] = [L]^{-1}[Qt]$$

$$[Bt_{syn}] = [L]^{-1}[Rt]$$

$$[L] = \begin{bmatrix} -L_d & 0 & L_{ad} & 0 & L_{ad} & 0 \\ 0 & -L_q & 0 & L_{aq} & 0 & L_{aq} \\ -L_{ad} & 0 & L_{ffd} & 0 & L_{ad} & 0 \\ 0 & -L_{aq} & 0 & L_{11q} & 0 & L_{aq} \\ -L_{aq} & 0 & L_{ad} & 0 & L_{11d} & 0 \\ 0 & -L_{aq} & 0 & L_{aq} & 0 & L_{22q} \end{bmatrix} \tag{2.15}$$

$$[Qt] = \begin{bmatrix} \omega_0 R_a & -\omega L_q & 0 & \omega L_{aq} & 0 & \omega L_{aq} \\ \omega L_d & \omega_0 R_a & -\omega L_{ad} & 0 & -\omega L_{ad} & 0 \\ 0 & 0 & -\omega_0 R_{fd} & 0 & 0 & 0 \\ 0 & 0 & 0 & -\omega_0 R_{1q} & 0 & 0 \\ 0 & 0 & 0 & 0 & -\omega_0 R_{1d} & 0 \\ 0 & 0 & 0 & 0 & 0 & -\omega_0 R_{2q} \end{bmatrix}$$

$$[Rt] = \begin{bmatrix} \omega_0 & 0 & 0 \\ 0 & \omega_0 & 0 \\ 0 & 0 & \omega_0 \\ 0 & 0 & 0 \\ 0 & 0 & 0 \\ 0 & 0 & 0 \end{bmatrix}$$

here, the superscript ^{T} means matrix transpose.

The synchronous machine swing equation can be written as:

$$\frac{2H}{\omega_o}\frac{d\omega}{dt} = T_{MECH} - T_{ELEC} \tag{2.16}$$

$$\frac{d\delta}{dt} = \omega - \omega_o \tag{2.17}$$

In the above two equations (2.16 and 2.17), ω is in radians per second, the inertia constant H is in seconds, and the load angle δ is in radians, ω_o is the synchronous frequency (377 rad/sec) and the mechanical and electrical torques T_{MECH} and T_{ELEC} are in per unit.

In developing the equations of multi-machine systems, the equations of each synchronous machine expressed in its own d-q reference frame which rotates with its rotor must be expressed in a common reference frame. Usually, a reference frame rotating at synchronous speed is used as the common reference. Axis transformation equations are used to transform between the individual machine (d-q) reference frames and the common (R-I) reference frame [27].

2.3.2 Modeling of the transmission line

A series capacitor-compensated transmission line may be represented by the *RLC* circuit shown in Figure 2.3 [28]. In the voltage phasor diagram shown in Figure 2.4, the rotor angle δ is the angle (in elec. rad) by which the q-axis leads the reference voltage V_b. The differential equations for the circuit elements, after applying Park's transformation [28], can be expressed in the d-q reference frame by the following matrix expressions.

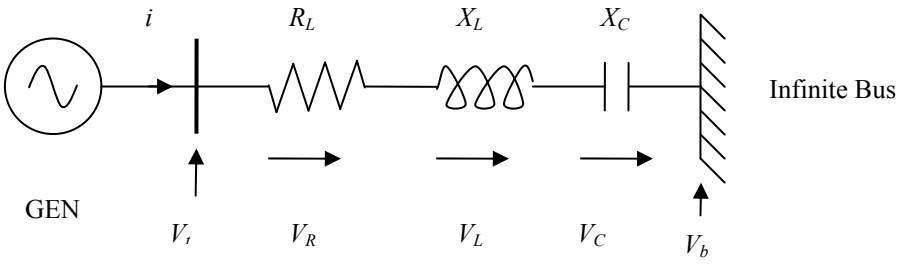

Figure 2.3: A series capacitor-compensated transmission line.

The voltage across the resistance:

$$\begin{bmatrix} V_{Rd} \\ V_{Rq} \end{bmatrix} = \begin{bmatrix} R_L & 0 \\ 0 & R_L \end{bmatrix} \begin{bmatrix} i_d \\ i_q \end{bmatrix} \tag{2.18}$$

The voltage across the inductance:

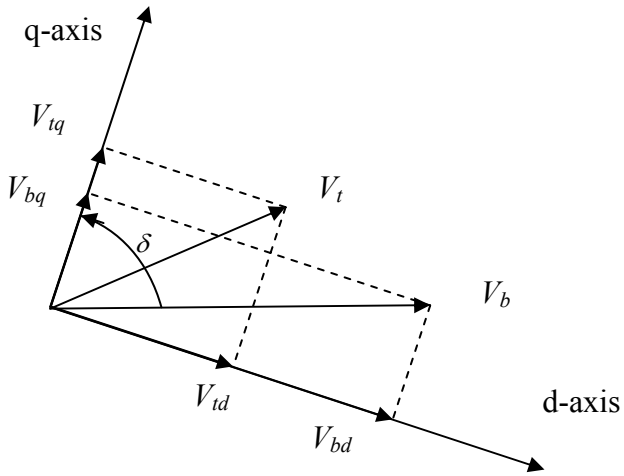

Figure 2.4: Voltage phasor diagram.

$$\begin{bmatrix} V_{Ld} \\ V_{Lq} \end{bmatrix} = \begin{bmatrix} 0 & -\frac{\omega}{\omega_0} X_L \\ \frac{\omega}{\omega_0} X_L & 0 \end{bmatrix} \begin{bmatrix} i_d \\ i_q \end{bmatrix} + \begin{bmatrix} \frac{X_L}{\omega_0} & 0 \\ 0 & \frac{X_L}{\omega_0} \end{bmatrix} \begin{bmatrix} \frac{di_d}{dt} \\ \frac{di_q}{dt} \end{bmatrix} \tag{2.19}$$

The voltage across the capacitor:

$$\begin{bmatrix} \frac{dV_{Cd}}{dt} \\ \frac{dV_{Cq}}{dt} \end{bmatrix} = \begin{bmatrix} \omega_0 X_C & 0 \\ 0 & \omega_0 X_C \end{bmatrix} \begin{bmatrix} i_d \\ i_q \end{bmatrix} + \begin{bmatrix} 0 & \omega \\ -\omega & 0 \end{bmatrix} \begin{bmatrix} V_{Cd} \\ V_{Cq} \end{bmatrix} \tag{2.20}$$

The overall equations of the transmission line can be written as

$$\begin{bmatrix} \frac{dV_{Cd}}{dt} \\ \frac{dV_{Cq}}{dt} \\ V_{td} \\ V_{tq} \end{bmatrix} = [Att] \begin{bmatrix} V_{Cd} \\ V_{Cq} \end{bmatrix} + [Rt1] \begin{bmatrix} \frac{di_d}{dt} \\ \frac{di_q}{dt} \end{bmatrix} + [Rt2] \begin{bmatrix} i_d \\ i_q \end{bmatrix} + [Btt][V_b] \tag{2.21}$$

where

$$[Att] = \begin{bmatrix} 0 & \omega \\ -\omega & 0 \\ 1 & 0 \\ 0 & 1 \end{bmatrix}$$

$$[Rt1]=\begin{bmatrix} 0 & 0 \\ 0 & 0 \\ \frac{X_L}{\omega_0} & 0 \\ 0 & \frac{X_L}{\omega_0} \end{bmatrix}$$

$$[Rt2]=\begin{bmatrix} \omega_0 X_C & 0 \\ 0 & \omega_0 X_C \\ R_L & -\frac{\omega}{\omega_0} X_L \\ \frac{\omega}{\omega_0} X_L & R_L \end{bmatrix} \qquad (2.22)$$

$$[Btt]=\begin{bmatrix} 0 \\ 0 \\ \sin\delta \\ \cos\delta \end{bmatrix}$$

2.3.3 Excitation system

The block diagram representation of the excitation system used in this study is shown in Figure 2.5, and the corresponding data are given in Appendix A [28].

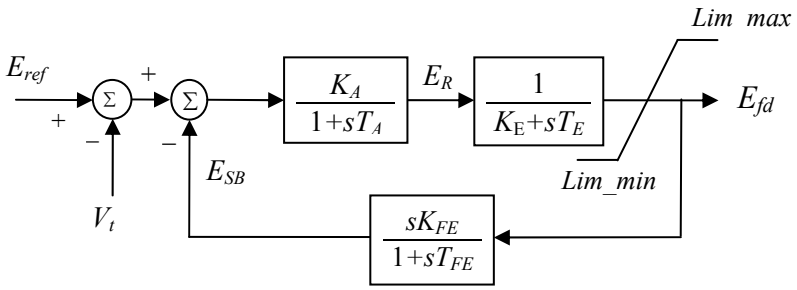

Figure 2.5: Block diagram of the excitation system.

Utilizing the relationship between the excitation system output voltage and the field voltage given by $E_{fd}=\frac{L_{ad}}{R_{fd}}e_{fd}$, the state-space equation of the excitation system can be derived from its block diagram and is given by

$$\left[\frac{dX_v}{dt}\right] = [At_v][X_v] + [Bt_v]\begin{bmatrix} V_t \\ E_{ref} \end{bmatrix} \tag{2.23}$$

where

$$[X_v] = \begin{bmatrix} e_{fd} & E_R & E_{SB} \end{bmatrix}^T$$

$$[At_v] = \begin{bmatrix} -\frac{K_E}{T_E} & \frac{1}{T_E}\frac{R_{fd}}{L_{ad}} & 0 \\ 0 & -\frac{1}{T_A} & -\frac{K_A}{T_A} \\ -\frac{K_E K_F}{T_E T_F}\frac{L_{ad}}{R_{fd}} & \frac{K_F}{T_F T_E} & -\frac{1}{T_F} \end{bmatrix} \tag{2.24}$$

$$[Bt_v] = \begin{bmatrix} 0 & 0 \\ -\frac{K_A}{T_A} & \frac{K_A}{T_A} \\ 0 & 0 \end{bmatrix}$$

2.3.4 Modeling of the transformer

The three-phase transformer is constructed by using three single-phase transformers connected in Delta (LV side)/Y grounded (HV side). The transformer leakage and magnetizing reactances as well as the winding resistances and core loss are represented in the model.

2.3.5 Modeling of system loads

The system loads are modeled in these studies by constant impedances. The formula, which is used in calculating the load impedances, is given by [29]:

$$Z_{Load} = \frac{|V_{Load}|^2}{P_{Load} - jQ_{Load}} \tag{2.25}$$

where

Z_{Load} = load impedance.

V_{Load} = load voltage.

P_{Load} = load real power.

Q_{Load} = load reactive power.

2.4 A Sample Case Study

In the studies conducted in this thesis, the ElectroMagnetic Transient Program (EMTP-RV) is used for modeling the various system components and producing the time-domain simulation results [30]. Due to the initialization process in the EMTP-RV, simulation results will be displayed starting at time equal four seconds. Moreover, faults are assumed to occur at t = 5 seconds.

Figure 2.6 shows the power flow results for the bus voltages and the line real power flows of the system under study. Figure 2.7 shows the transient time responses of the generator load angles and speeds (measured respectively with respect to the load angle and speed of generator 1), the bus voltages and the real power flows in the transmission lines during and after clearing a three-cycle, three-phase fault at the middle of transmission line L_3. The following observations can be made from examining these two figures:

1. The power flow results show heavy power transfers along the two compensated lines L_1 and L_2.
2. The system is stable after fault clearing. The generator load angles and speeds reach steady states. The bus voltages drop immediately at the instant of fault inception but recover after fault clearing.
3. The low frequency oscillations in the generator load angles and speeds are poorly damped.
4. The system under study has three generators; therefore, it has two natural modes of oscillations [26]. In general, synchronous machines respond to disturbances by complex oscillations that involve several natural frequencies, but a particular machine or group of coherent machines may tend to favor one mode over all others [2]. This is the case for generators 2 and 3. As it can be seen from the load angle responses of these two generators, measured with respect to the load angle of generator 1 (Figure 2.7), generators 2 and 3 tend to oscillate at a single frequency (approximately 1.4 Hz).

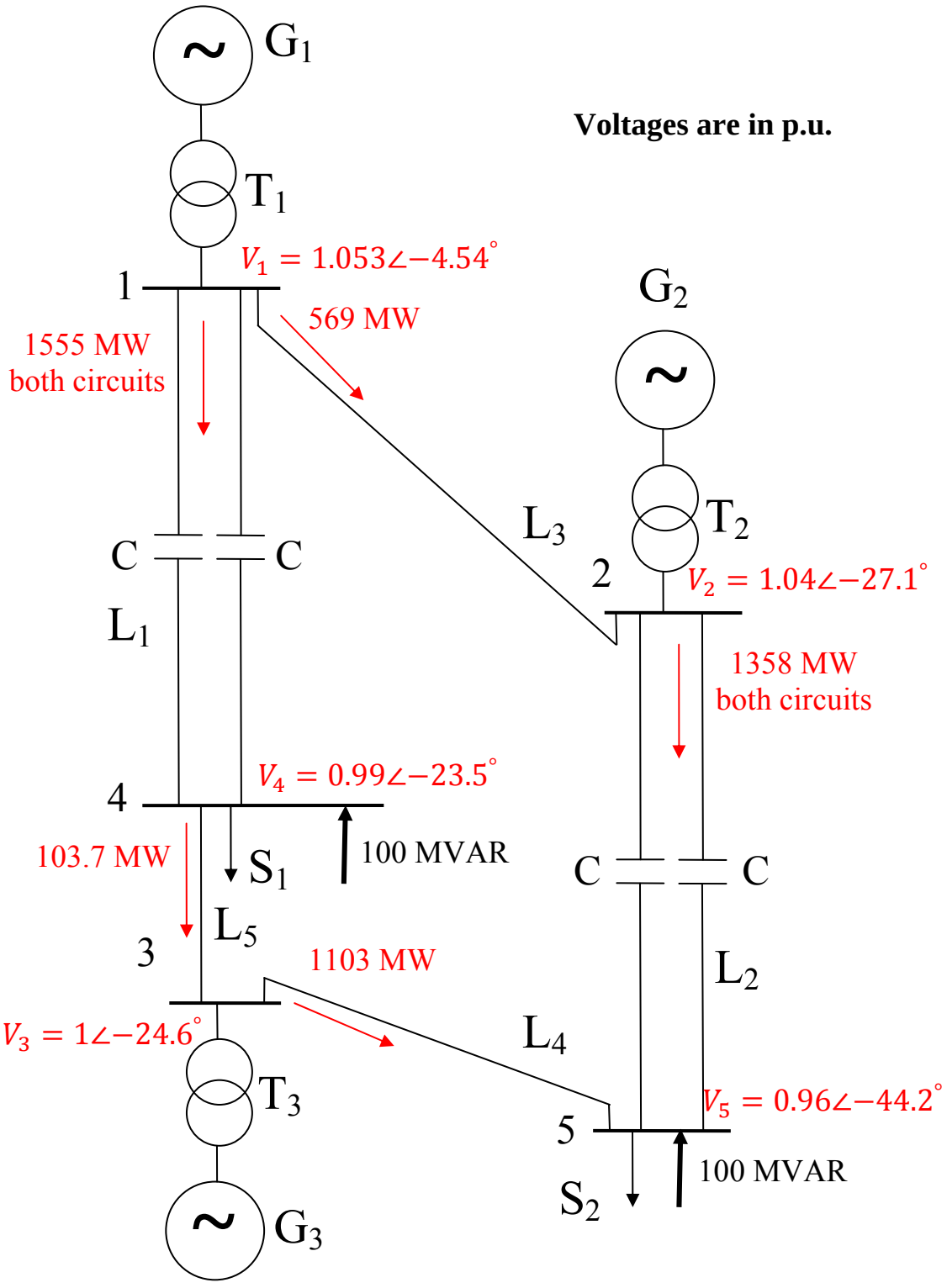

Figure 2.6: Power flow results of bus voltages and line real power flows of the system under study.

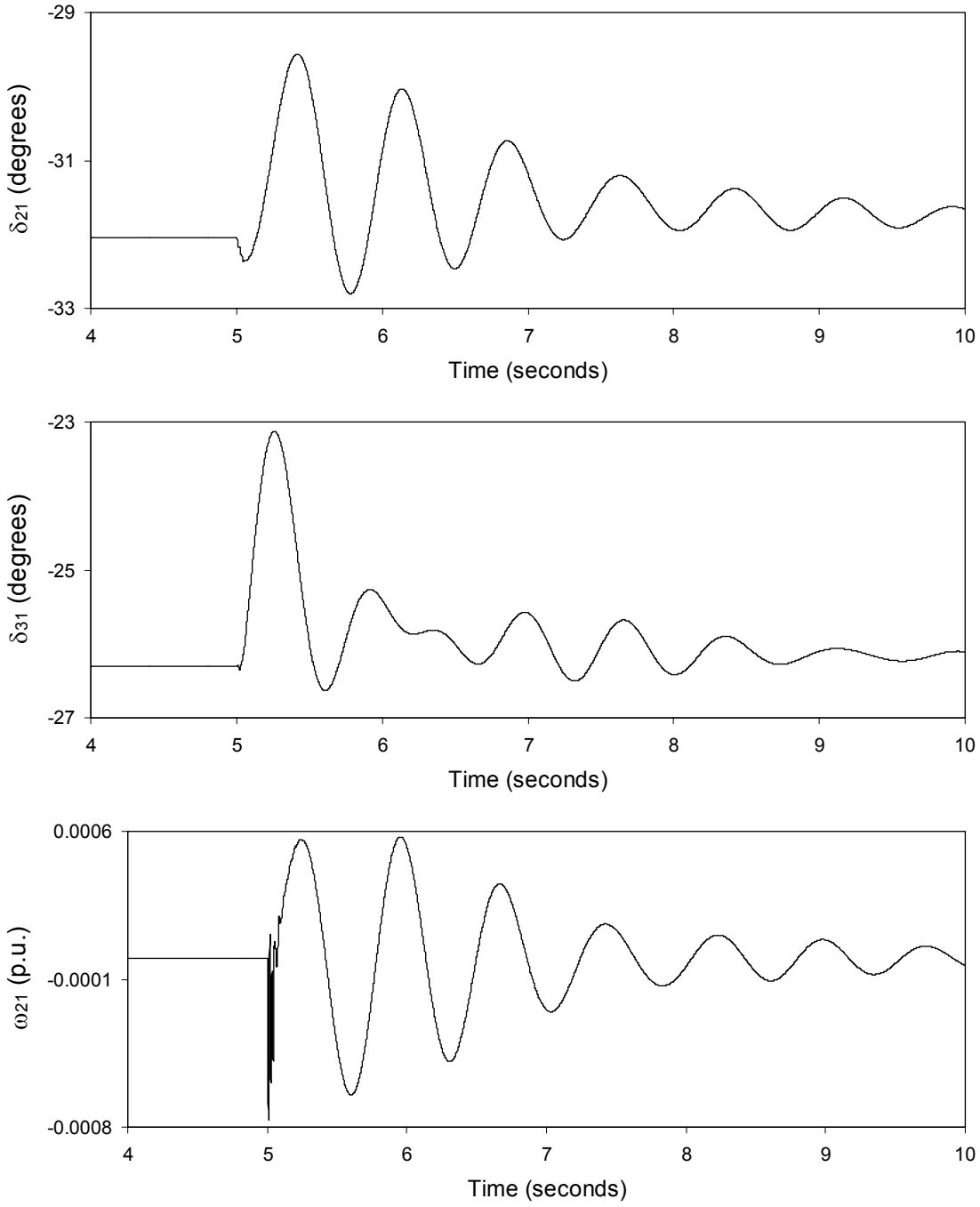

Figure 2.7: Transient time responses of the power system during and after clearing a three-cycle, three-phase fault at the middle of transmission line L_3.

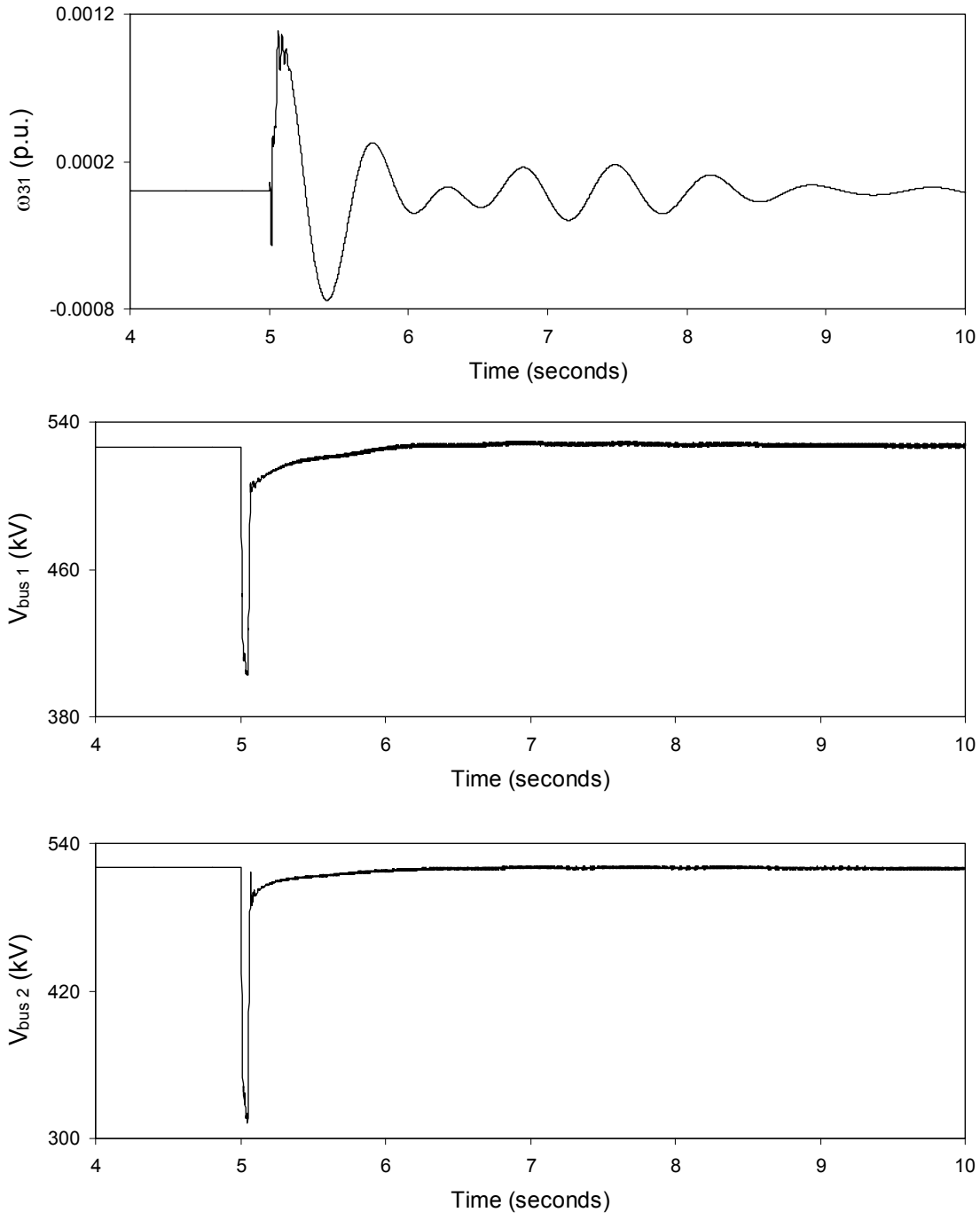

Figure 2.7: continued.

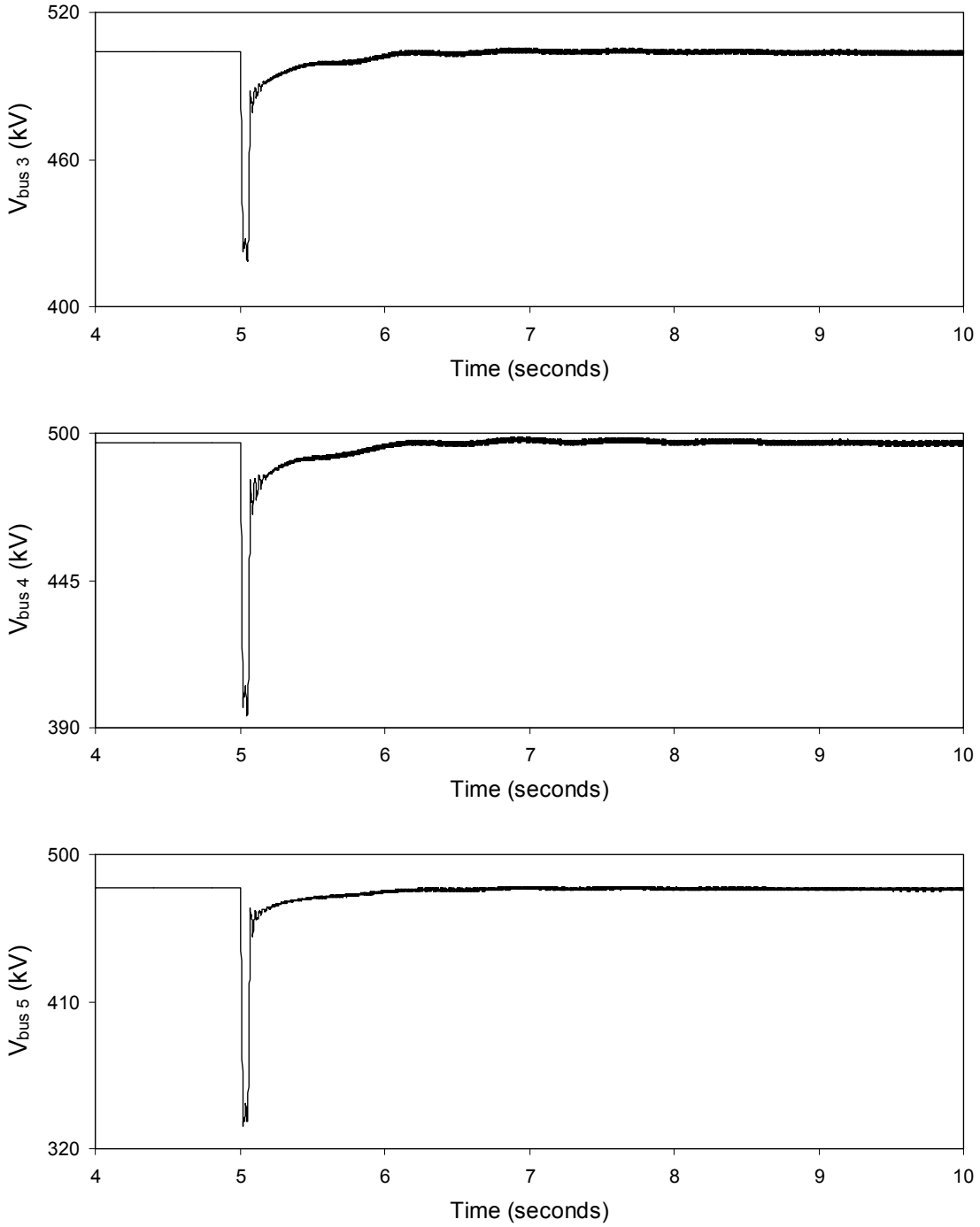

Figure 2.7: continued.

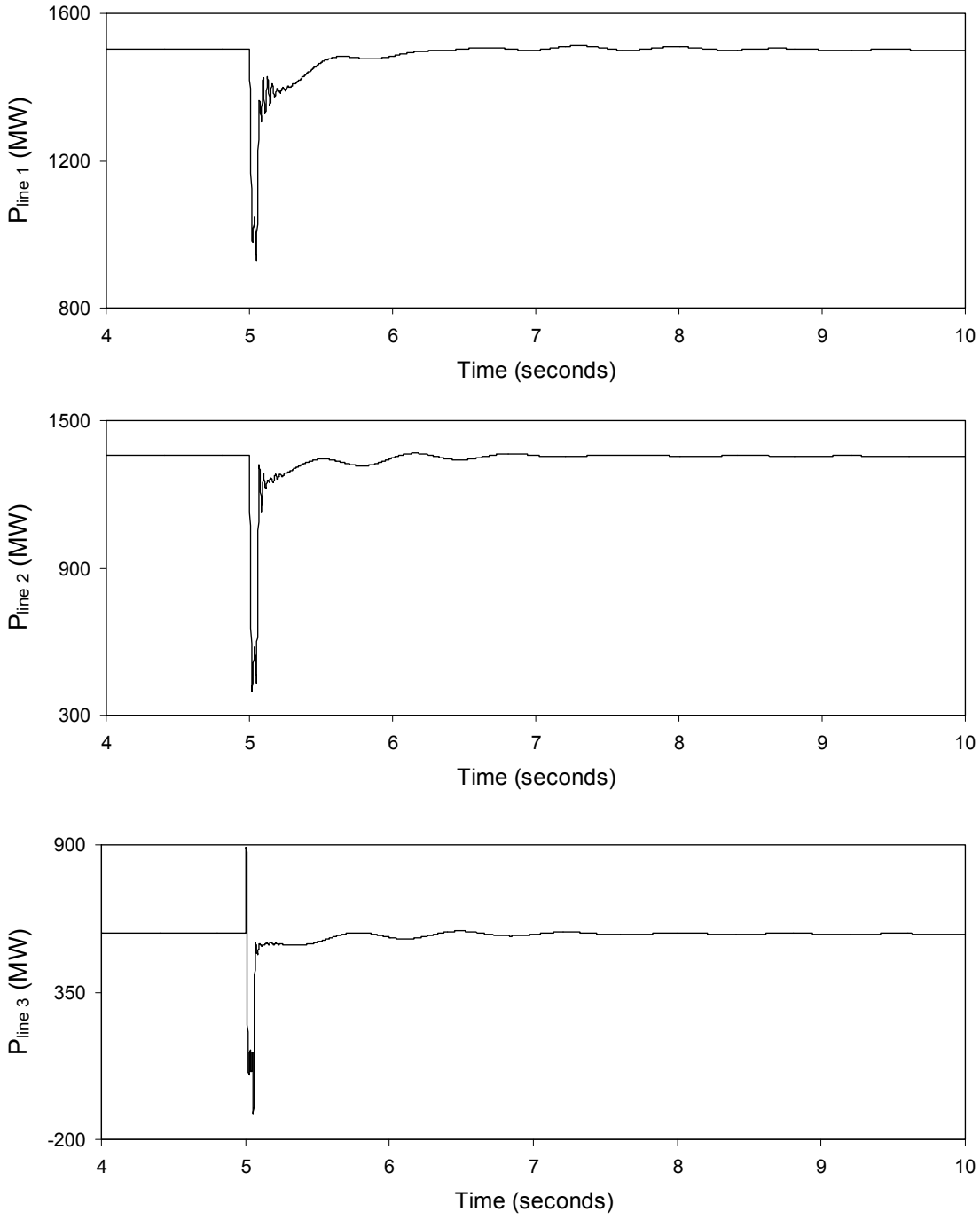

Figure 2.7: continued.

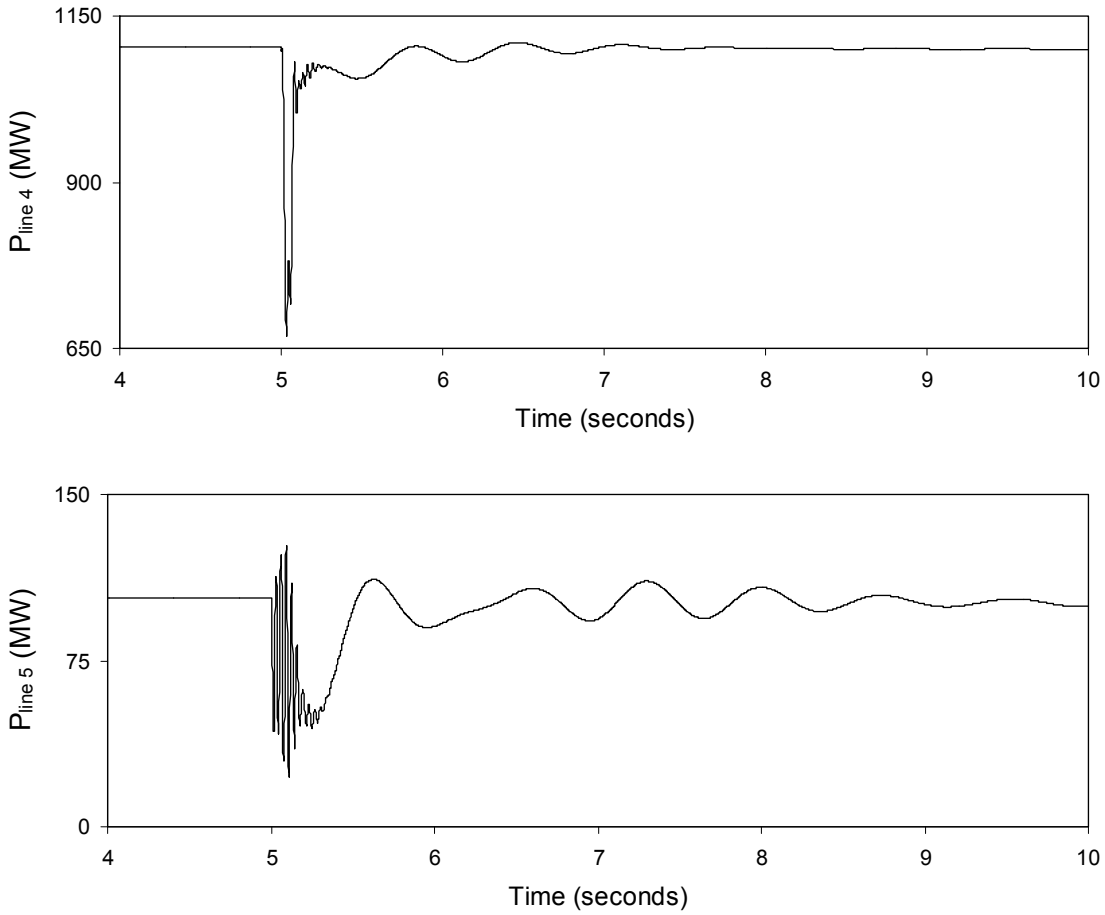

Figure 2.7: continued.

2.5 Summary

This chapter introduces the system used for the studies reported in this thesis and presentes the mathematical models of its various components. A digital time-domain simulation of a case study of the system during a three-phase fault is also presented and some observations are noted.

Chapter 3

THE THYRISTOR CONTROLLED SERIES CAPACITOR AND THE HYBRID SINGLE-PHASE- TCSC COMPENSATION SCHEME

3.1 General

This chapter presents the description and the basic principles of the TCSC as well as the derivation of its mathematical model. Modeling the hybrid single-phase-TCSC scheme in the ElectroMagnetic Transient Program (EMTP-RV) is also presented.

3.2 Thyristor Controlled Series Capacitor

The TCSC shown in Figure 3.1 consists of a number of series connected modules. In each module, the capacitor bank is provided with a parallel thyristor controlled inductor that circulates current pulses which add in phase with the line current. This boosts the capacitor voltage beyond the level that would be obtained by the line current alone. A Zinc oxide varistor is included in each module for secure overvoltage protection of the TCSC. Each thyristor is triggered once per cycle and has a conduction interval that is shorter than a half-cycle of the rated frequency. If the additional voltage created by the circulating current pulses is controlled to be proportional to the line current, the transmission system will perceive the TCSC as having a virtually increased reactance beyond the physical reactance of the capacitor. This feature which is referred to "vernier control" can be used for short-time transient control. The upper limit for vernier operation is a function of the line current magnitude and time spent at the operating point. Moreover, this scheme can provide an accurate setting of the compensation degree with a high resolution as well as a subsynchronous resonance immune series compensation even at high compensation degrees [31], [32].

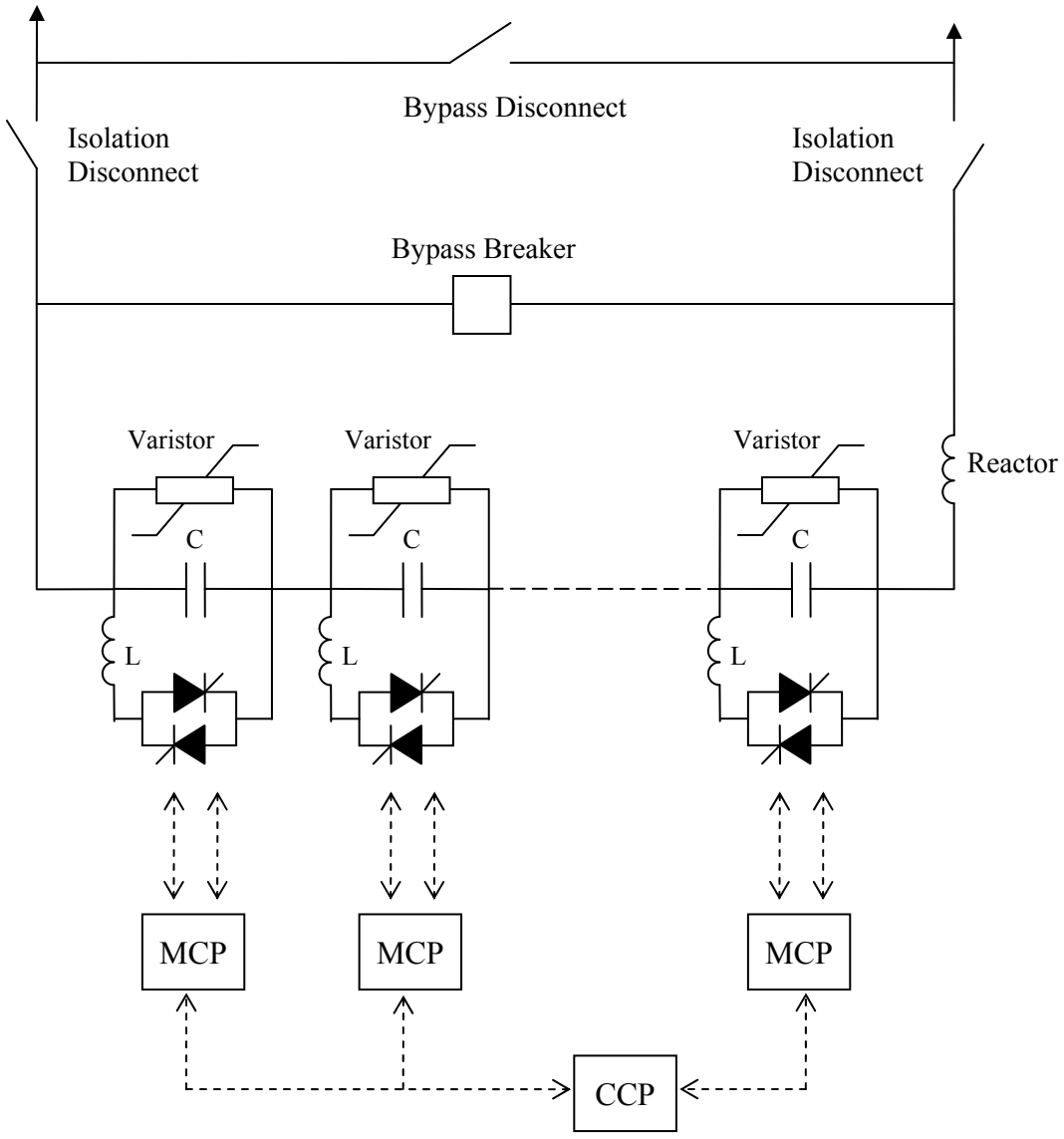

Figure 3.1: A multi-module TCSC.

The control and protection of TCSC are partitioned in two levels; common and module. Commands for both control and protective operations flow from the common level to the module levels. Status information is sent back from each module level. The design concept is to permit any module or combination of modules to be out of service while still being able to operate the remaining modules to benefit the power system.

The common-level protection detects problems affecting all modules, and as such, generally requires bypassing all modules with the bypass breaker. The module-level protection detects problems affecting a single-module and as such, may only initiate protective actions within the affected module. The thyristor switches allow for bypassing individual modules by continuous gating the thyristors, and this is an effective protective action for many potential internal failures (e.g., capacitor failure). However, for some serious problems within a module (e.g., varistor failure), protective actions may involve bypassing all modules with the bypass breaker.

3.3 Operation of the TCSC

3.3.1 Basic principles [33]

A simple understanding of TCSC functioning can be realized by analyzing the behavior of the circuit shown in Figure 3.2 which consists of a variable inductor connected in parallel with a fixed capacitor. The equivalent impedance, Z_{eq}, of this LC combination is expressed as:

$$Z_{eq} = -j\frac{1}{\omega C - \frac{1}{\omega L}} \tag{3.1}$$

The impedance of the capacitor alone, however, is given by $X_c = -j\frac{1}{\omega C}$.

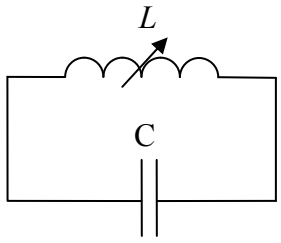

Figure 3.2: A variable inductor connected in parallel with a fixed capacitor.

If $\omega C - \left(\frac{1}{\omega L}\right) > 0$ or, in other words, $\omega L > \frac{1}{\omega C}$, the reactance of the fixed capacitor is less than that of the parallel-connected variable reactor and that this combination provides a variable-capacitive reactance are both implied. Moreover, this inductor increases the equivalent-capacitive reactance of the LC combination above that of the fixed capacitor.

If $\omega C - \left(\frac{1}{\omega L}\right) = 0$, a resonance develops that results in an infinite-capacitive impedance. If, however, $\omega C - \left(\frac{1}{\omega L}\right) < 0$, the LC combination provides inductance above the value of the fixed inductor. This situation corresponds to the inductive-vernier mode of the TCSC operation.

In the variable-capacitive mode of the TCSC, as the inductive reactance of the variable inductor is increased, the equivalent-capacitive reactance is gradually decreased. The minimum equivalent-capacitive reactance is obtained for extremely large inductive reactance or when the variable inductor is open-circuited, in which the value is equal to the reactance of the fixed capacitor itself.

The behavior of the TCSC is similar to that of the parallel LC combination. The difference is that the LC-combination analysis is based on the presence of pure sinusoidal voltage and current in the circuit, whereas in the TCSC, the voltage and current are not sinusoidal because of the thyristor switchings. The analysis in this case is presented in Section 3.4.

3.3.2 Modes of TCSC operation

There are three modes of TCSC operation:

1. Bypassed-Thyristor Mode: the thyristors are made to fully conduct resulting in a continuous sinusoid of flow current through the thyristor valves (Figure 3.3(a)). The TCSC module behaves like a parallel capacitor-inductor combination. The net current through the module, however, is inductive, for the susceptance of the reactor is chosen to be greater than that of the capacitor.
2. Blocked-Thyristor Mode: the firing pulses of the thyristor valves are blocked. The TCSC module is reduced to a fixed capacitor (Figure 3.3(b)).
3. Partially Conducting Thyristor or Vernier Mode: This mode allows the TCSC to behave either as a continuously controllable capacitive reactance or as a continuously controllable inductive reactance. It is achieved by varying the thyristor-pair firing angle in an appropriate range. In practice, the TCSC operates only in the *capacitive-vernier-control* mode. In such a mode, the thyristors are fired when the capacitor voltage and the capacitor current have opposite polarity. This condition causes the reactor current to have a direction opposite to that of the capacitor current, thereby, resulting in a loop-

current flow in the TCSC controller. The loop current increases the voltage across the fixed capacitor, effectively enhancing the equivalent capacitive reactance and the series compensation level for the same value of line current. To preclude resonance, the firing angle α of the forward facing thyristor, as measured from the positive reaching a zero crossing of the capacitor voltage, is constrained in the range $\alpha_{\min} \le \alpha \le 180^\circ$. This constraint provides a continuous vernier of the TCSC module reactance. The loop current increases as α is decreased from 180° to $\alpha_{\min}$. The maximum TCSC reactance permissible with $\alpha = \alpha_{\min}$ is typically two-and-half to three times the capacitor reactance at fundamental frequency.

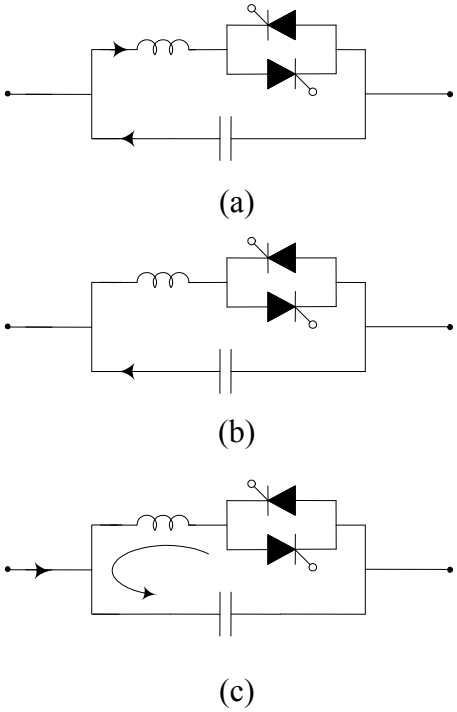

Figure 3.3: TCSC modes of operation: (a) bypassed-thyristor mode, (b) blocked-thyristor mode, (c) vernier mode.

3.4 Analysis of the TCSC

The following "approximate" analysis of TCSC operation in the vernier-control mode is performed based on the simplified TCSC circuit shown in Figure 3.4 [33]. Transmission line current is assumed to be the independent-input-variable and is modeled as an external current source, $i_s(t)$. Moreover, it is assumed that the line current is sinusoidal, as field tests have demonstrated that very few harmonics exist in the line current [12].

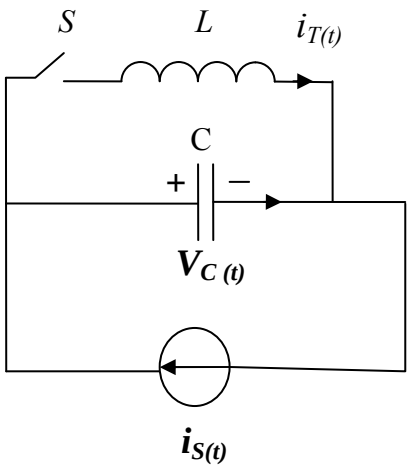

Figure 3.4: A simplified TCSC circuit.

The current through the fixed-series capacitor, *C*, is expressed as

$$C\frac{dv_c}{dt} = i_s(t) - i_T(t).u \tag{3.2}$$

The switching variable *u* is equal to 1 when the thyristor valves are conducting (switch S is closed). When the thyristor valves are blocked (switch S is open), *u* = 0. The thyristor current, $i_T(t)$ can be described as

$$L\frac{di_T}{dt} = v_c.u \tag{3.3}$$

Let the line current, $i_s(t)$ be represented by

$$i_s(t) = I_m \cos\omega t \tag{3.4}$$

Equations (3.3) and (3.4) can be solved with the knowledge of the instants of switching. In equidistant firing-pulse control, for balanced TCSC operation, the thyristors are switched on twice in each cycle of the line current at instants t_1 and t_3 given by

$$t_1 = -\frac{\beta}{\omega} \tag{3.5}$$

$$t_3 = \frac{\pi - \beta}{\omega} \tag{3.6}$$

where β is the angle of advance (before the forward voltage becomes zero). Or,

$$\beta = \pi - \alpha; \qquad 0 < \beta < \beta_{\max} \tag{3.7}$$

The firing angle α is generated using a reference signal that can be in phase with the capacitor voltage. The thyristor switch S turns off at the instant t_2 and t_4 defined as:

$$t_2 = t_1 + \frac{\sigma}{\omega} \tag{3.8}$$

$$t_4 = t_3 + \frac{\sigma}{\omega} \tag{3.9}$$

where σ is the conduction angle and,

$$\sigma = 2\beta \tag{3.10}$$

Solving the TCSC equations (3.2 to 3.4) results in the steady-state thyristor current i_T, as:

$$i_T(t) = \frac{k^2}{k^2 - 1} IMG \left[\cos \omega t - \frac{\cos \beta}{\cos k\beta} \cos \omega_r t \right]; \quad -\beta \le \omega t \le \beta \tag{3.11}$$

where

$$\omega_r = \frac{1}{\sqrt{LC}} \tag{3.12}$$

$$k = \frac{\omega_r}{\omega} = \sqrt{\frac{1}{\omega L} \frac{1}{\omega C}} = \sqrt{\frac{X_C}{X_L}} \tag{3.13}$$

and X_C is the nominal reactance of the fixed capacitor only. The steady-state capacitor voltage at the instant $\omega t = -\beta$ is expressed by:

$$v_{C1} = \frac{IMG\ X_C}{k^2 - 1} (\sin \beta - k \cos \beta \tan k\beta) \tag{3.14}$$

At $\omega t = \beta$, $i_T = 0$, and the capacitor voltage is given by:

$$v_C(\omega t = \beta) = v_{C2} = -v_{C1} \tag{3.15}$$

The capacitor voltage is finally obtained as:

$$v_C(t) = \frac{IMG\ X_C}{k^2 - 1} \left[-\sin \omega t + k \frac{\cos \beta}{\cos k\beta} \sin \omega_r t \right]; \quad -\beta \le \omega t \le \beta \tag{3.16}$$

$$v_C(t) = v_{C2} + IMG\ X_C (\sin \omega t - \sin \beta); \qquad \beta < \omega t < \pi - \beta \tag{3.17}$$

Because the nonsinusoidal capacitor voltage, v_C, has odd symmetry about the axis $\omega t = 0$, the fundamental component, V_{CF}, is obtained as:

$$V_{CF} = \frac{4}{\pi}\int_0^{\pi/2} v_c(t)\sin\omega t\, d(\omega t) \tag{3.18}$$

The equivalent TCSC reactance is computed as the ratio of V_{CF} to I_m:

$$\begin{aligned} X_{TCSC} = \frac{V_{CF}}{I_m} &= X_C - \frac{X_C^2}{(X_C - X_L)}\frac{2\beta + \sin 2\beta}{\pi} \\ &+ \frac{4X_C^2}{(X_C - X_L)}\frac{\cos^2\beta}{(k^2-1)}\frac{(k\tan k\beta - \tan\beta)}{\pi} \end{aligned} \tag{3.19}$$

The net reactance of the TCSC in per unit of X_C, denoted by X_{net} (= X_{TCSC}/X_C, sometimes called the boost factor) can be expressed as:

$$\begin{aligned} X_{net} &= 1 - \frac{X_C}{(X_C - X_L)}\frac{\sigma + \sin\sigma}{\pi} + \frac{4X_C}{(X_C - X_L)}\frac{\cos^2 0.5\sigma}{(k^2-1)} \\ &\cdot \frac{(k\tan 0.5\sigma\, k - \tan 0.5\sigma)}{\pi} \end{aligned} \tag{3.20}$$

Because the TCSC is used mainly as a capacitive device, the convention is to define positive reactance as capacitive and negative reactance as inductive. As an example, $X_{net} = +2$ implies that the thyristors are fired so that the resulting circulating current in the fixed capacitor – thyristor controlled reactor loop causes a 60-Hz voltage of $2X_C I_{line}$ p.u. to appear across the fixed capacitor, which lags the line current by 90^o.

The traditional boost control method (constant firing angle delay (CFAD)) controls the firing angle $\beta = \pi - \alpha$ of the thyristor. A rather non-linear relationship exists between the boost factor *kB* and the steady state conduction angle $\sigma = 2\beta$, making *kB* very sensitive to the instant of triggering when the TCSC operates at a high boost factor. Further, at transients, a complicated dynamic characteristic governs the relationship between the firing angle and the conduction angle. Instead of controlling the thyristor firing angle, another control scheme, named 'Synchronous Voltage Reversal' (SVR), is being used. It aims to control the instant when the capacitor voltage crosses zero [34], [35]. This eliminates the non-linearity in the boost control and results in that the TCSC apparent impedance at subsynchronous frequencies appears as inductive. Furthermore, at low boost factors, SVR controlled TCSC can provide much better SSR damping than conventional CFAD control [36]. In the studies conducted in this thesis, the SVR control is used.

3.5 The Hybrid Single-Phase-TCSC Compensation Scheme

Figure 3.5 shows a phase imbalanced hybrid series capacitive compensation scheme using a TCSC [37], [38]. In such a scheme, the series capacitive compensation in one phase is created using a single-phase TCSC in series with a fixed capacitor (C_c), and the other two phases are compensated by fixed series capacitors (C). The TCSC control is initially set such that its equivalent compensation at the power frequency combined with the fixed capacitor C_c yield a resultant compensation equal to the other two phases. Thus, the phase balance is maintained at the power frequency while at any other frequency, a phase imbalance is created. Mathematically, this can be explained as follows:

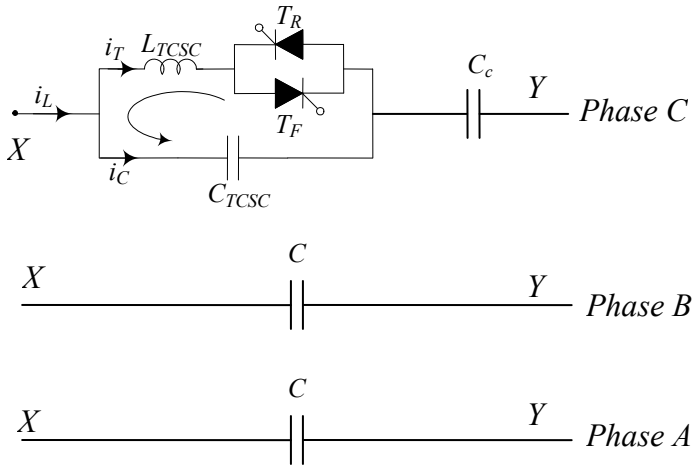

Figure 3.5: The hybrid single-phase TCSC compensation scheme.

1) At the power frequency, the series reactance between buses X and Y, in Figure 3.5, in phases a, b, and c are given by:

$$X_a = X_b = \frac{1}{j\omega_o C} \tag{3.21}$$

$$X_c = \frac{1}{j\omega_o C_c} - jX_{TCSCo} \tag{3.22}$$

where $-jX_{TCSCo}$ is the effective capacitive reactance of the TCSC at the power frequency such that $X_a = X_b = X_c$.

2) During any other frequency, f_e, including subsynchronous frequencies,

$$X_c = \frac{1}{j\omega_e C_c} - jX_{TCSCo} - j\Delta X_{TCSC} \tag{3.23}$$

The first terms in (3.22) and (3.23) are different because of the difference in frequency. The third term in (3.23) represents the change in the effective capacitive reactance of the TCSC due to the action of the TCSC supplemental controller.

3.6 Modeling of the Single-Phase TCSC in the EMTP-RV

The single-phase TCSC is modeled in the EMTP-RV as a single module using an ideal thyristor pair and an RC snubber circuit as shown in Figure 3.6. A Phase Locked Loop (PLL) is used to extract phase information of the fundamental frequency line current, which will be used to synchronize TCSC operation. The thyristor gating control is based on the Synchronous Voltage Reversal (SVR) technique [34] - [36]. The TCSC impedance is measured in terms of a boost factor *kB*, which is the ratio of the apparent reactance of the TCSC seen from the line to the physical reactance of the TCSC capacitor bank. A positive value of *kB* is considered for capacitive operation. A low-pass filter based estimation algorithm is used to estimate the voltage and the current phasors. A boost measurement block performs complex impedance calculations for the boost factor of the TCSC as *kB* = Imag $\{\hat{V}_C / \hat{I}_C\} / X_{CTCSC}$, where, $\hat{V}_C$ and $\hat{I}_C$ are the estimated phase voltage and current and X_{CTCSC} is the capacitive reactance of the TCSC capacitor branch at the fundamental frequency. A proportional-integral (PI) control based boost level controller is implemented to control the TCSC boost level to the desired value by adjusting the instant of the expected capacitor voltage zero crossing. The integral part of the controller helps in removing the steady state errors. The controller parameters were determined by performing repeated time domain simulations for the different operating conditions. This algorithm uses the difference between the actual boost level and the reference boost level (*err*) shown in Figure 3.6 as an objective function. The algorithm starts with arbitrary initial values for the control parameters and calculates the values of the objective function each time. The control parameters are incremented for the next iteration and the procedure is repeated until the objective function approaches a minimum value (below a threshold value). The procedure described above is widely used by industry for tuning of controller parameters. The multiple simulations run

based tuning procedure similar to the above was reported in [39], [40]. The optimum values of the parameters obtained for the different compensation degrees are given in Appendix B.

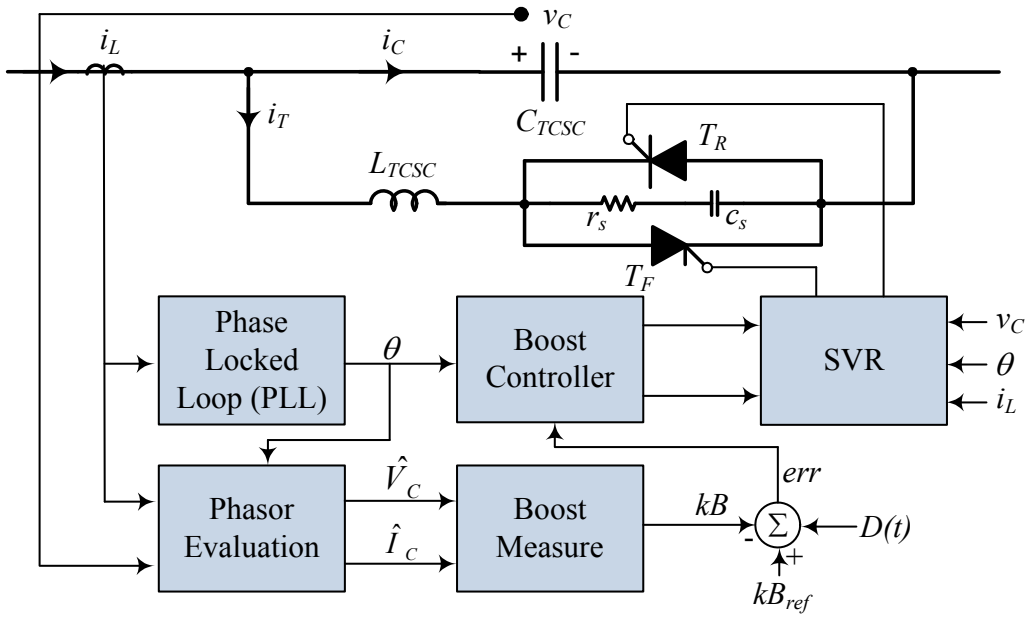

Figure 3.6: Block diagram of a TCSC controller.

In Figure 3.6, kB_{ref} is the TCSC boost level set point and $D(t)$ is the supplementary control signal for damping low frequency oscillations. The Synchronous Voltage Reversal block solves for angle γ from the non-linear relation, $u_{CZ} = X_o i_{LM}\left[\lambda\gamma - \tan(\lambda\gamma)\right]$, where u_{CZ} is the estimated capacitor voltage at the desired instant when the capacitor voltage zero crossing occurs, i_{LM} is the measured value of the line current i_L, X_0 is the TCSC capacitor reactance at the TCSC resonance frequency, λ is the ratio between the TCSC resonance frequency and the system fundamental frequency and γ is the angle difference between the firing time and the voltage zero-crossing. The value of γ is used to calculate the exact firing instants of the individual thyristors. The non-linear relationship between the boost factor and the thyristor firing angle α is shown in Figure 3.7.

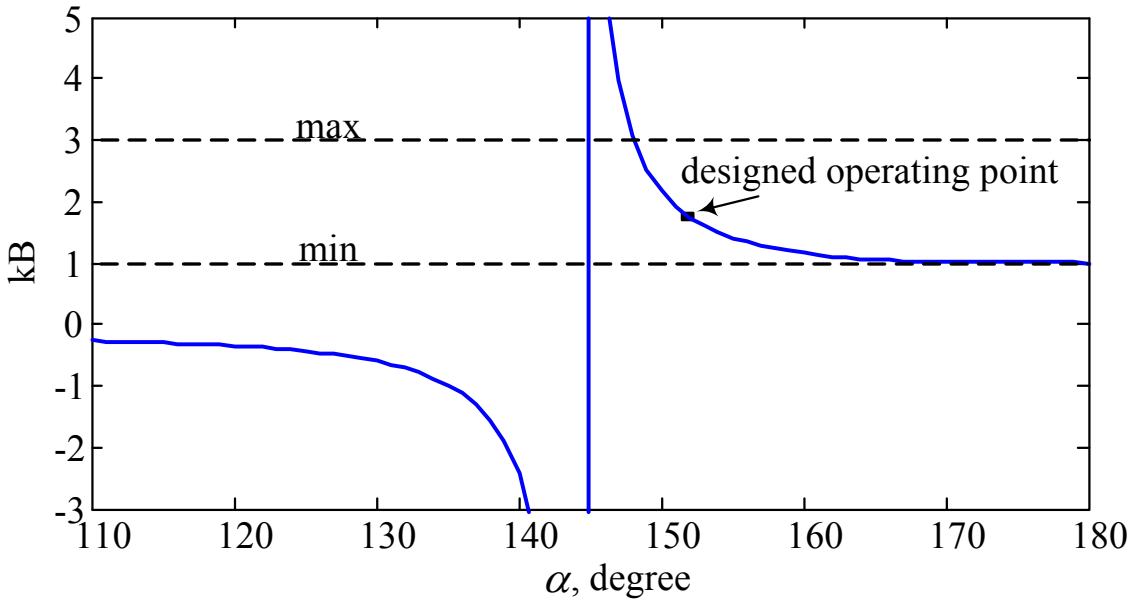

Figure 3.7: TCSC boost factor as a function of the thyristor firing angle α.

The most striking feature of the TCSC is that it behaves like an inductor at subsynchronous frequencies. This prevents the occurrence of a series resonance within a certain critical frequency band. On the other hand, the TCSC behaves like a capacitor at the power frequency. The transition of the virtual reactance of the TCSC from inductive to capacitive outside the subsynchronous frequency band is achieved by means of a reactance controller (like the SVR technique), providing a controllable capacitive reactance around the power frequency as shown in Figure 3.8 [41]. The details of the SVR algorithm are given in [34], [35].

3.7 Summary

This chapter presents the description, basic principles and the derivation of the mathematical model of the TCSC. Modeling the hybrid single-phase TCSC in the ElectroMagnetic Transient Program (EMTP-RV) is also presented. This model is incorporated in the system under study (Figure 2.1) replacing the fixed compensations in lines L_1 and L_2. The effectiveness of the hybrid single-phase compensation scheme in damping power system oscillations is investigated in the next chapter.

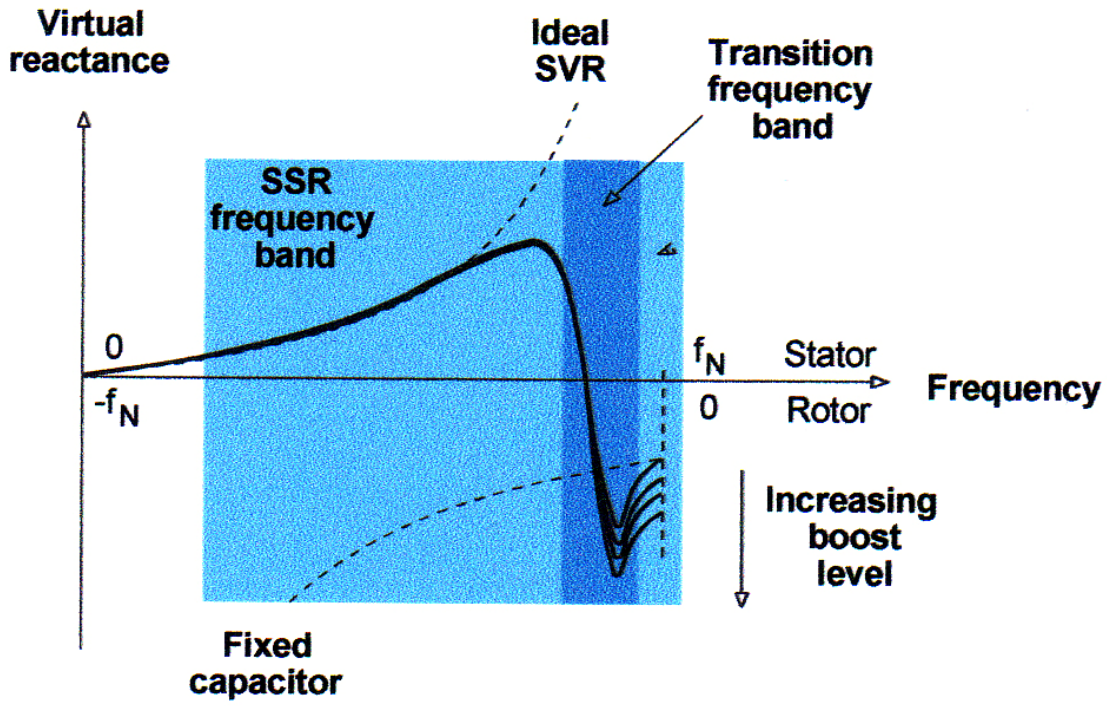

Figure 3.8: Effect of the SVR technique on the virtual reactance of the TCSC.

Chapter 4

DAMPING POWER SYSTEM OSCILLATIONS USING THE HYBRID SINGLE-PHASE-TCSC COMPENSATION SCHEME

4.1 General

The control offered by the TCSC is an 'impedance' type control, i.e. the inserted voltage is proportional to the line current. This type of control normally is best suited to applications in power flow corridors, where a well-defined phase angle difference exists between the ends of the transmission line to be compensated and controlled. A TCSC can also be used, however, to provide additional damping to the electromechanical (0.5 - 2 Hz) power oscillations as it provides fast speed of response and executes any switching patterns without such restrictions that might apply for mechanical breakers.

In this chapter, the effectiveness of the hybrid single-phase-TCSC compensation scheme in damping power system oscillations is investigated. For this purpose, the scheme is assumed to be installed in one or more circuits of lines L_1 and L_2 replacing the fixed series capacitor compensations as well as in the uncompensated line L_3. The performance of the scheme in each case study is compared to the corresponding case with only fixed capacitor compensation.

4.2 TCSC Power Oscillations Damping Controller

The TCSC can be made to vary the series-compensation level dynamically in response to the controller-input signal so that the resulting changes in the power flow enhance the system damping. The traditional type of controller for Power Oscillations Damping (POD) purposes uses cascade-connected washout filters and linear lead-lag compensators to generate the desired reactance modulation signal. The purpose of the wash-out filters is to eliminate the average and extract the oscillating part of the input signal. The lead-lag compensators provide the desired phase shift at the oscillations frequency. Such a controller is illustrated in Figure 4.1 [24], [42], [43]. In some situations, a simple controller consists of only the washout filters can have a better

performance than that of the lead-lag controller. Such a controller, shown in Figure 4.2 can be regarded as a proportional type controller.

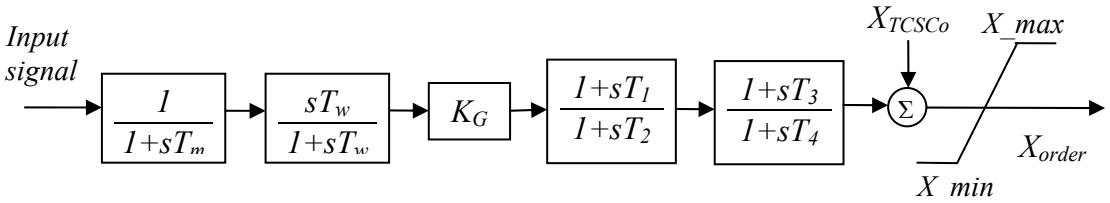

Figure 4.1: Structure of a lead-lag POD controller.

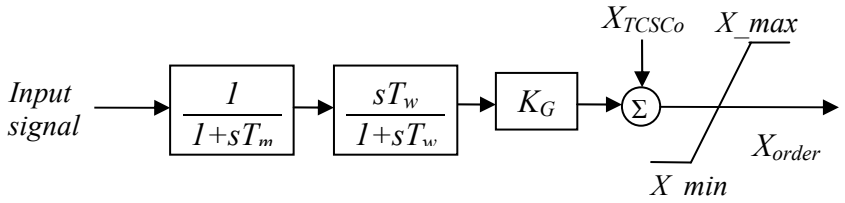

Figure 4.2: Structure of a simple POD controller.

The selection of the appropriate input (stabilizing) signal is an important issue in the design of an effective and robust controller. The selected input signal must yield correct control action when a severe fault occurs in the system. As an example, it was reported in [44] that if the real power is used as the input signal of a pure derivative controller, the output control signal may cause negative damping effects in the presence of disturbances involving large changes in the generator power angles.

The input signals could be local (e.g. real power flows) or remote (e.g. load angles or speed deviations of remote generators). If a wide-area network of Synchronized Phasor Measurement (SPM) units is available, then the remote signals can be downloaded at the controller in real time without delay [45] - [49]. In the studies conducted in this thesis, the generator load angles and speeds, measured with respect to the load angle and speed of a reference generator, as well as the real power flows in lines L_1 and L_2 are used as input signals.

It is worth noting here that due to the inherent imbalance nature of the hybrid single-phase-TCSC compensation scheme during transients, the design of the TCSC supplemental controller using classical linear control techniques would be very difficult, if not, virtually impossible to achieve. However, nonlinear control theories for TCSC applications have been found to have a significant potential in recent years [50]. Some of the examples are; variable-

structure controllers (VSCs), model reference adaptive controllers and self-tuning controllers. VSCs are capable of maintaining a desired response characteristic almost independently of the system structure. The design of any of such controllers is, however, beyond the level of being a part of a Master research project. In the studies conducted in this thesis, the supplemental controller parameters are determined by performing multiple time domain simulations with the aim of improving the transient responses of the system. In the case of multiple controllers, simultaneous tuning of the parameters of the controllers is performed to ensure that satisfactory dynamic and steady-state performances are met whilst minimizing or preventing undesirable interactions among controllers.

4.3 Case Study I: The Hybrid Single-Phase-TCSC Compensation Scheme is Installed in one Circuit of Line L_1

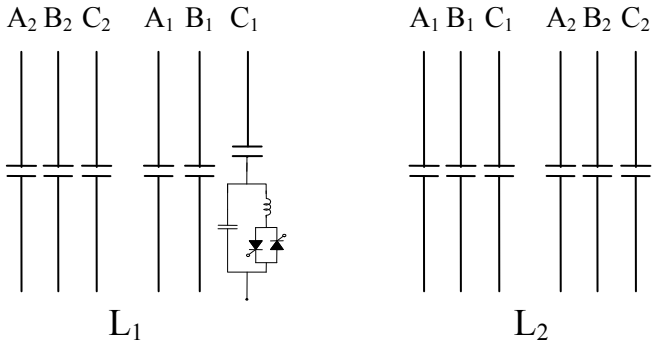

Figure 4.3: Case study I: the hybrid single-phase-TCSC compensation scheme is installed in one circuit of line L_1.

The TCSC provides 50% of the total capacitive compensation ($X_{Cc} = X_{TCSC} = 0.5\ X_C$, Figure 3.5) and the stabilizing signal is δ_{21}. The generator load angles and speeds, measured with respect to generator 1 load angle and speed, and the transmission line real power flow responses during and after clearing a three-cycle, three-phase fault at bus 4 are illustrated in Figures 4.4 to 4.6 for the case when the TCSC supplemental controller is of a proportional type with a transfer function given by Equation 4.1. Figures 4.7 to 4.9 illustrate the responses of the same variables in the case when the TCSC supplemental controller is of a lead-lag type with a transfer function given by Equation 4.2.

$$G_P(s) = 0.45\frac{10}{(s+10)}\frac{3s}{(3s+1)} \qquad (4.1)$$

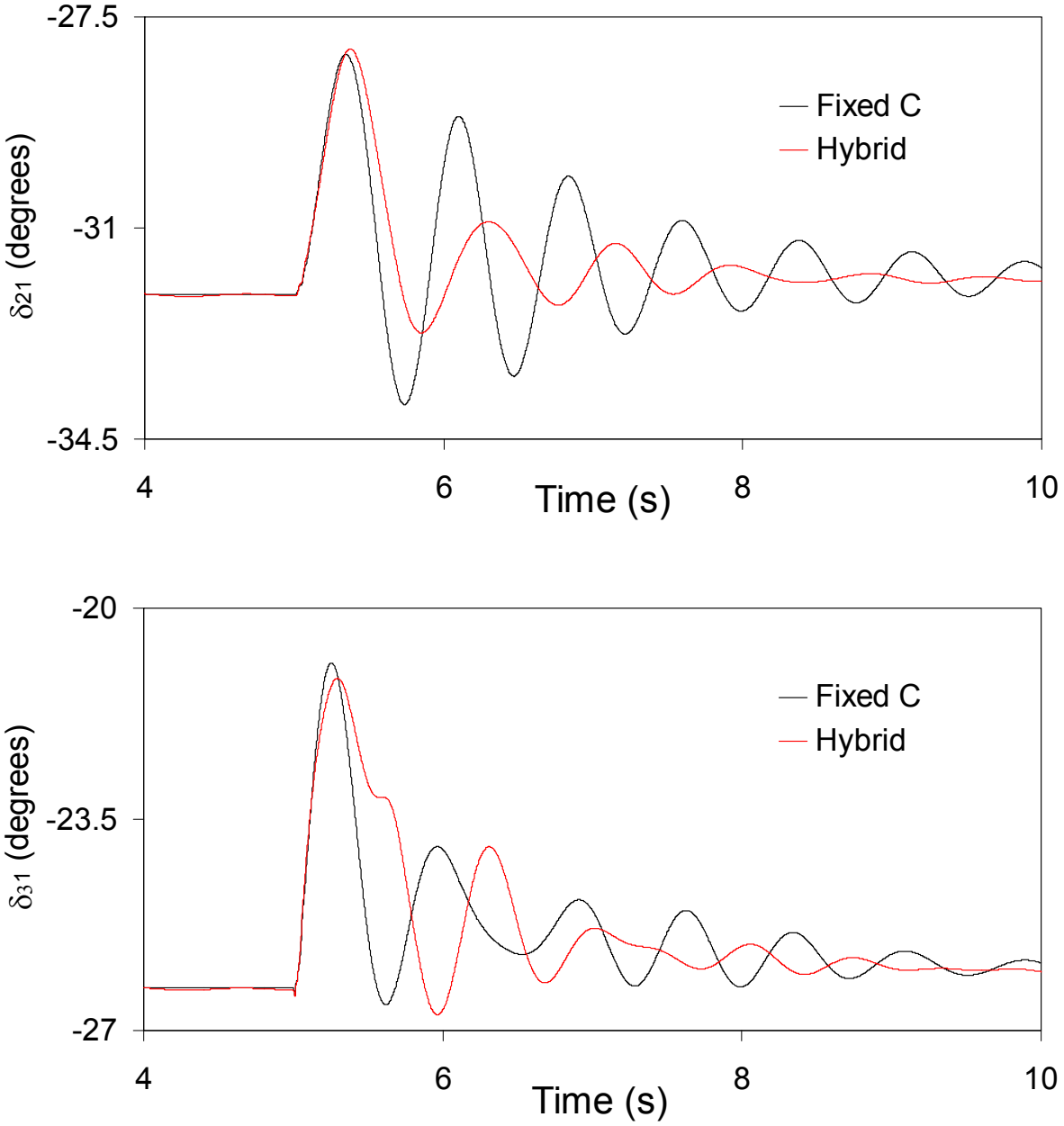

Figure 4.4: Generator load angles, measured with respect to generator 1 load angle, during and after clearing a three-cycle, three-phase fault at bus 4 (case study I, TCSC supplemental controller: proportional type).

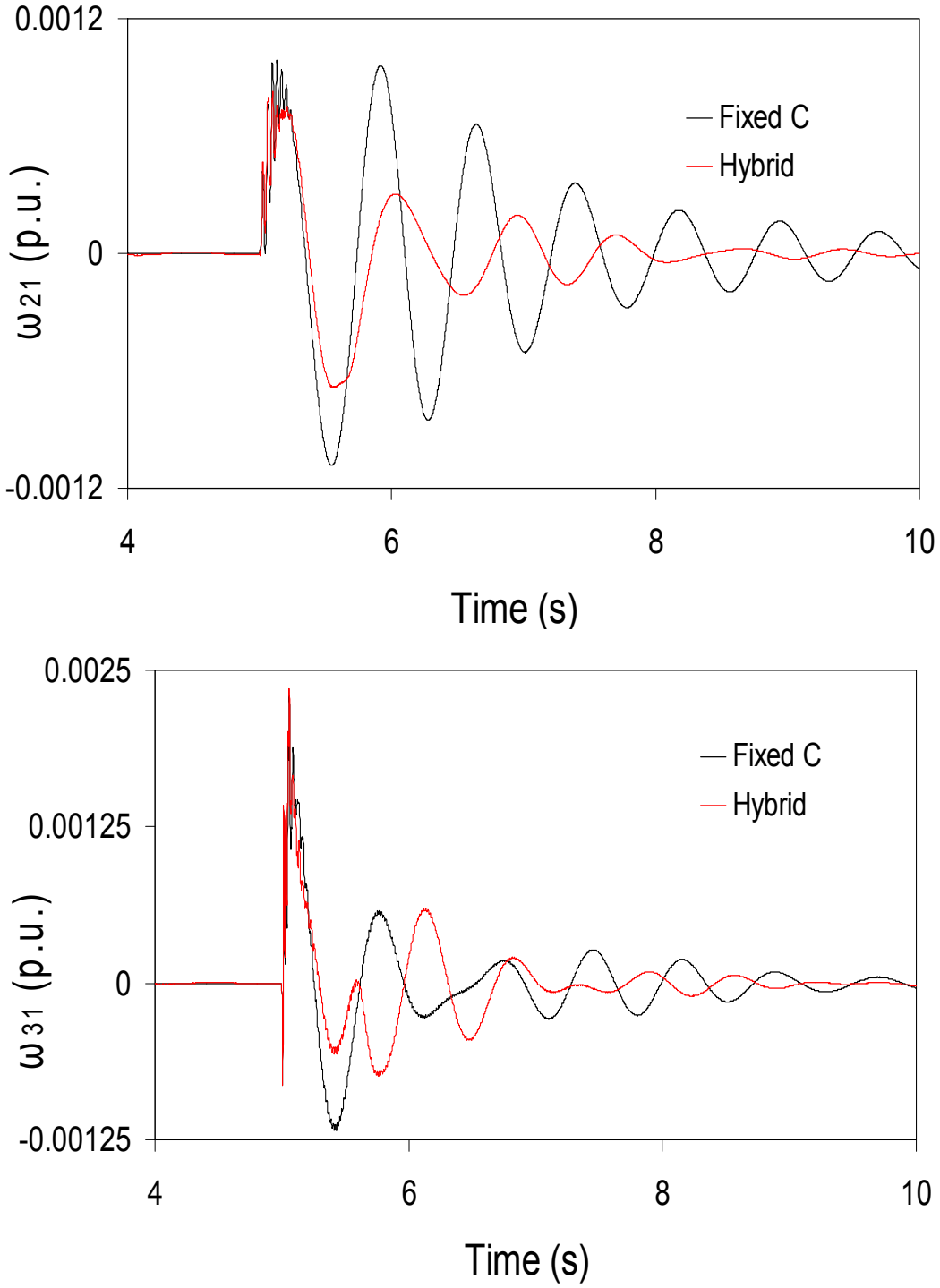

Figure 4.5: Generator speeds, measured with respect to generator 1 speed, during and after clearing a three-cycle, three-phase fault at bus 4 (case study I, TCSC supplemental controller: proportional type).

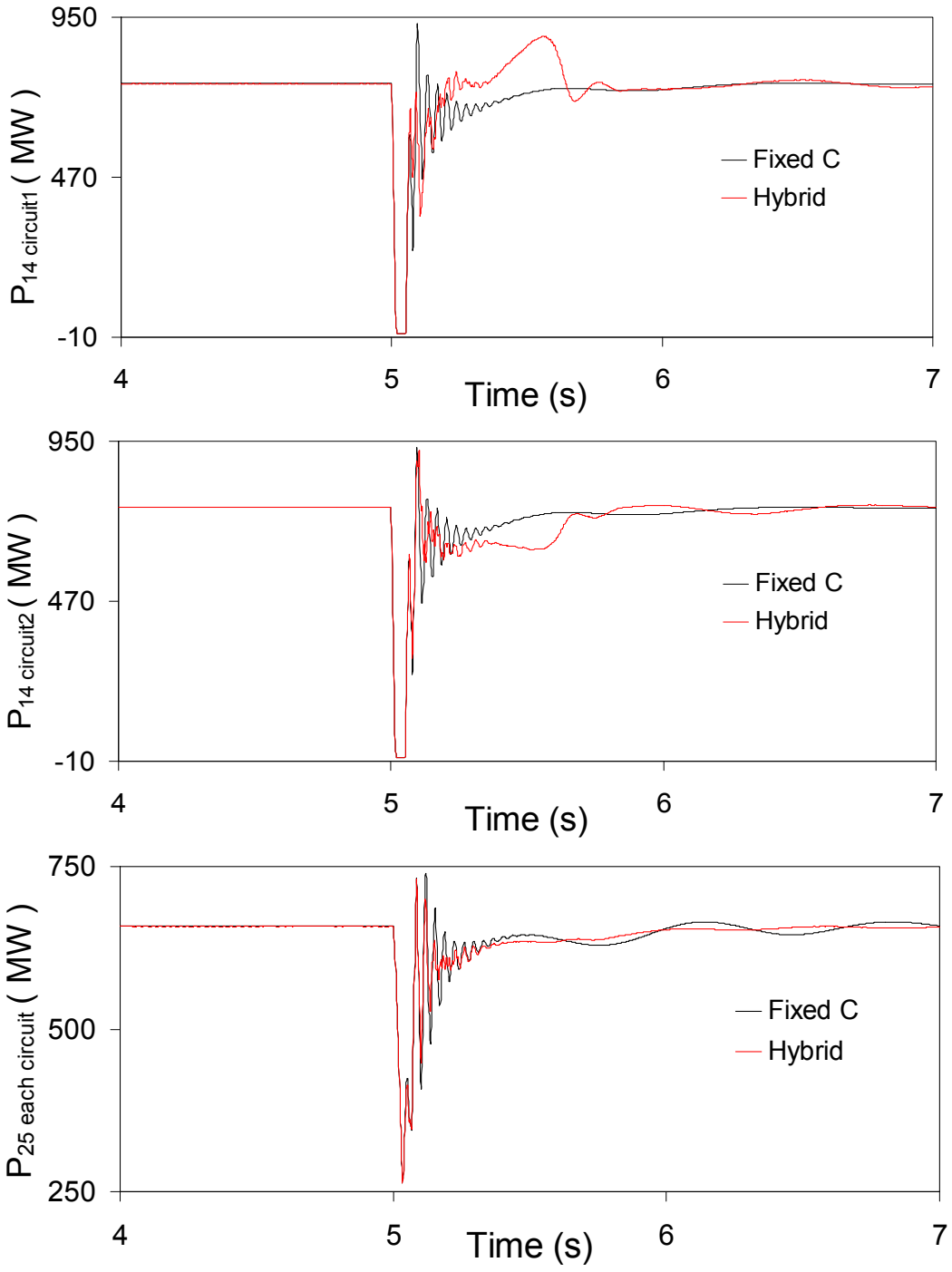

Figure 4.6: Transmission line real power flows during and after clearing a three-cycle, three-phase fault at bus 4 (case study I, TCSC supplemental controller: proportional type).

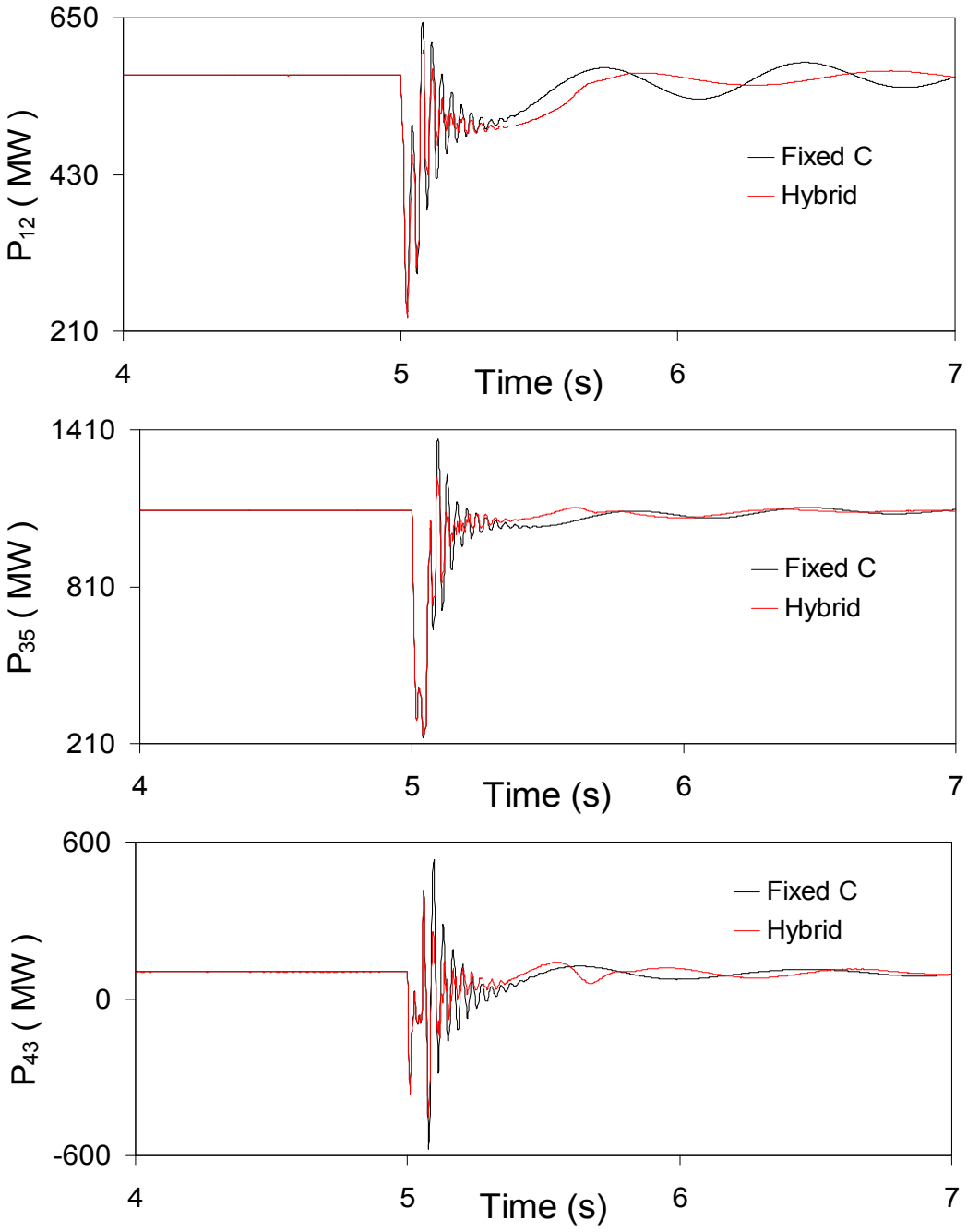

Figure 4.6: continued.

$$G_{L-L}(s) = 0.005 \frac{10}{(s+10)} \frac{3s(s+70)}{(3s+1)} \tag{4.2}$$

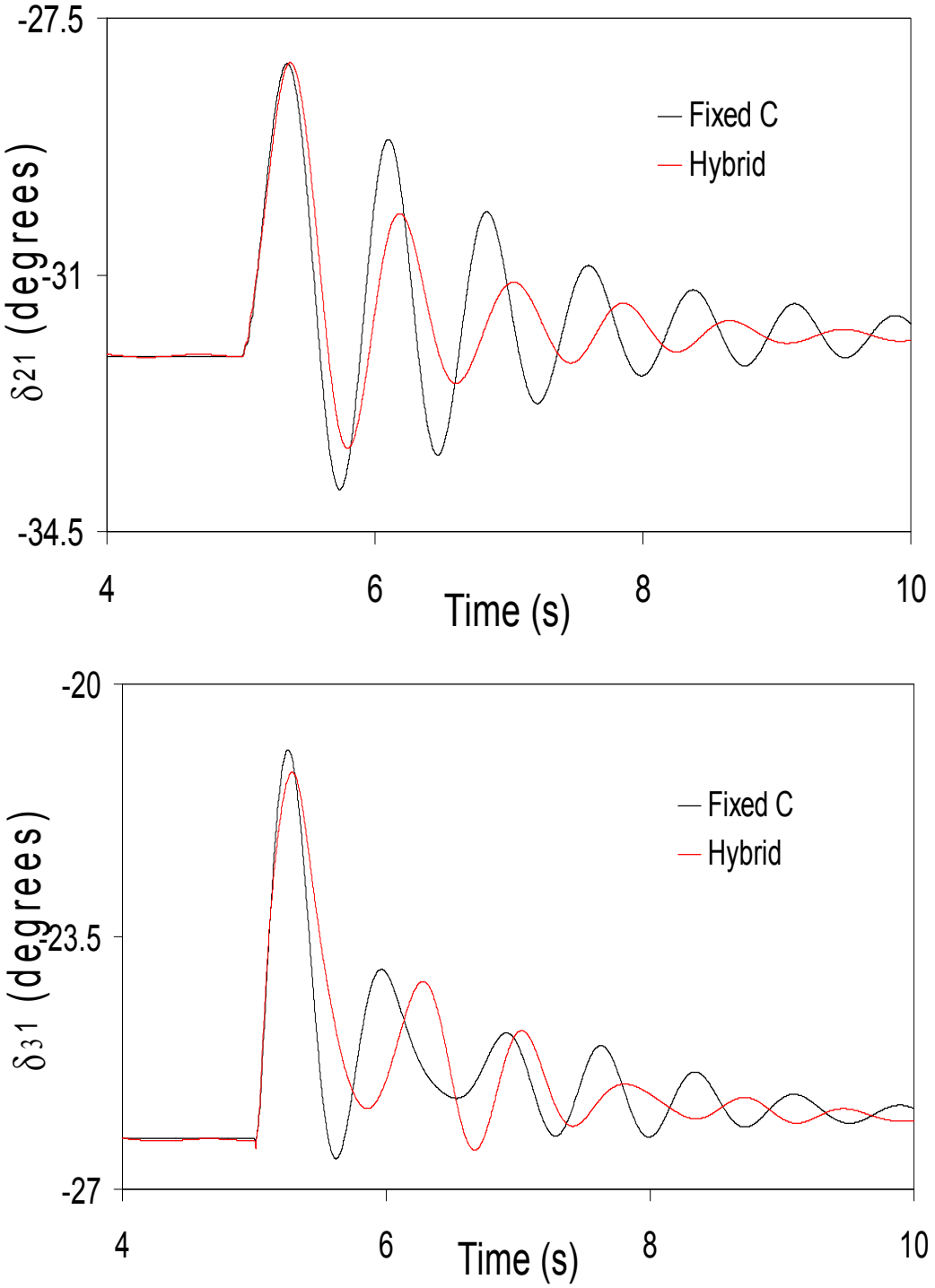

Figure 4.7: Generator load angles, measured with respect to generator 1 load angle, during and after clearing a three-cycle, three-phase fault at bus 4 (case study I, TCSC supplemental controller: lead-lag type).

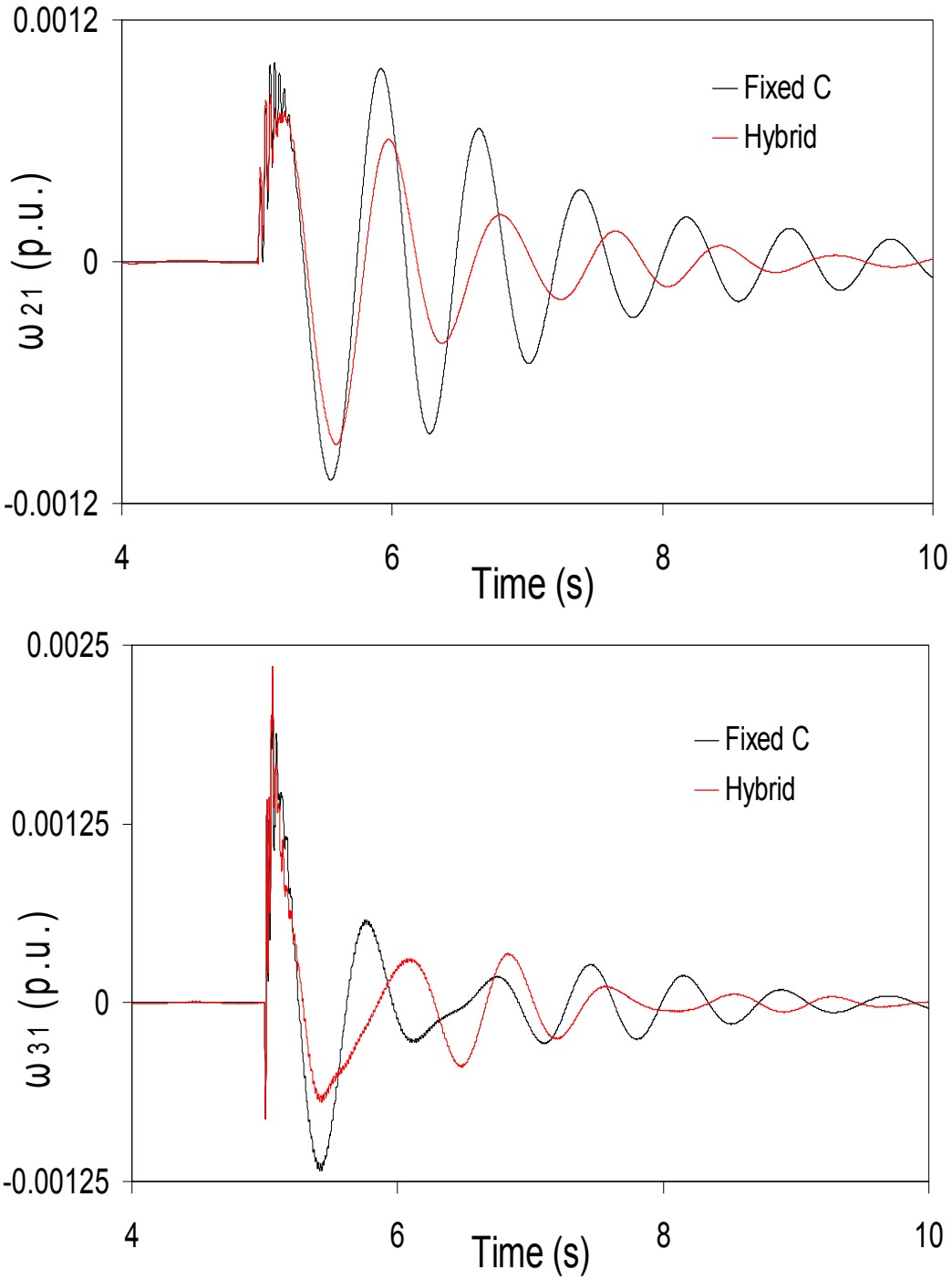

Figure 4.8: Generator speeds, measured with respect to generator 1 speed, during and after clearing a three-cycle, three-phase fault at bus 4 (case study I, TCSC supplemental controller: lead-lag type).

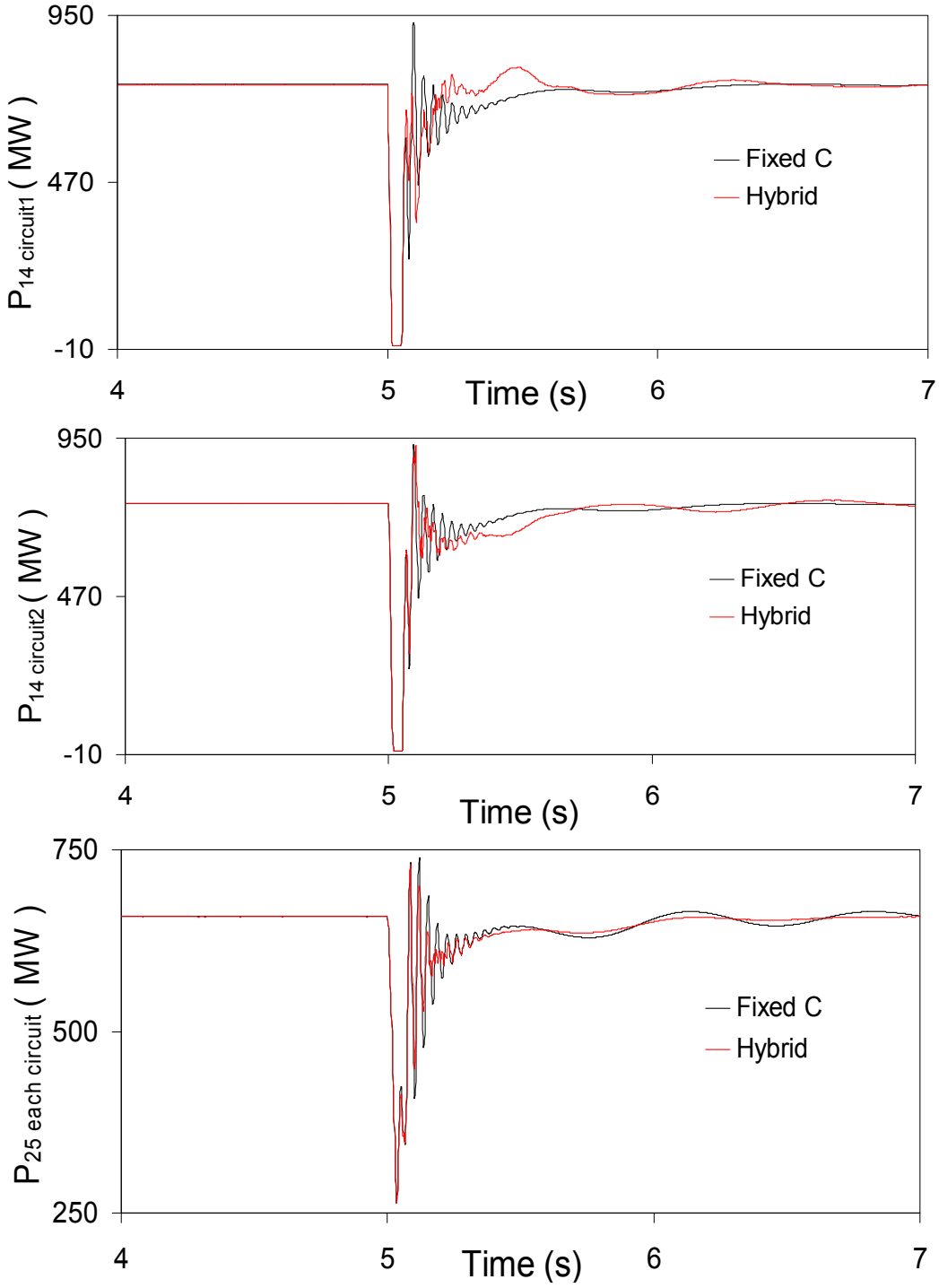

Figure 4.9: Transmission line real power flows during and after clearing a three-cycle, three-phase fault at bus 4 (case study I, TCSC supplemental controller: lead-lag type).

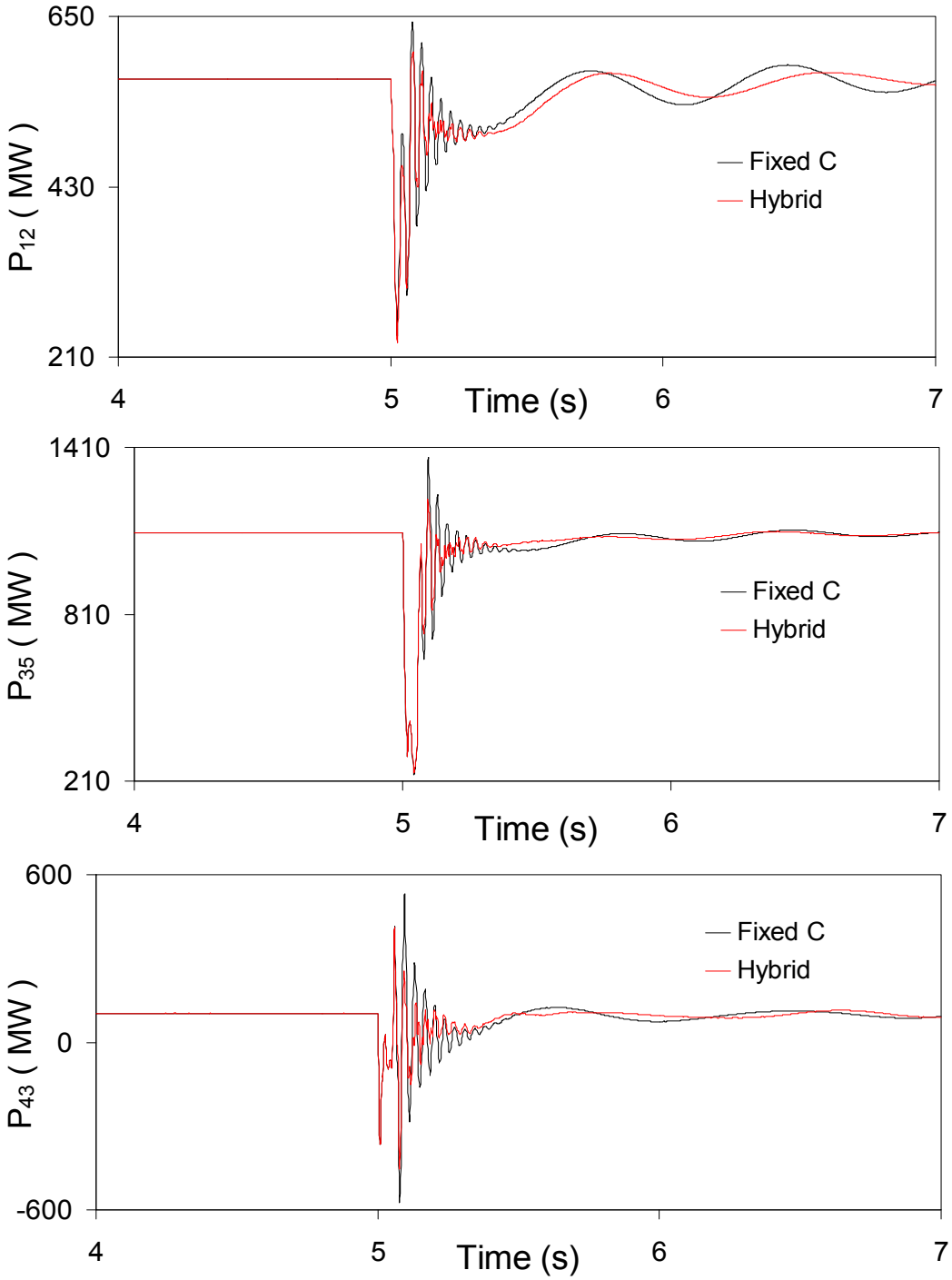

Figure 4.9: continued.

It can be seen from Figure 4.4 that in the case of fixed capacitor compensation, the system is first swing stable for this fault, but the post-contingency oscillations are not well damped. It can also be seen from Figures 4.4 and 4.7 that the effect of the TCSC supplemental controllers on the first swing is insignificant. The same figures show, however, that the TCSC supplemental controllers reduces the subsequent swings and provide a better damping than in the case of fixed capacitor compensation. Regarding the real line power flows, Figures 4.6 and 4.9 show that in the case of the hybrid single-phase TCSC scheme, high spikes occur during the fault period.

The comparison between the performance of the proportional and the lead-lag controllers of Equations 4.1 and 4.2 is shown in Figure 4.10. It can be seen from this figure that the proportional controller results in a relatively better system transient response in terms of the settling time.

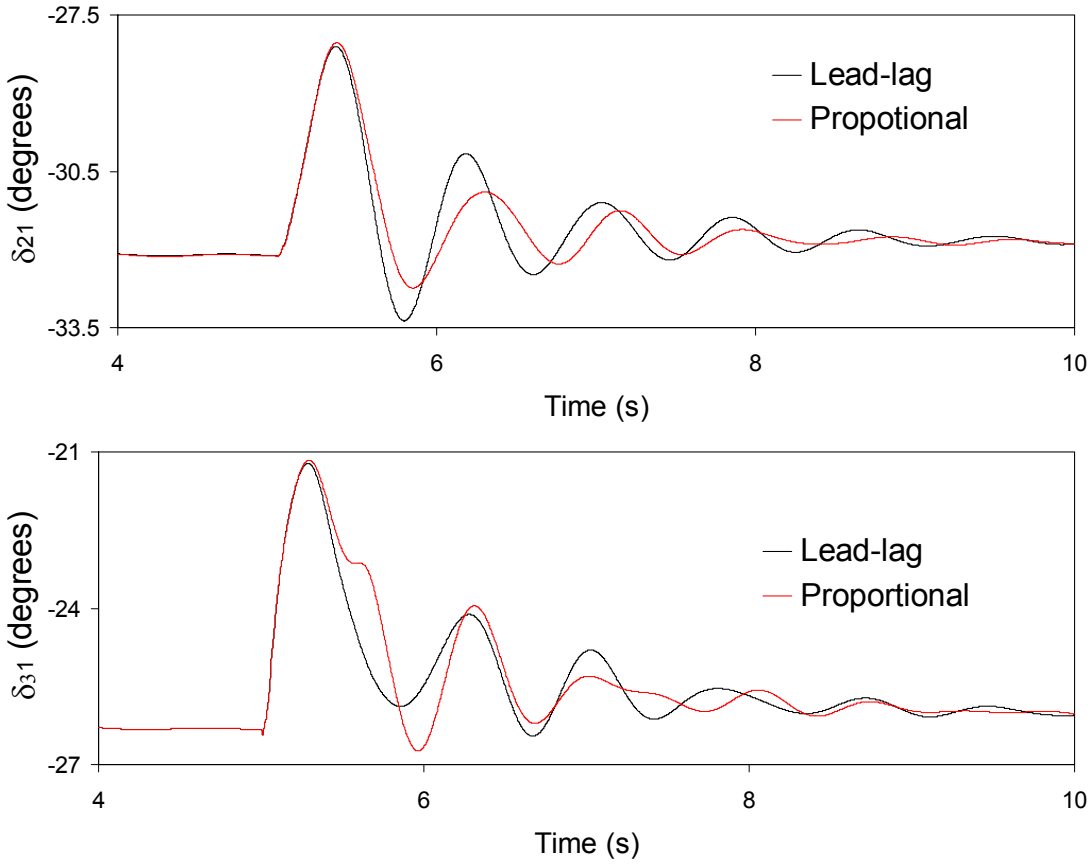

Figure 4.10: Generator load angles, measured with respect to generator 1 load angle, during and after clearing a three-cycle, three-phase fault at bus 4 (case study I).

4.4 Case Study II: The Hybrid Single-Phase-TCSC Compensation Scheme is Installed in one Circuit of Line L_2

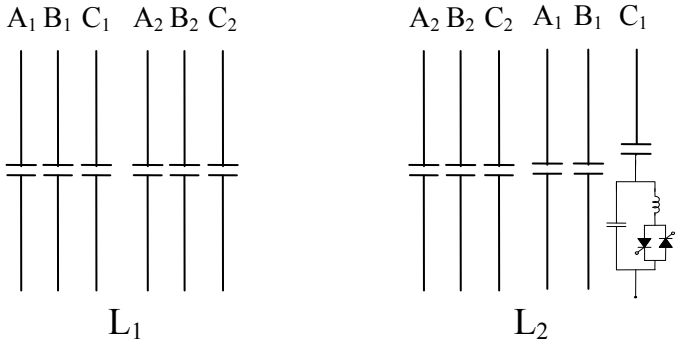

Figure 4.11: Case study II: the hybrid single-phase-TCSC compensation is installed in one circuit of line L_2.

The TCSC provides 50% of the total capacitive compensation and the stabilizing signal is δ_{21}. The generator load angles and speeds, measured with respect to generator 1 load angle and speed, and the transmission line real power flow responses during and after clearing a three-cycle, three-phase fault at bus 5 are illustrated in Figures 4.12 to 4.14 for the case when the TCSC supplemental controller is of a proportional type with a transfer function given by Equation 4.3. The comparison between Figures 4.12 to 4.14 and Figures 4.7 to 4.9 shows that the system response is very similar to that of case study I.

$$G_{P1}(s) = -0.4\frac{10}{(s+10)}\frac{s}{(s+1)} \tag{4.3}$$

Figures 4.15 to 4.17 illustrate the generator load angles and speeds, measured with respect to generator 1 load angle and speed, and the transmission line real power flow responses during and after clearing a three-cycle, three-phase fault at bus 2. This is a severe disturbance as the fault is at the terminals of a generating station. Time domain simulation results (not documented in this thesis) have shown that with a proportional controller and 50% of the total capacitive compensation provided by the TCSC, satisfactory system damping is not achievable. When the TCSC is set to provide the total degree of compensation (i.e. $X_{Cc} = 0$), Figures 4.15 to 4.17 show that a slight improvement in the system damping is obtained with the TCSC supplemental controller is of a lead-lag type with a transfer function given by Equation 4.4 and the stabilizing signal is δ_{21}.

$$G_{P2}(s) = -0.02\frac{10}{(s+10)}\frac{3s(s+10)}{(3s+1)} \tag{4.4}$$

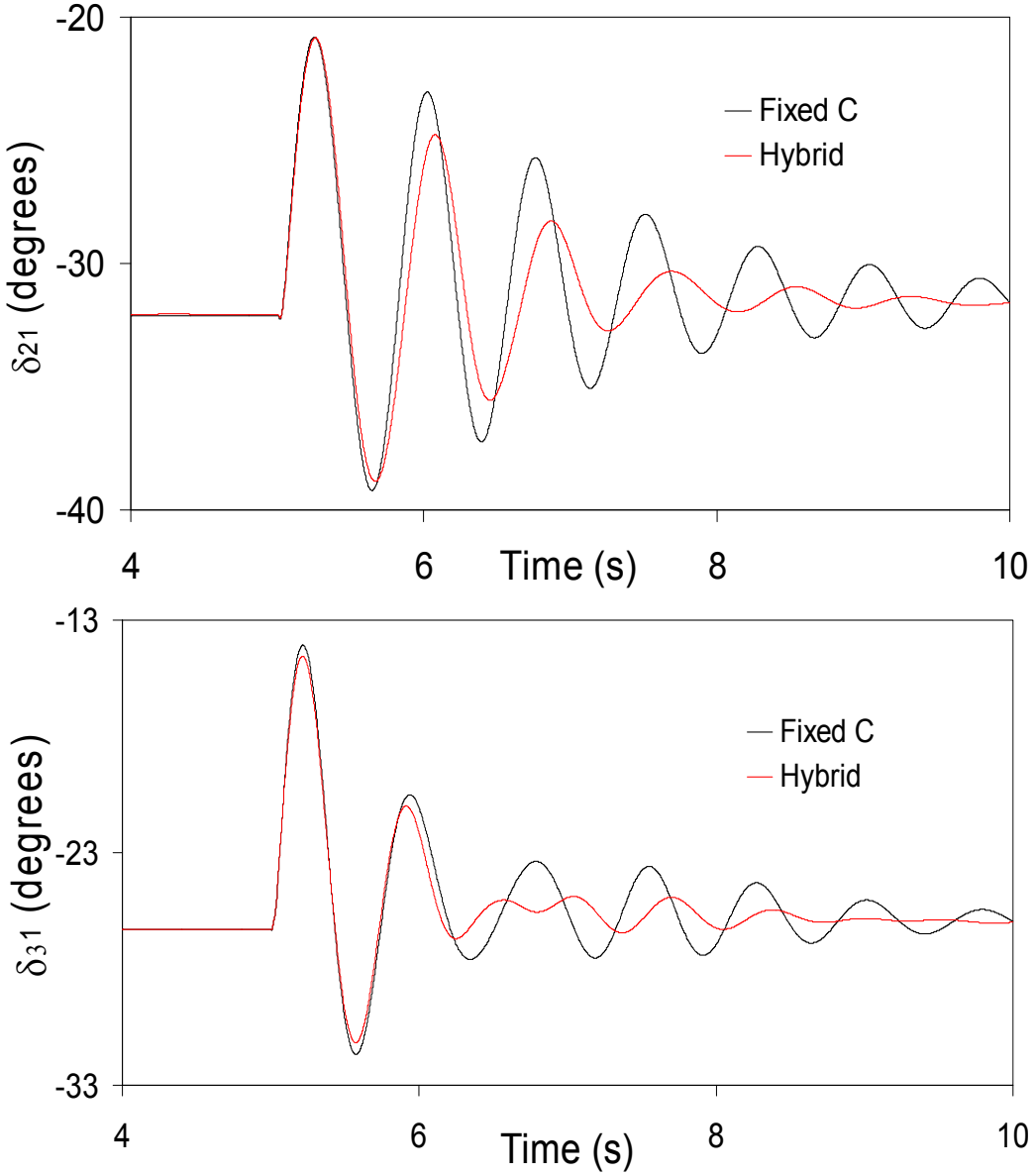

Figure 4.12: Generator load angles, measured with respect to generator 1 load angle, during and after clearing a three-cycle, three-phase fault at bus 5 (case study II).

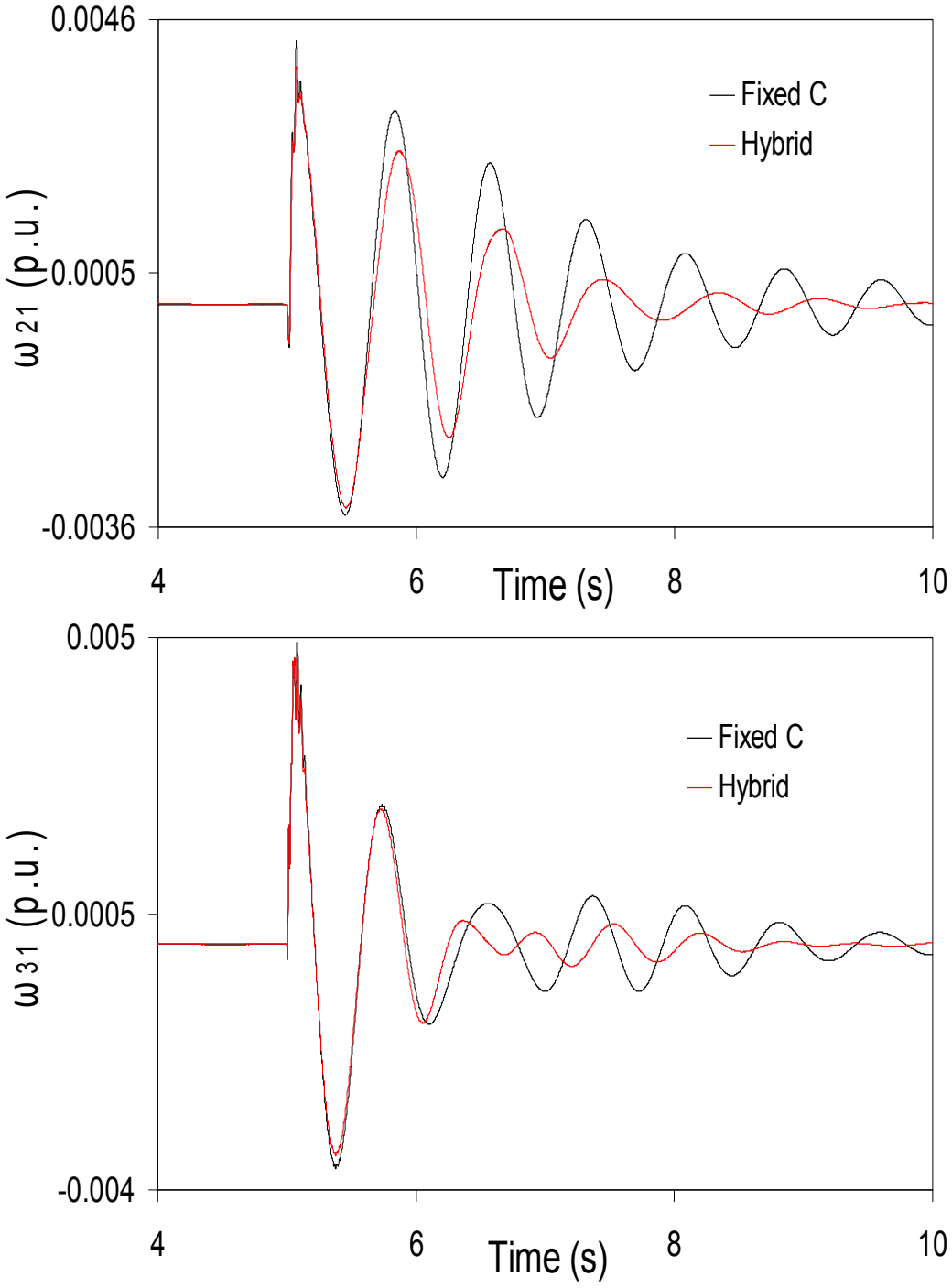

Figure 4.13: Generator speeds, measured with respect to generator 1 speed, during and after clearing a three-cycle, three-phase fault at bus 5 (case study II).

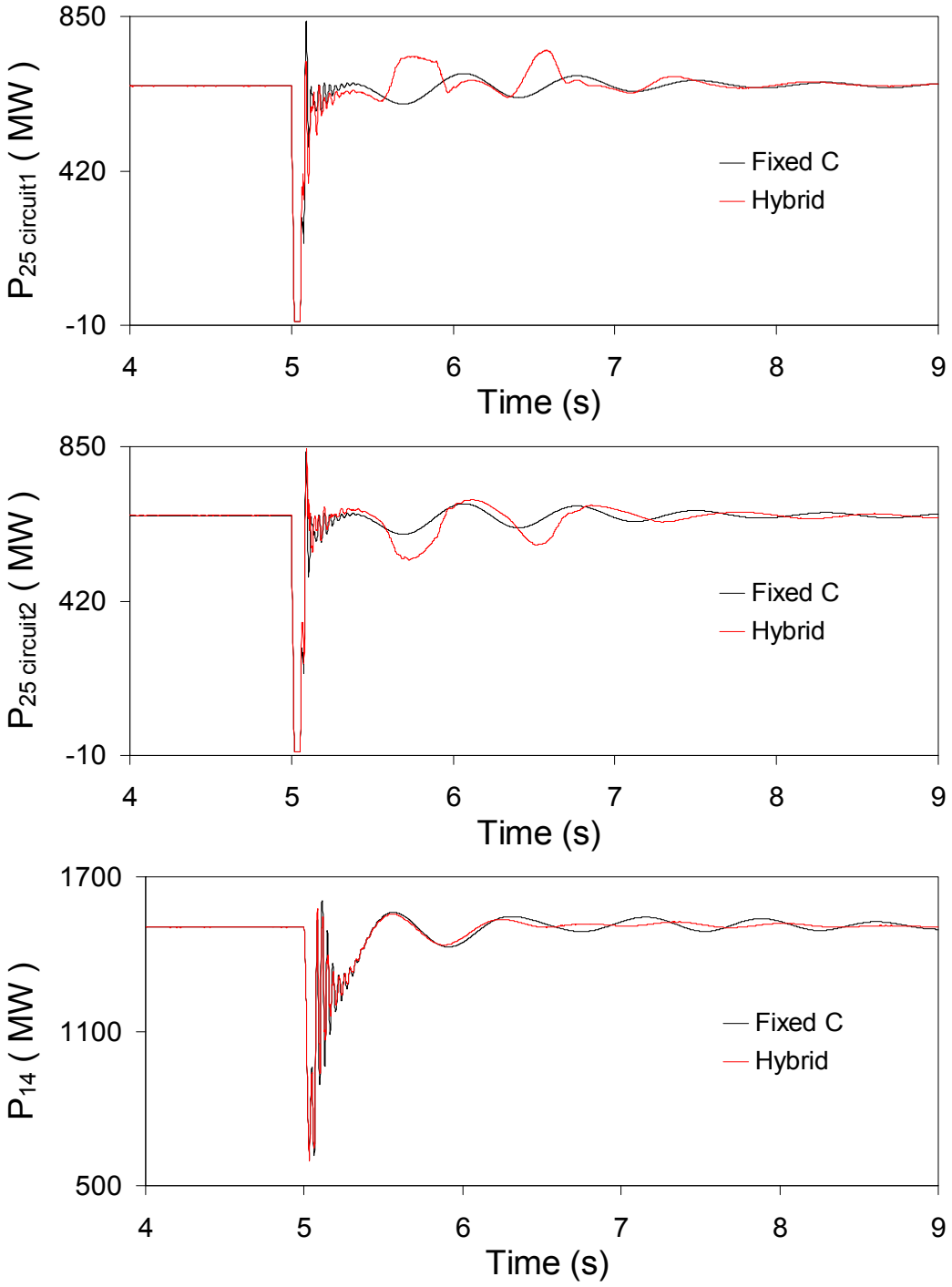

Figure 4.14: Transmission line real power flows during and after clearing a three-cycle, three-phase fault at bus 5 (case study II).

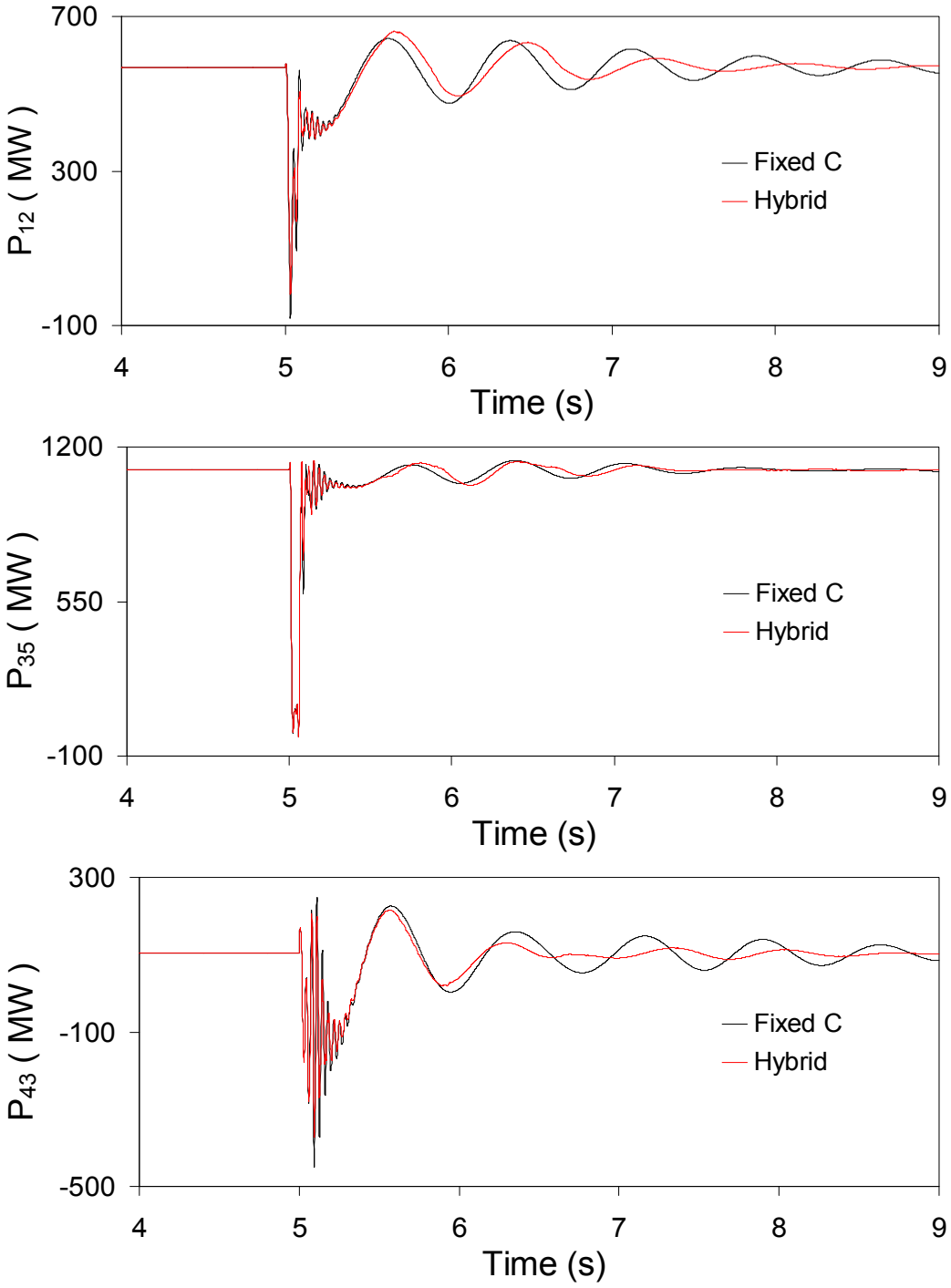

Figure 4.14: Continued.

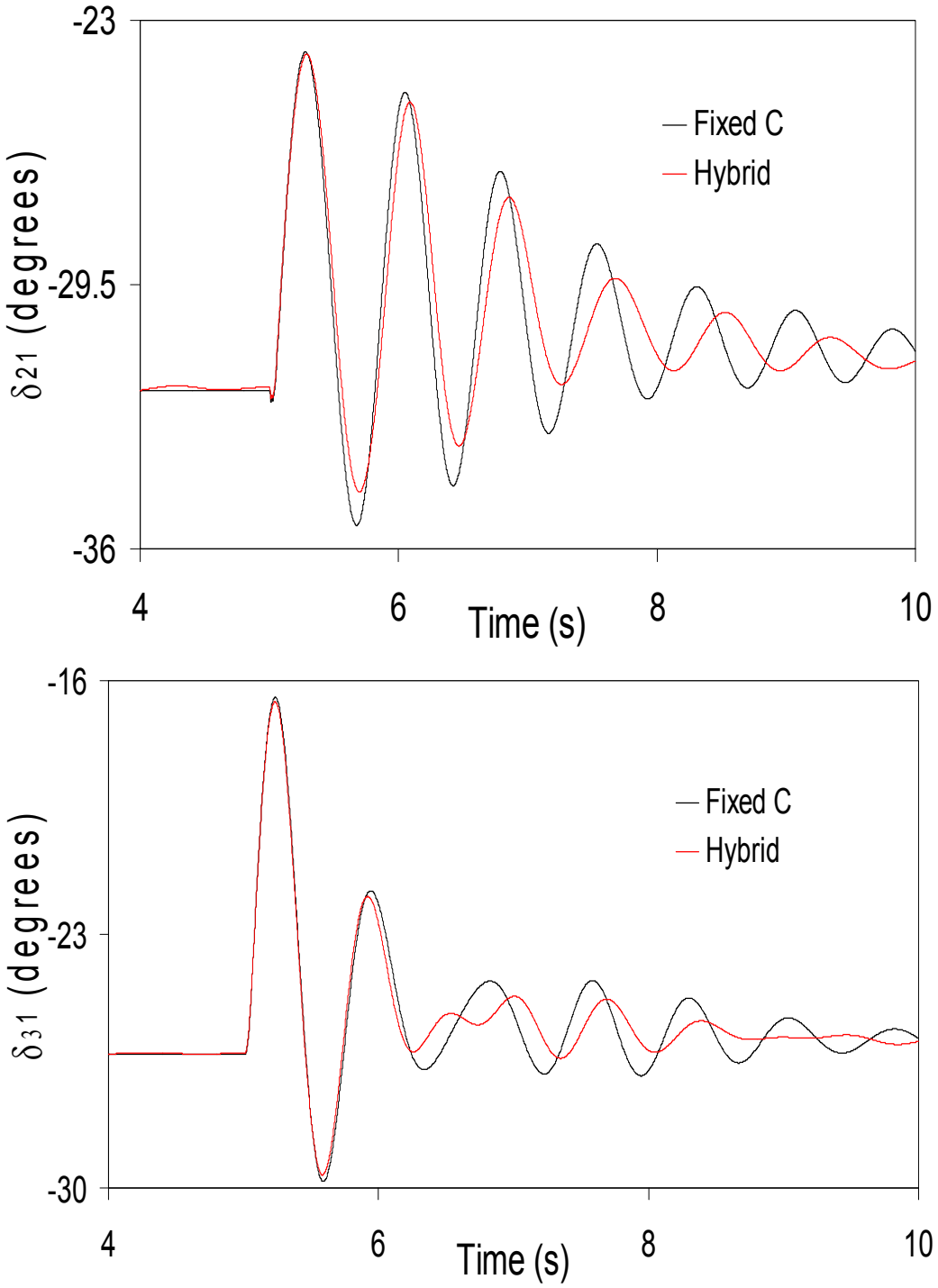

Figure 4.15: Generator load angles, measured with respect to generator 1 load angle, during and after clearing a three-cycle, three-phase fault at bus 2 (case study II).

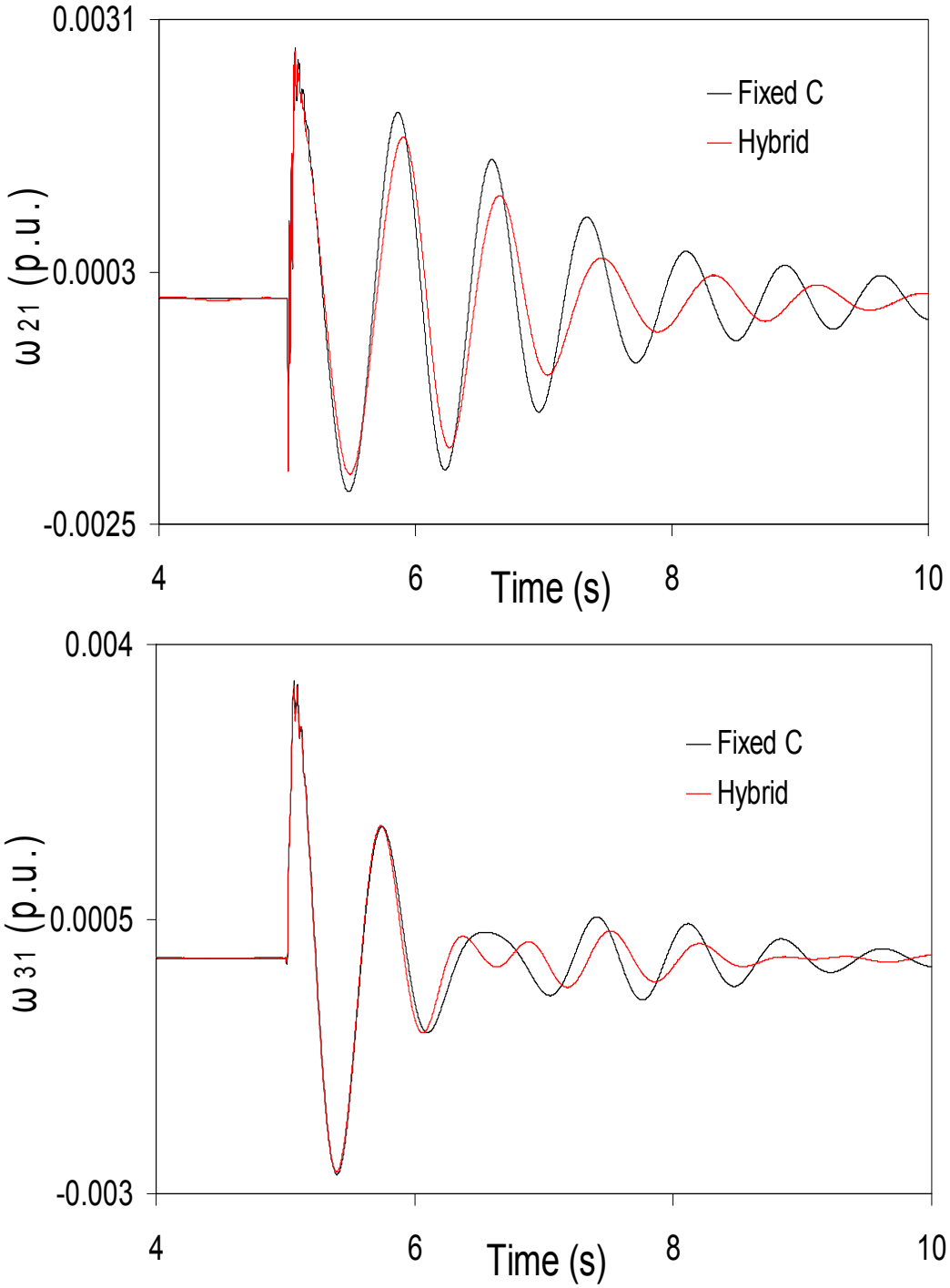

Figure 4.16: Generator speeds, measured with respect to generator 1 speed, during and after clearing a three-cycle, three-phase fault at bus 2 (case study II).

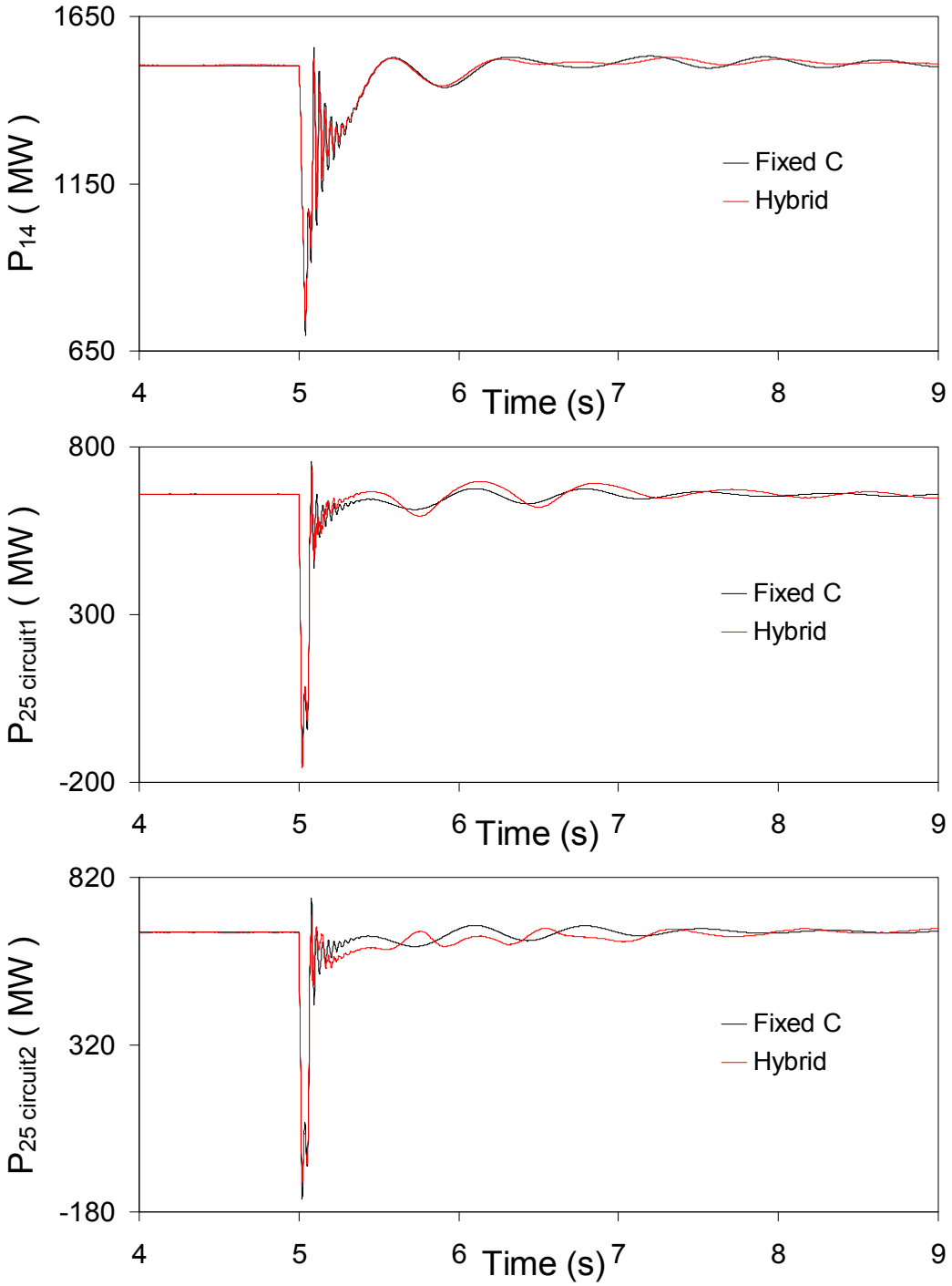

Figure 4.17: Transmission line real power flows during and after clearing a three-cycle, three-phase fault at bus 2 (case study II).

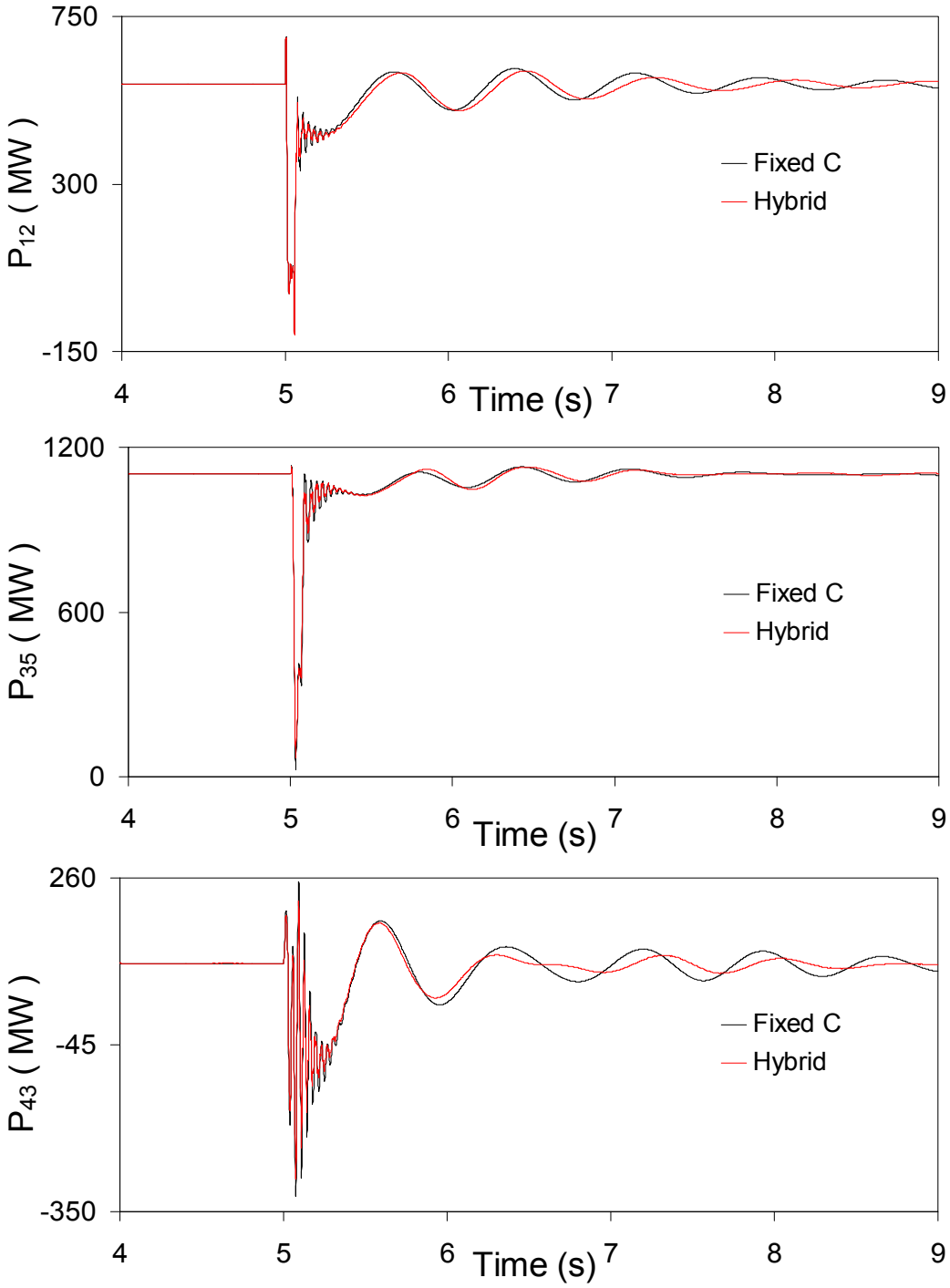

Figure 4.17: Continued.

4.5 Case Study III: The Hybrid Single-Phase-TCSC Compensation Scheme is Installed in both Circuits of Line L_1

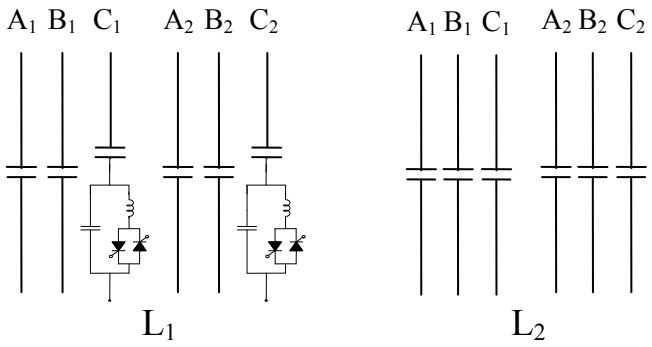

Figure 4.18: Case study III: the hybrid single-phase-TCSC compensation scheme is installed in both circuits of line L_1.

Each TCSC provides 50% of the total capacitive compensation and the stabilizing signal is δ_{21} for both controllers. The generator load angles and speeds, measured with respect to generator 1 load angle and speed, and the transmission line real power flow responses during and after clearing a three-cycle, three-phase fault at bus 4 are illustrated in Figures 4.19 to 4.21 for the case when the TCSC supplemental controllers are of a proportional type with a transfer function:

$$G_{P-\delta 21}(s) = 0.25\frac{10}{(s+10)}\frac{3s}{(3s+1)} \tag{4.5}$$

The level of the dynamic capacitive compensation provided by the TCSCs is twice of that in Case Study I. As a result, there are some reductions in the first swings as shown in Figure 4.19. In general, a reduction in the first swing is an indication of an enhancement in the transient stability of the system. It can also be seen from Figures 4.19 and 4.20 that the hybrid single-phase TCSC scheme is effective in damping the subsequent swings with a better damping than in the case of fixed capacitor compensation.

The effect of the input signal on damping the low frequency oscillations is examined through the use of two new signals, namely the relative deviation between generators 2 and 1 speeds, ω_{21} and the deviation in the real power flow in line L_1, P_{L1}. Satisfactory system transient responses and damping were not achievable with either signal, if the proportional type controller of Equation 4.5 is employed. The possibility of using a different controller for each signal was

explored. This resulted in designing proportional (for ω_{21}) and lead-lag (for P_{L1}) controllers with the transfer functions given respectively, in Equations 4.6 and 4.7.

$$G_{P-\omega 21}(s) = -600\frac{10}{(s+10)}\frac{0.1s}{(0.1s+1)} \tag{4.6}$$

$$G_{PL1}(s) = 0.5\frac{10}{(s+10)}\frac{0.5s}{(0.5s+1)}\frac{(s+0.1)}{(s+0.2)}\frac{(s+0.5)}{(s+3)} \tag{4.7}$$

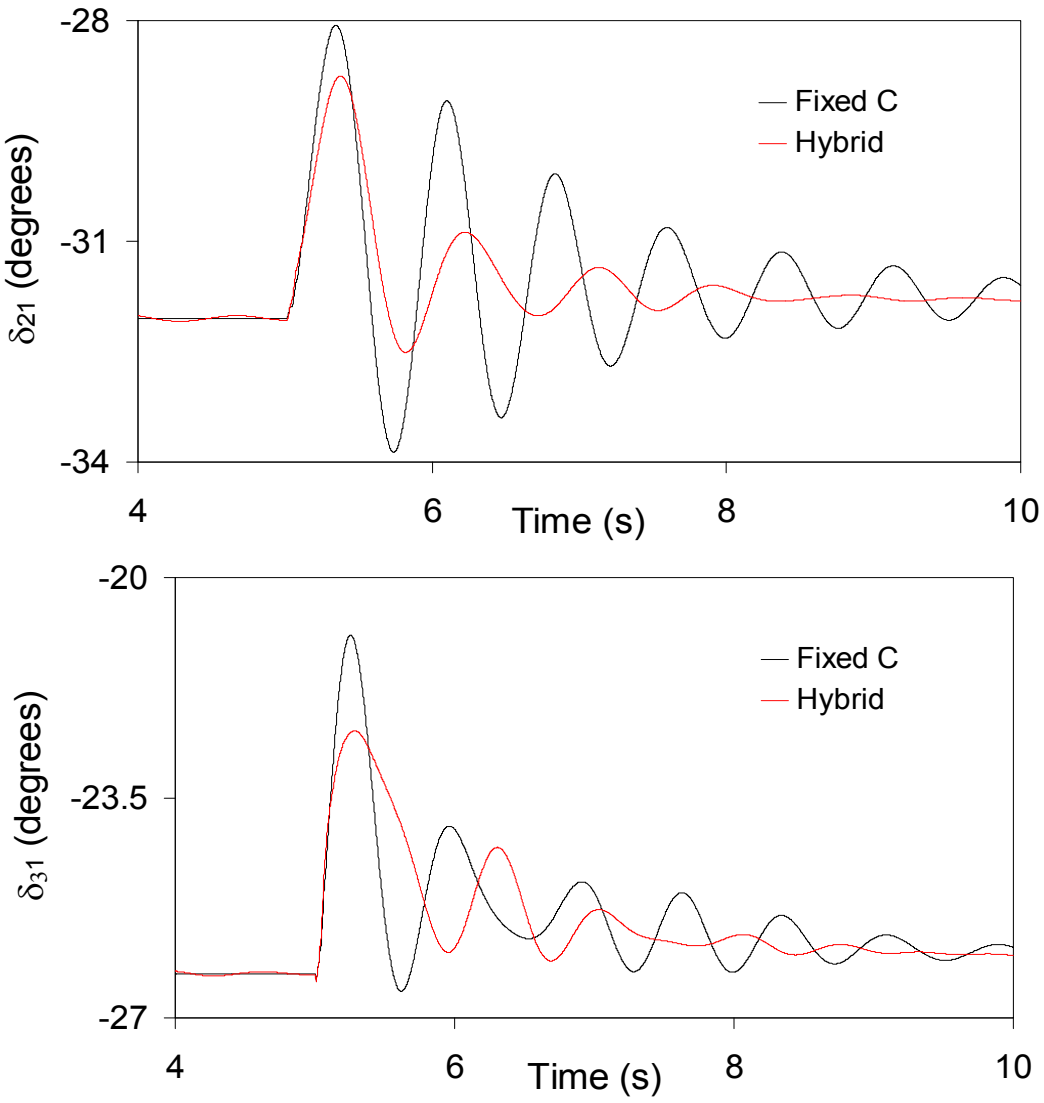

Figure 4.19: Generator load angles, measured with respect to generator 1 load angle, during and after clearing a three-cycle, three-phase fault at bus 4 (case study III).

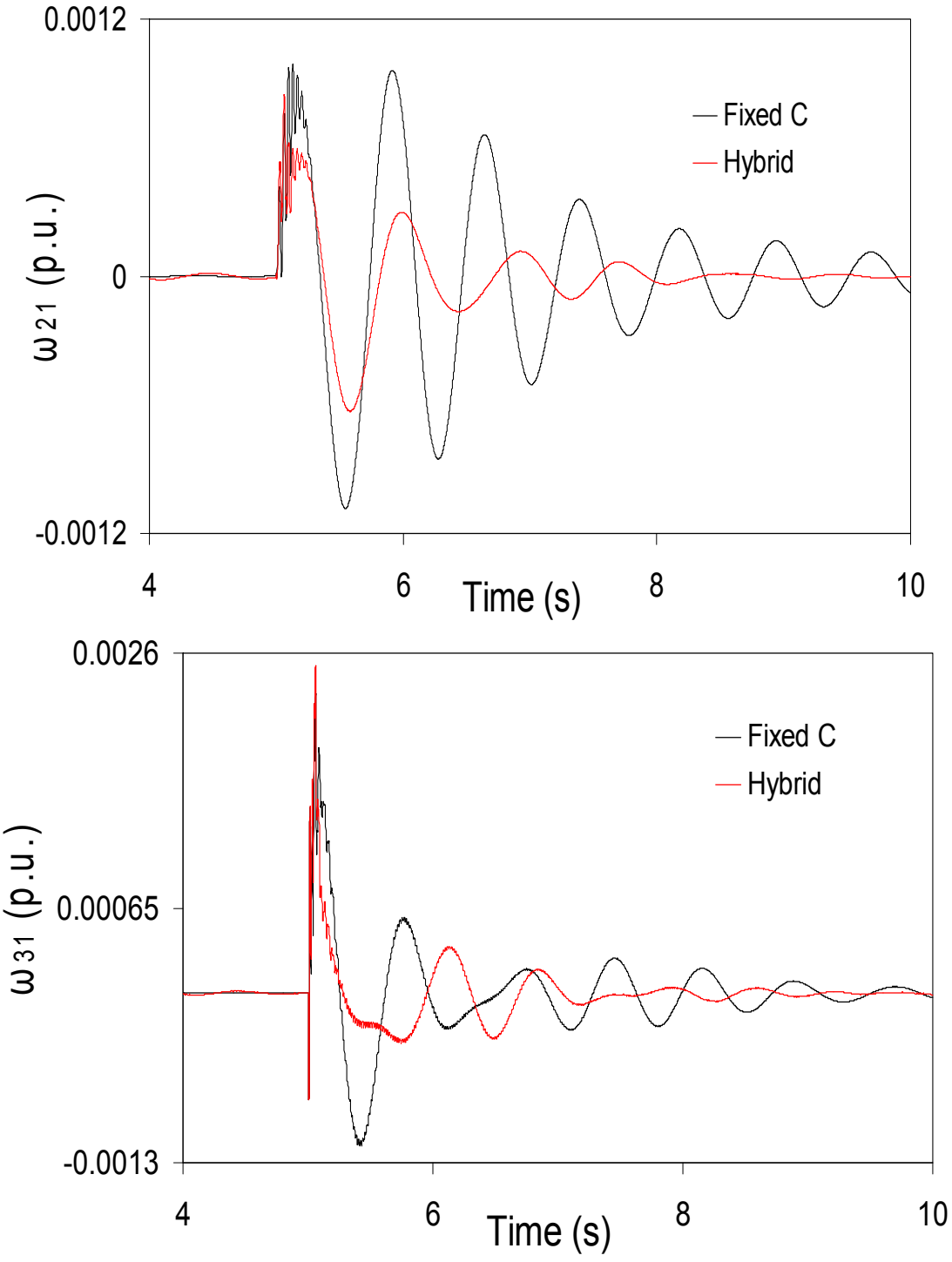

Figure 4.20: Generator speeds, measured with respect to generator 1 speed, during and after clearing a three-cycle, three-phase fault at bus 4 (case study III).

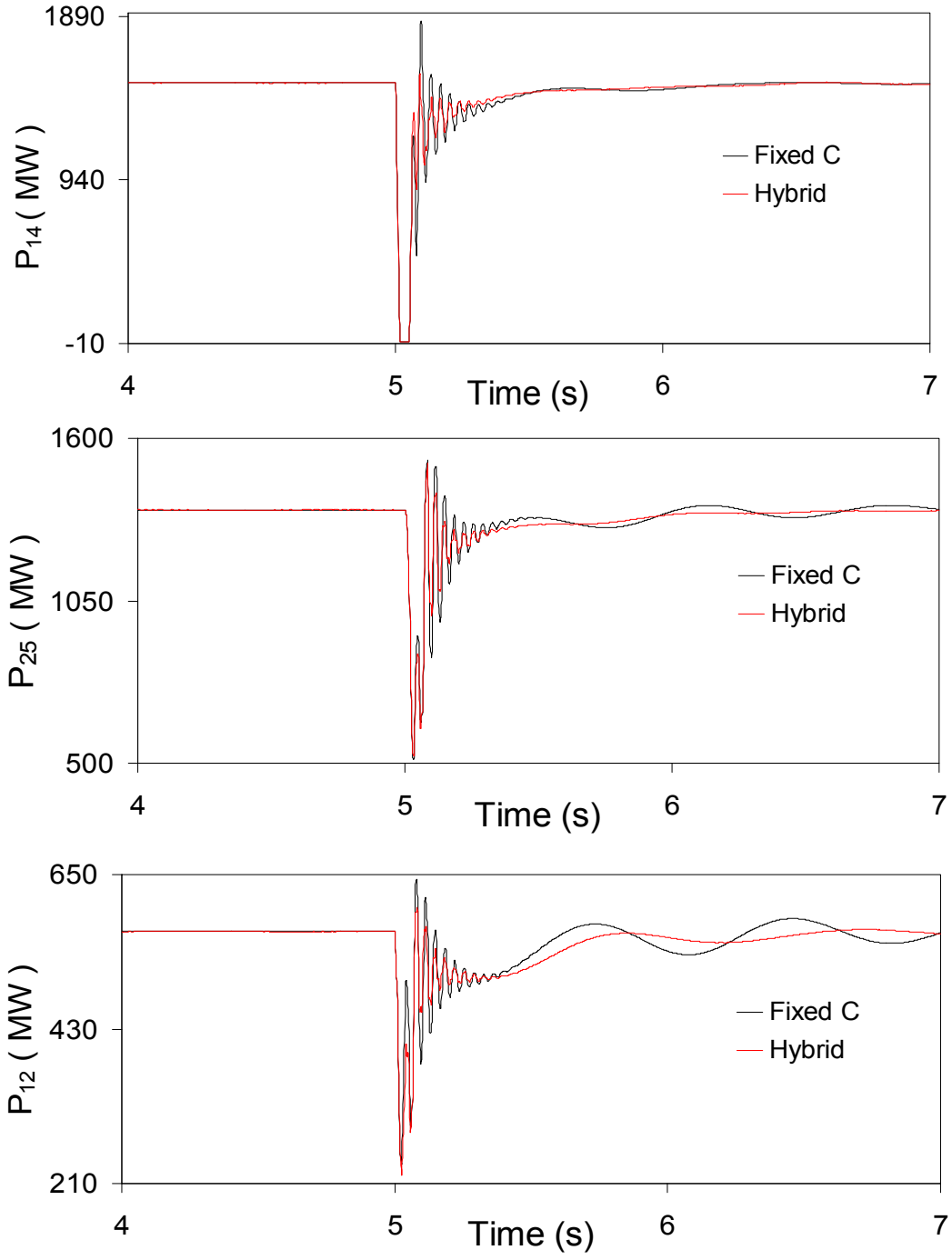

Figure 4.21: Transmission line real power flows during and after clearing a three-cycle, three-phase fault at bus 4 (case study III).

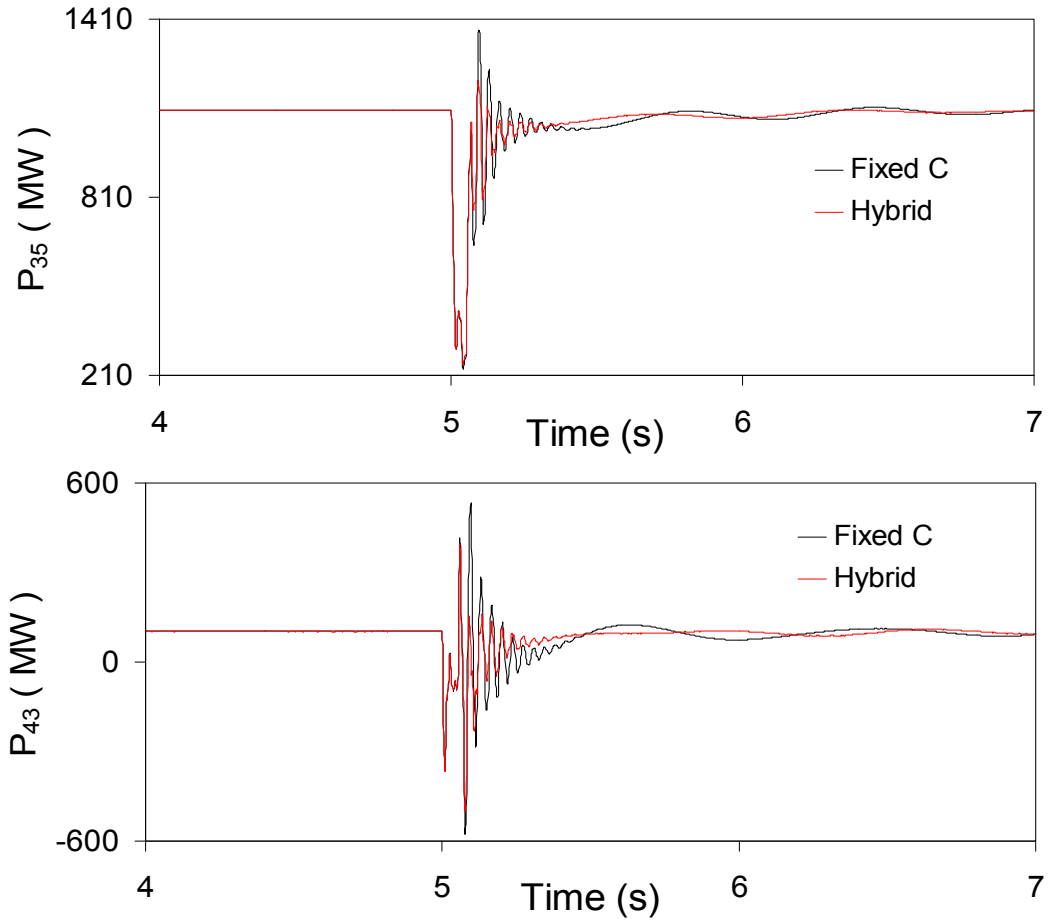

Figure 4.21: Continued.

A comparison between the system responses to the three controllers is shown in Figure 4.22. It can be seen from this figure that the system transient responses in the three cases are comparable. The response in the case of the input signal δ_{21} is still relatively the best, especially near steady-state. This should be expected due to the direct relationship between the relative load angles and the generators that yield the problem. Moreover, although the system response in the case of the input signal P_{L1} is very satisfactory, two lead-lag stages are required in order to acquire such a response.

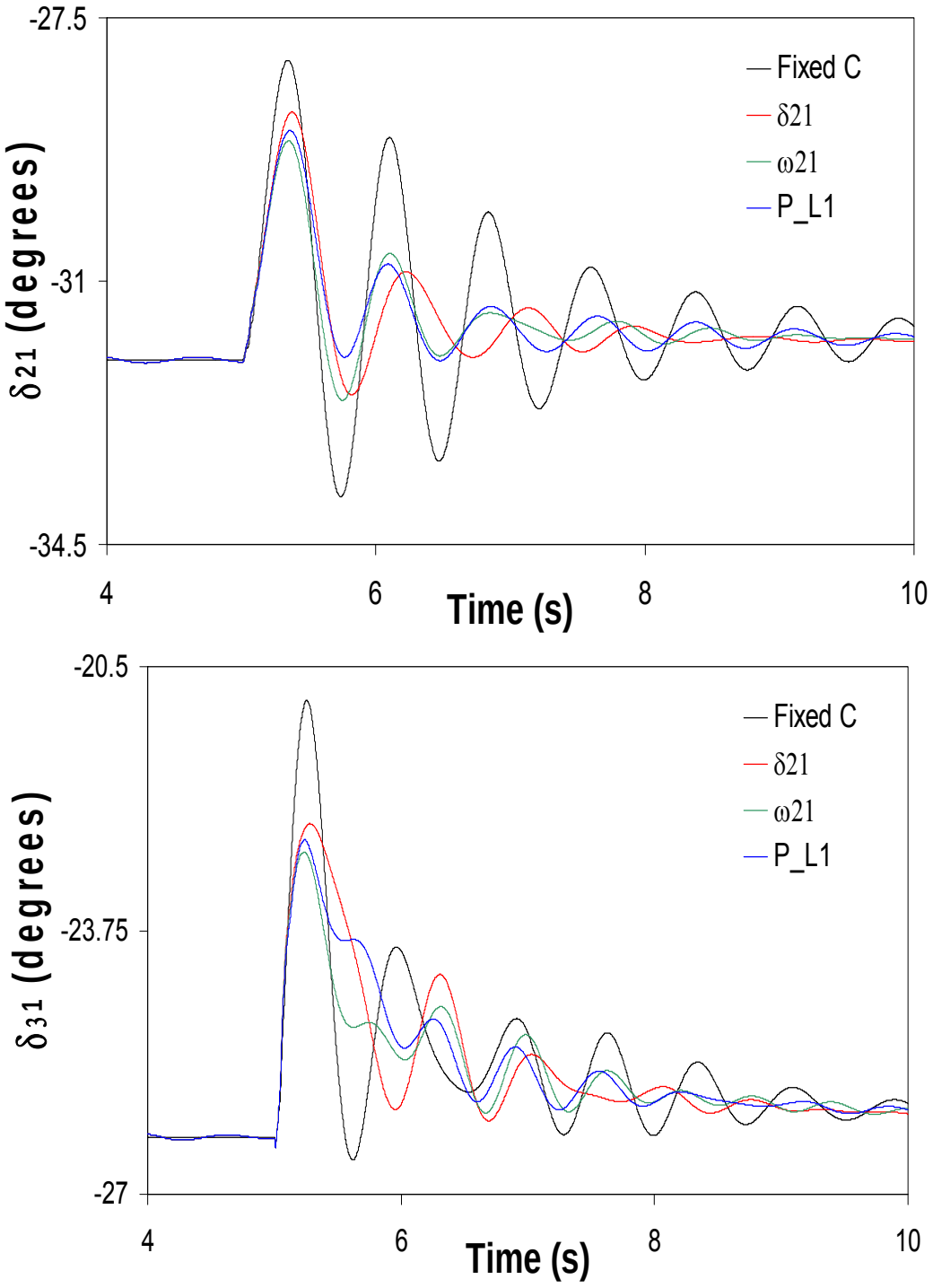

Figure 4.22: Generator load angles, measured with respect to generator 1 load angle, during and after clearing a three-cycle, three-phase fault at bus 4 (case study III, effect of the stabilizing signal).

4.6 Case Study IV: The Hybrid Single-Phase-TCSC Compensation Scheme is Installed in all Circuits of Lines L_1 and L_2

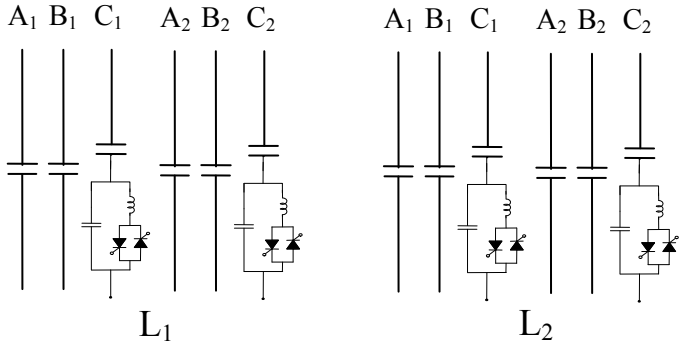

Figure 4.23: Case study IV: the hybrid single-phase-TCSC compensation scheme is installed in all circuits of lines L_1 and L_2.

Each TCSC provides 50% of the total capacitive compensation and the disturbance is a three-cycle, three-phase fault at bus 4. Four different combinations of stabilizing signals (tabulated in Table 4.1) are examined in order to determine the combination that would result in the best system transient time responses. The final results of the time-domain simulation studies (controllers tuning) are shown in Figure 4.24 which illustrates the generator load angles, measured with respect to generator 1 load angle, during and after fault clearing. The transfer functions of the TCSC supplemental controllers for the four combinations are given in Table 4.2.

Table 4.1: The four examined combinations of stabilizing signals.

Combination	Each TCSC in L_1	Each TCSC in L_2
1	δ_{21}	δ_{21}
2	δ_{31}	δ_{21}
3	δ_{31}	P_{L2}
4	P_{L1}	δ_{21}

It can be seen from Figure 4.24 that the best damping of the relative load angle responses are achieved with the δ_{21}- δ_{21} combination. The second best damped responses are obtained with the δ_{31}- δ_{21} combination. Again, these results should be expected due to the direct relationship between the relative load angles and the generators that yield the problem. It can also be seen from Figure 4.24 that the worst damped responses are obtained with P_{L1}- δ_{21} combination which results also in the increase of the first swings.

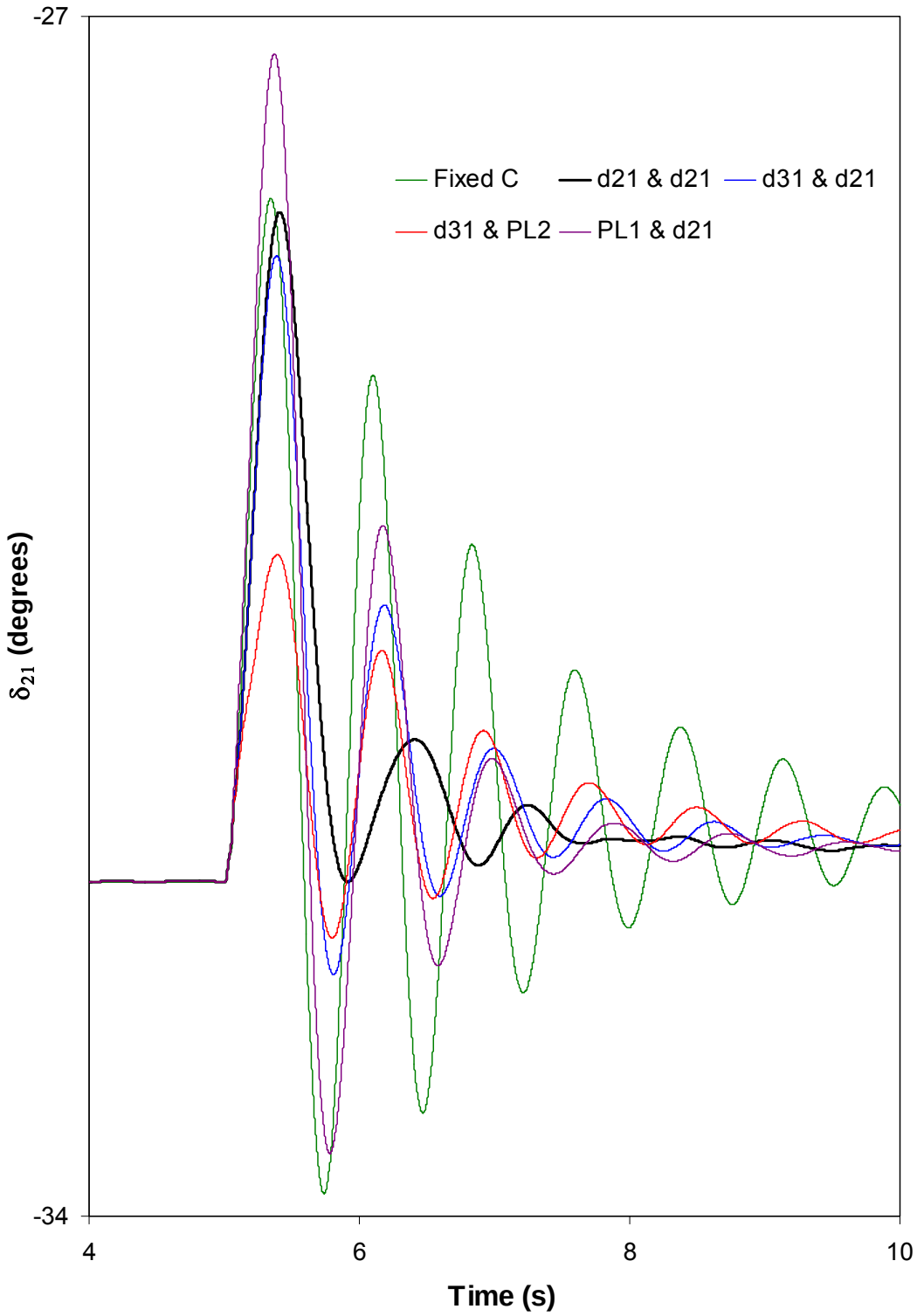

Figure 4.24: Generator load angles, measured with respect to generator 1 load angle, during and after clearing a three-cycle, three-phase fault at bus 4 (case study IV).

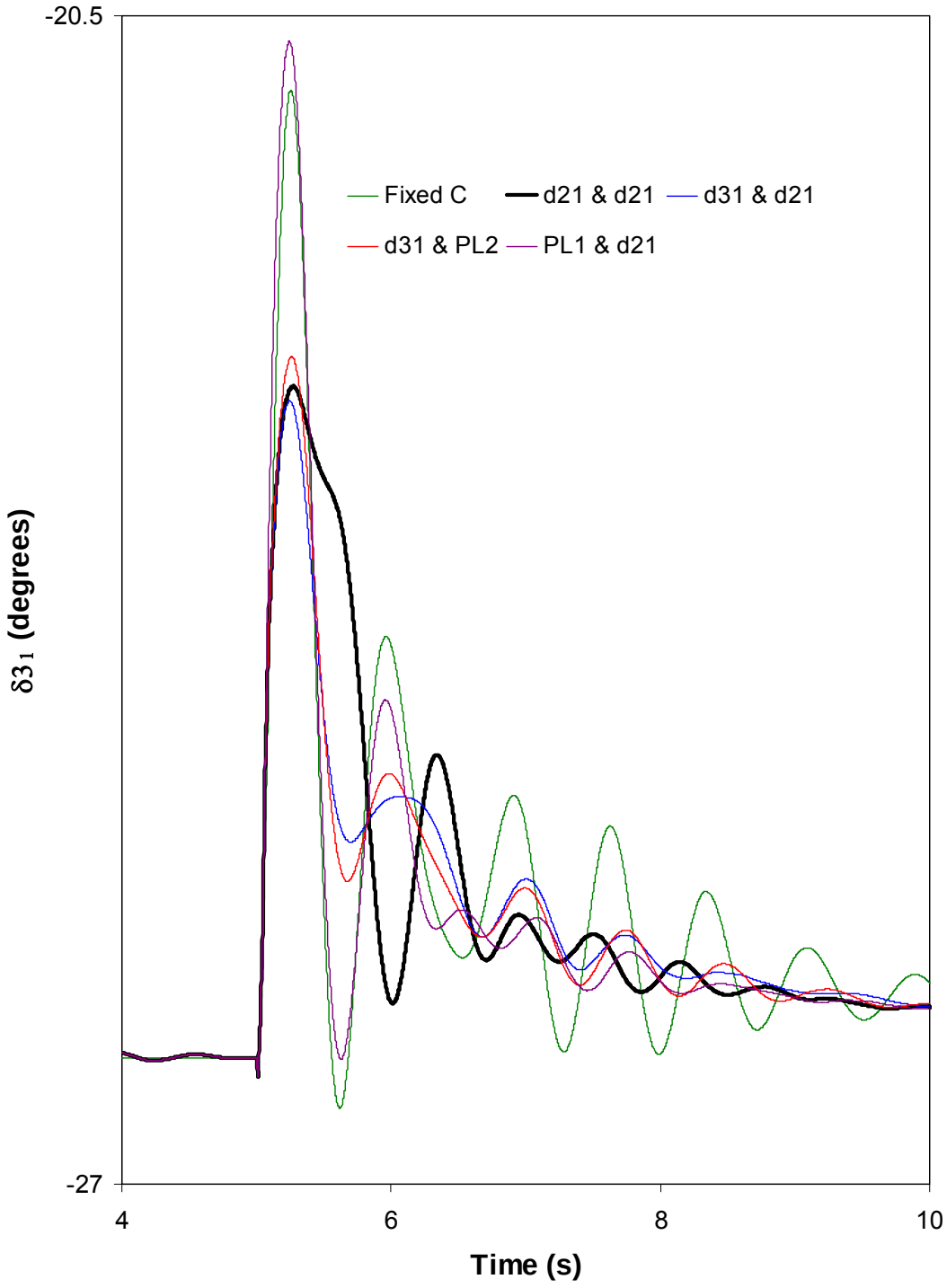

Figure 4.24: Continued.

Table 4.2: Transfer functions of the TCSC supplemental controllers.

Combination	Each TCSC in L_1	Each TCSC in L_2
1	$G(s)=0.25\frac{10}{(s+10)}\frac{3s}{(3s+1)}$	$G(s)=-0.15\frac{10}{(s+10)}\frac{3s}{(3s+1)}$
2	$G(s)=0.05\frac{10}{(s+10)}\frac{3s}{(3s+1)}$	$G(s)=-0.15\frac{10}{(s+10)}\frac{3s}{(3s+1)}$
3	$G(s)=0.1\frac{10}{(s+10)}\frac{3s}{(3s+1)}$	$G(s)=-0.4\frac{10}{(s+10)}\frac{3s}{(3s+1)}$
4	$G(s)=-0.25\frac{10}{(s+10)}\frac{3s}{(3s+1)}$	$G(s)=-0.25\frac{10}{(s+10)}\frac{3s}{(3s+1)}$

Having established that δ_{21}- δ_{21} are the best stablizing input signals, Figure 4.25 and 4.26 illustrate respectively, the transient time responses of the generator speeds (relative to the speed of generator 1) and the real power flow on the five transmission lines. The variations of the TCSC modulated reactances are shown in Figures 4.27 and 4.28. It is interesting to point out from Figure 4.27 that at the instant of fault clearing, the TCSC net reactance in line L_1 is inductive.

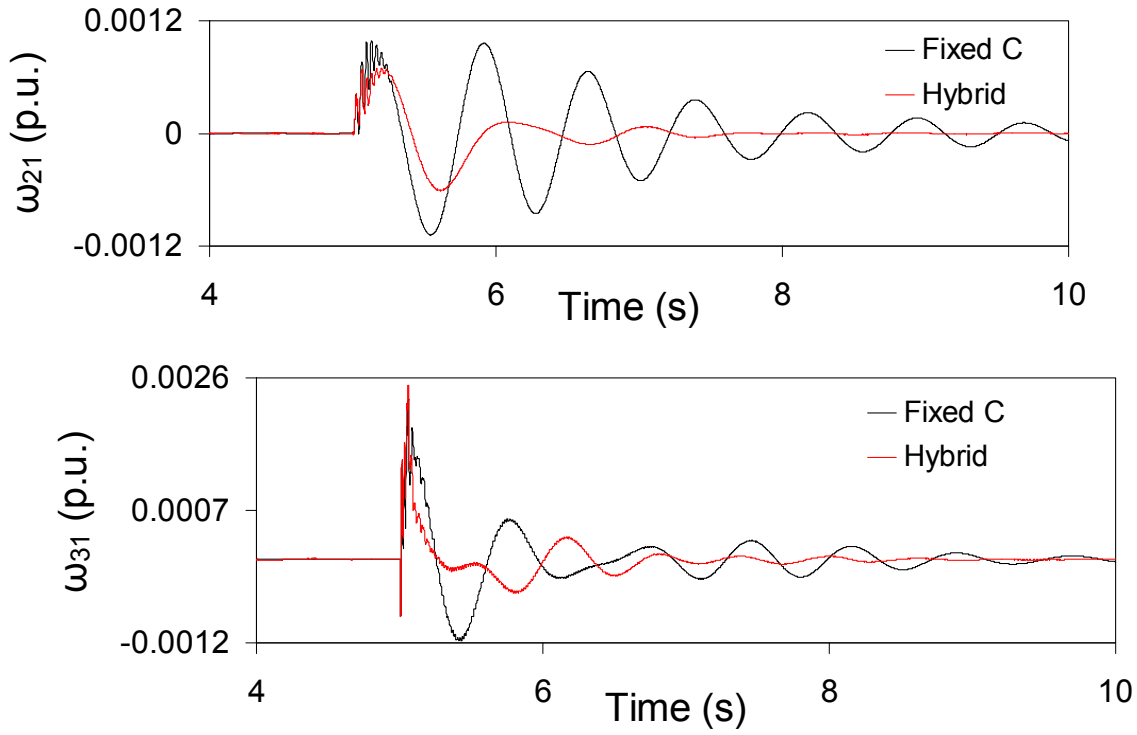

Figure 4.25: Generator speeds, measured with respect to generator 1 speed, during and after clearing a three-cycle, three-phase fault at bus 4 (case study IV, input signals are δ_{21} for both TCSC controllers).

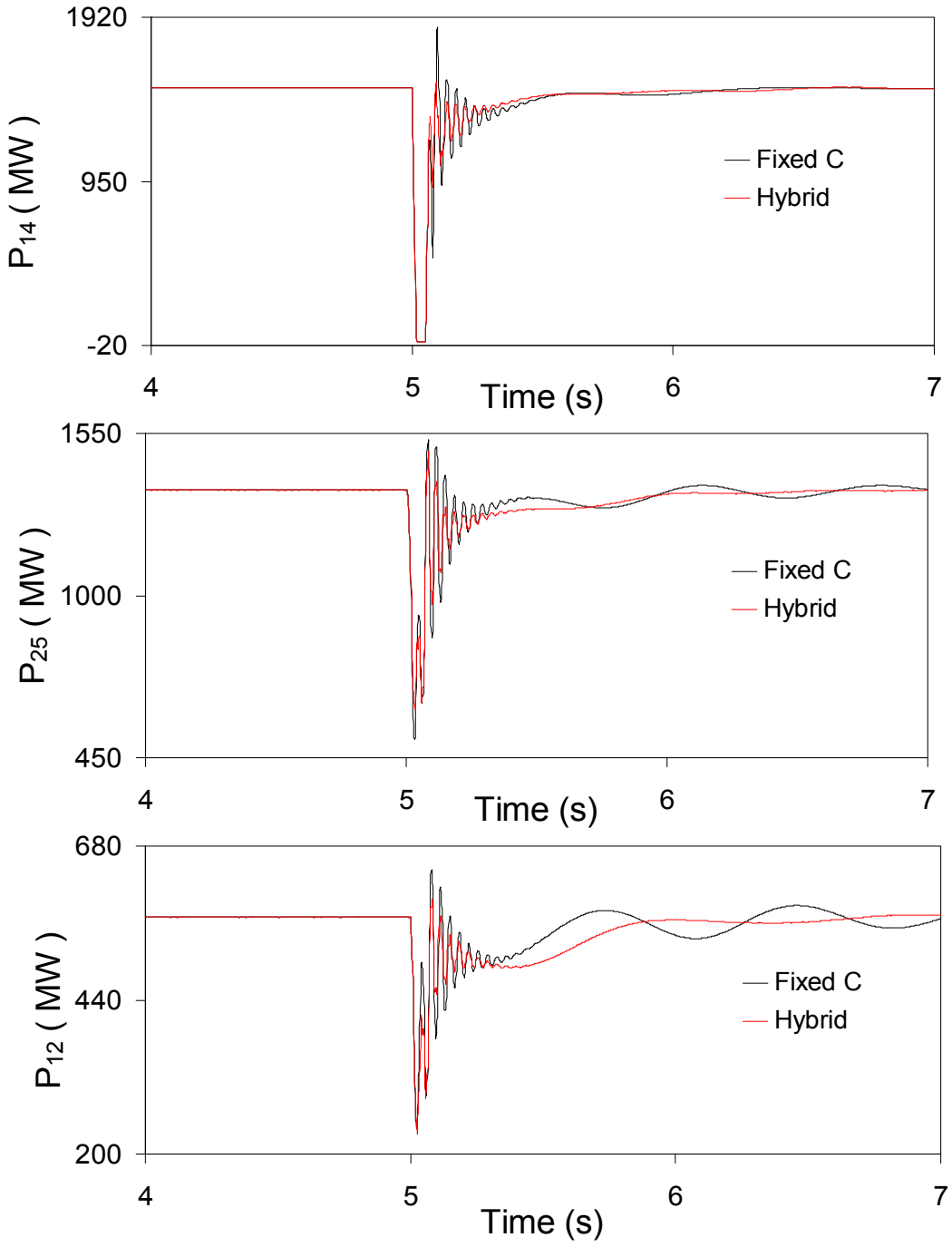

Figure 4.26: Transmission line real power flows during and after clearing a three-cycle, three-phase fault at bus 4 (case study IV, input signals are δ_{21} for both TCSC controllers).

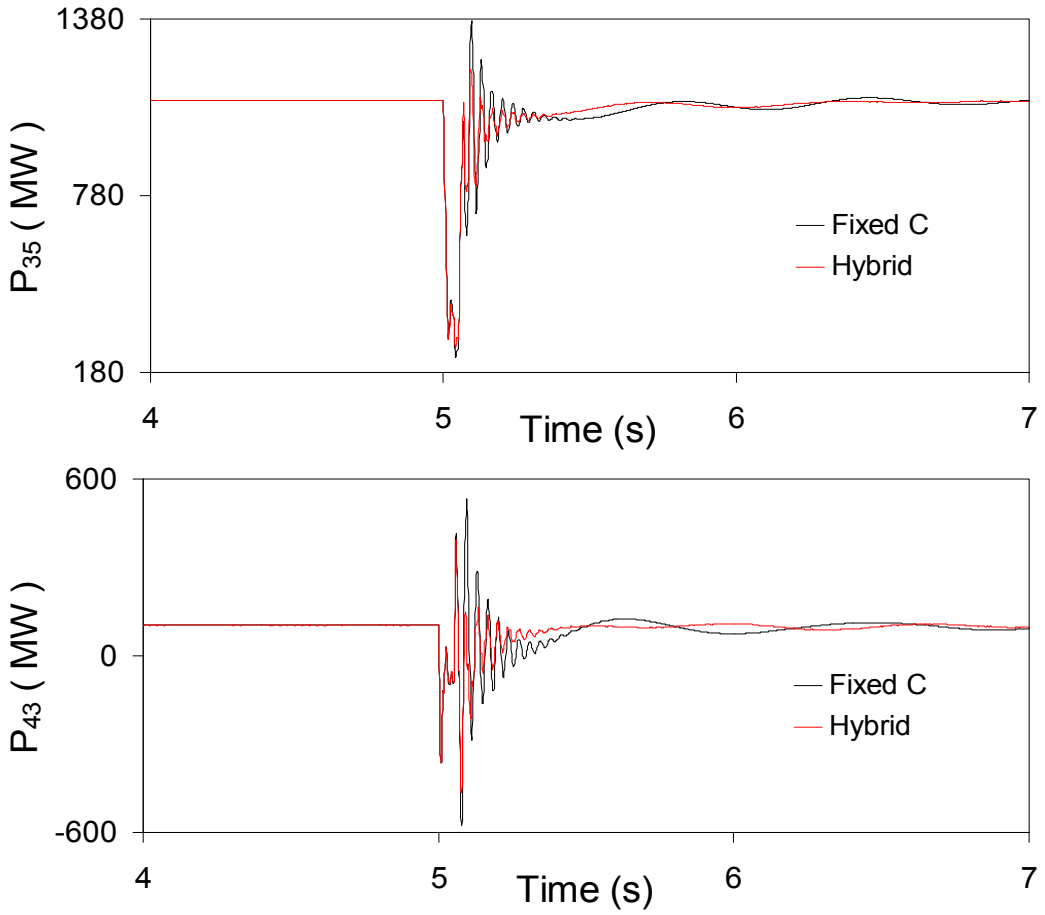

Figure 4.26: Continued.

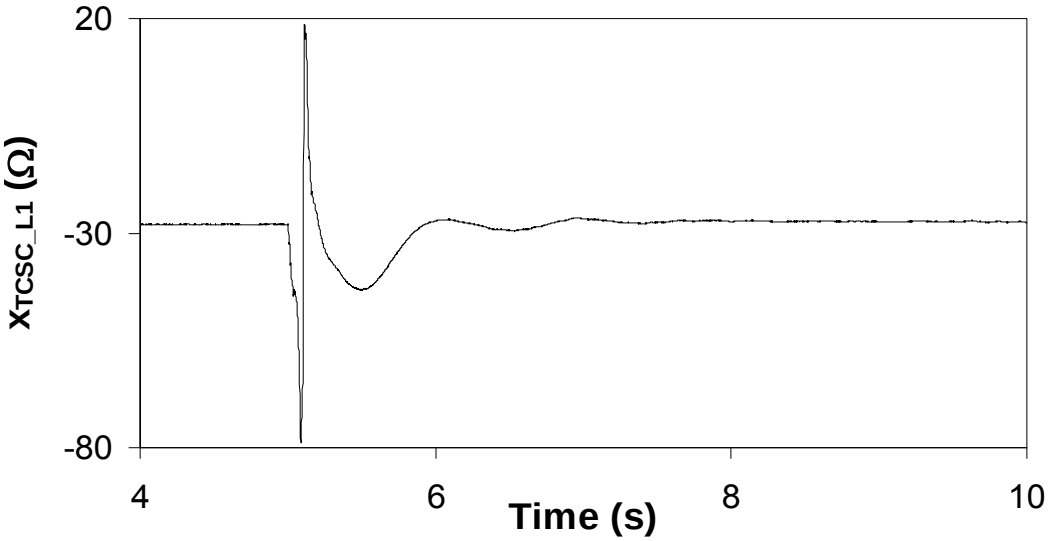

Figure 4.27: Variations of line L_1 TCSC reactance during and after clearing a three-cycle, three-phase fault at bus 4 (case study IV, input signals are δ_{21} for both TCSC controllers).

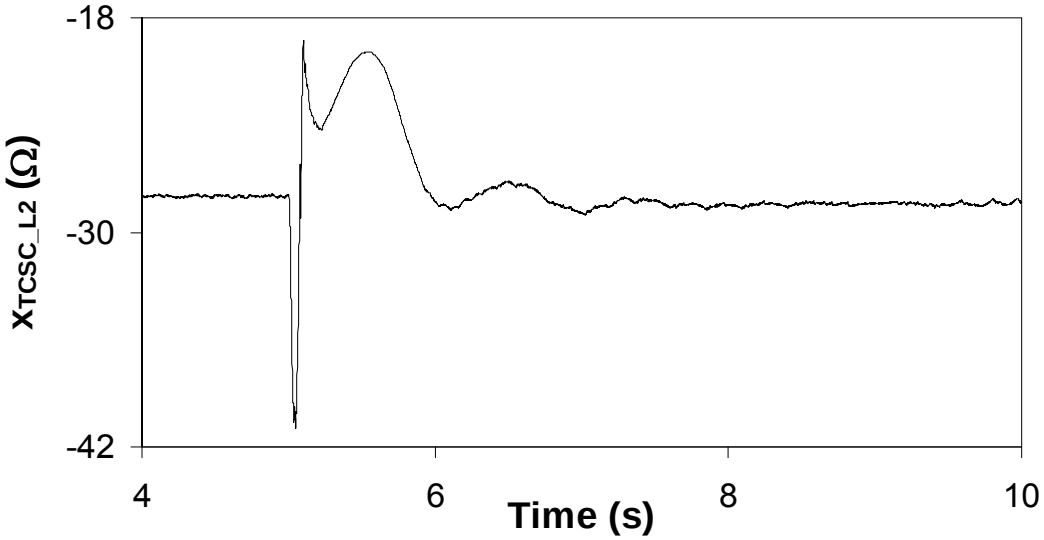

Figure 4.28: Variations of line L_2 TCSC reactance during and after clearing a three-cycle, three-phase fault at bus 4 (case study IV, input signals are δ_{21} for both TCSC controllers).

4.6.1 Performance of the scheme at a different loading profile

Each TCSC provides 50% of the total capacitive compensation and the stabilizing signal is δ_{21}. Moreover, the disturbance is a three-cycle, three-phase fault at bus 4. Load S_1 is increased by 600 MW while load S_2 is reduced by the same amount. The power flow results for the bus voltages and the line real power flows of the system under study are shown in Figure 4.29. The comparison between this figure and Figure 2.6 shows that the direction of the real power flow between buses 4 and 3 is reversed.

Figure 4.30 illustrates the generator load angles, measured with respect to generator 1 load angle, during and after fault clearing. The transfer functions of the TCSC supplemental controllers are given in Table 4.3. It can be seen from Figure 4.30 that, at this loading condition, the hybrid single-phase-TCSC scheme provides again a better damping performance to system oscillations compared to fixed capacitor compensation. It is observed, however, that there is a slight increase in the first swing of δ_{21}.

Table 4.3: Transfer functions of the TCSC supplemental controllers with the stabilizing signal δ_{21}.

Each TCSC in L_1	Each TCSC in L_2
$G(s) = 0.3\frac{10}{(s+10)}\frac{3s}{(3s+1)}$	$G(s) = -0.15\frac{10}{(s+10)}\frac{3s}{(3s+1)}$

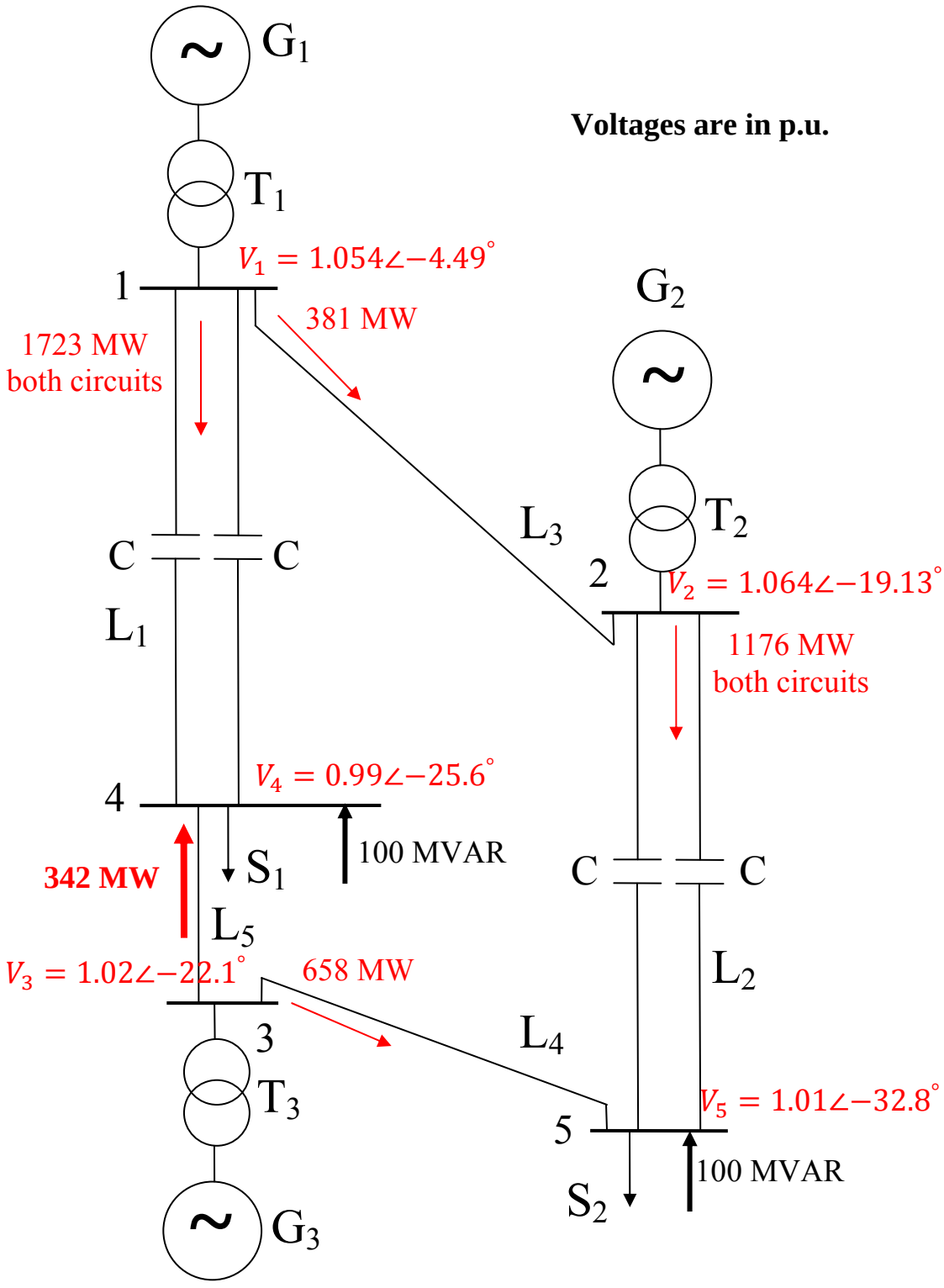

Figure 4.29: Power flow results of bus voltages and line real power flows of the system under study.

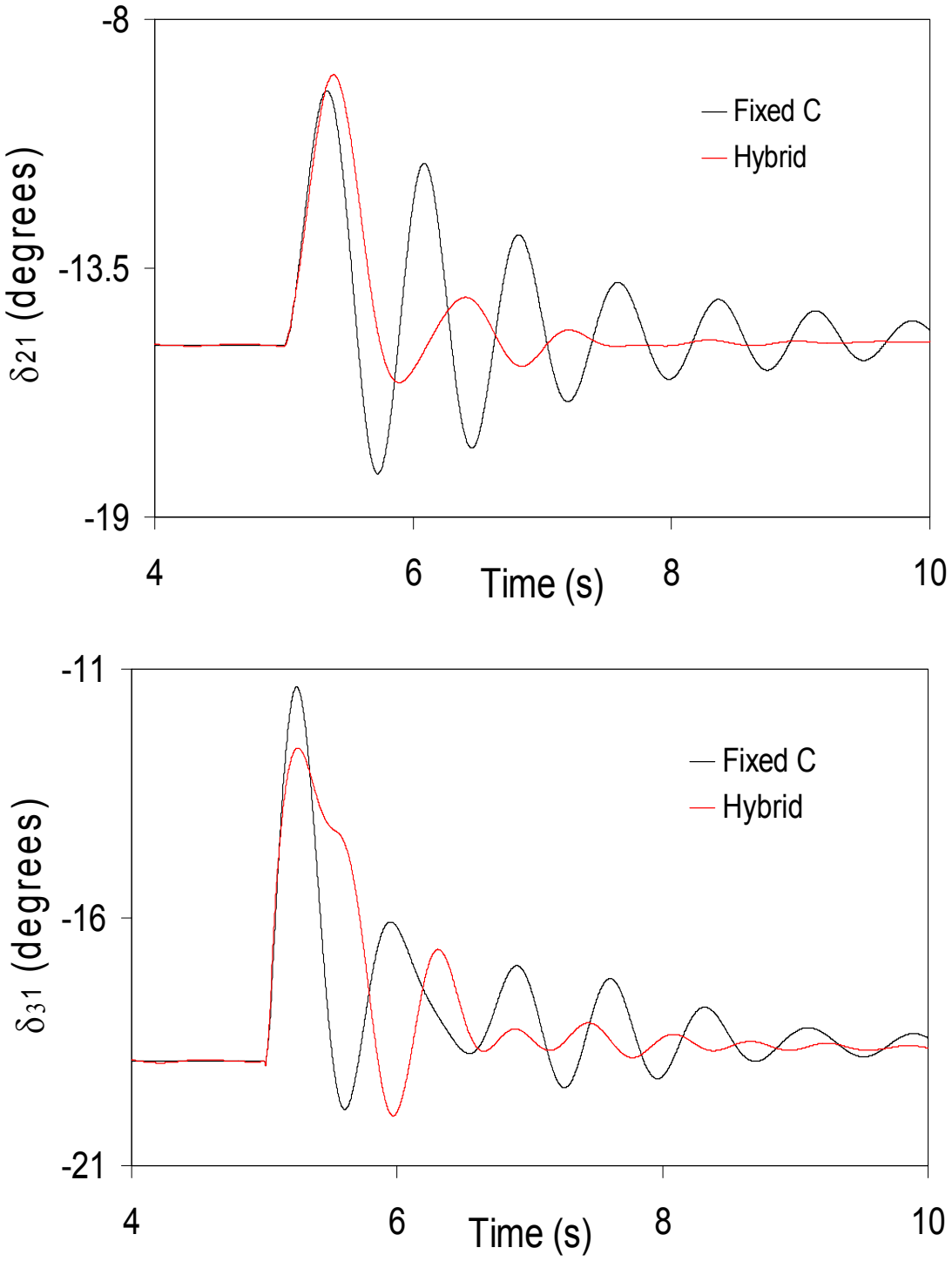

Figure 4.30: Generator load angles, measured with respect to generator 1 load angle, during and after clearing a three-cycle, three-phase fault at bus 4 (case study IV at a different loading profile, stabilizing signal: δ_{21}).

4.6.2 Performance of a dual-channel TCSC supplemental controller

Any of the four signals, δ_{21}, δ_{31}, P_{L1} and P_{L2} contains the system's two natural modes of oscillations and can be used to add damping to these modes as it has been demonstrated in Sections 4.3 to 4.6. The sum of two properly selected signals, however, should result in a more effective damping. The reason is that the two natural modes of oscillations are, in general, not in phase. A dual-channel controller would adjust separately the gain and phase of each mode of oscillations and, thus, provides a better damping. The performance of the dual-channel TCSC supplemental controller shown in Figure 4.31 in damping power system oscillations is examined using the six pairs of signals given in Table 4.4. It is assumed again that each TCSC provides 50% of the total capacitive compensation and that the disturbance is a three-cycle, three-phase fault at bus 4. Moreover, investigations are conducted on the system with the pre-fault load flow in Figure 4.29.

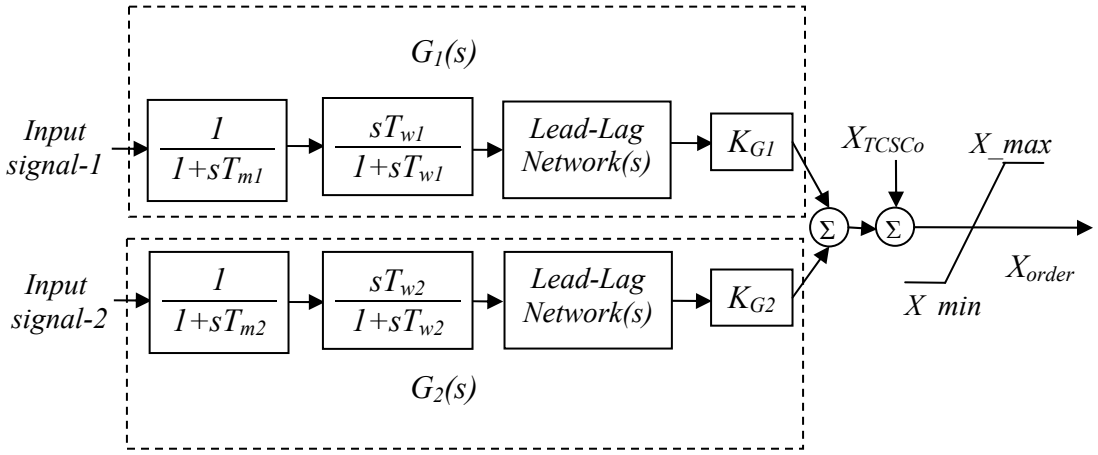

Figure 4.31: Structure of a dual-channel POD controller.

The final results of the time-domain simulation studies (controllers tuning) are shown in Figure 4.32 which illustrates the generator load angles, measured with respect to generator 1 load angle, during and after fault clearing. These results (in red color) are compared to the hybrid case of Figure 4.30. The transfer functions of the TCSC supplemental controllers for the six pairs of signals are given in Tables 4.5 and 4.6.

Table 4.4: The six examined combinations of stabilizing signals.

Pair number	Each TCSC (input signal-1, input signal-2)
1	δ_{21}, δ_{31}
2	δ_{21}, P_{L1}
3	δ_{21}, P_{L2}
4	δ_{31}, P_{L1}
5	δ_{31}, P_{L2}
6	P_{L1}, P_{L2}

Table 4.5: Transfer functions of the dual- channel TCSC supplemental controllers in L_1.

Pair number	Each TCSC in L_1
1	$G_1(s) = 0.2\frac{10}{(s+10)}\frac{3s}{(3s+1)}$ $G_2(s) = -0.2\frac{10}{(s+10)}\frac{3s}{(3s+1)}$
2	$G_1(s) = 0.25\frac{10}{(s+10)}\frac{0.5s}{(0.5s+1)}$ $G_2(s) = -0.5\frac{60}{(s+60)}\frac{0.01s}{(0.01s+1)}$
3	$G_1(s) = 0.3\frac{10}{(s+10)}\frac{s}{(s+1)}$ $G_2(s) = -1\frac{60}{(s+60)}\frac{0.01s}{(0.01s+1)}$
4	$G_1(s) = 0.28\frac{10}{(s+10)}\frac{3s}{(3s+1)}$ $G_2(s) = -2.5\frac{60}{(s+60)}\frac{0.01s}{(0.01s+1)}\frac{(s+0.1)}{(s+0.2)}\frac{(s+0.5)}{(s+3)}$
5	$G_1(s) = 0.28\frac{10}{(s+10)}\frac{3s}{(3s+1)}$ $G_2(s) = -2.5\frac{60}{(s+60)}\frac{0.01s}{(0.01s+1)}\frac{(s+0.1)}{(s+0.2)}\frac{(s+0.5)}{(s+3)}$
6	$G_1(s) = -0.5\frac{10}{(s+10)}\frac{3s}{(3s+1)}$ $G_1(s) = \frac{10}{(s+10)}\frac{3s}{(3s+1)}$

Table 4.6: Transfer functions of the dual- channel TCSC supplemental controllers in L_2.

Pair number	Each TCSC in L_2
1	$G_1(s) = 0.2\frac{10}{(s+10)}\frac{3s}{(3s+1)}$ $G_2(s) = -0.2\frac{10}{(s+10)}\frac{3s}{(3s+1)}$
2	$G_1(s) = 0.25\frac{10}{(s+10)}\frac{0.5s}{(0.5s+1)}$ $G_2(s) = -0.5\frac{60}{(s+60)}\frac{0.01s}{(0.01s+1)}$
3	$G_1(s) = 0.3\frac{10}{(s+10)}\frac{s}{(s+1)}$ $G_2(s) = -1\frac{60}{(s+60)}\frac{0.01s}{(0.01s+1)}$
4	$G_1(s) = 0.26\frac{10}{(s+10)}\frac{s}{(s+1)}$ $G_2(s) = 2\frac{60}{(s+60)}\frac{0.01s}{(0.01s+1)}\frac{(s+0.1)}{(s+0.2)}\frac{(s+0.5)}{(s+3)}$
5	$G_1(s) = 0.26\frac{10}{(s+10)}\frac{s}{(s+1)}$ $G_2(s) = 2\frac{60}{(s+60)}\frac{0.01s}{(0.01s+1)}\frac{(s+0.1)}{(s+0.2)}\frac{(s+0.5)}{(s+3)}$
6	$G_1(s) = 0.5\frac{10}{(s+10)}\frac{3s}{(3s+1)}$ $G_1(s) = \frac{-10}{(s+10)}\frac{3s}{(3s+1)}$

It can be seen from Figure 4.32 that the best damping of the relative load angle responses are achieved with pair 2 (δ_{21}, P_{L1}). The second and third best damped responses are very close and are obtained with pairs 5 and 4. It can also be seen from Figure 4.32 that the worst damped responses are obtained with pair 6, namely P_{L1}, P_{L2}.

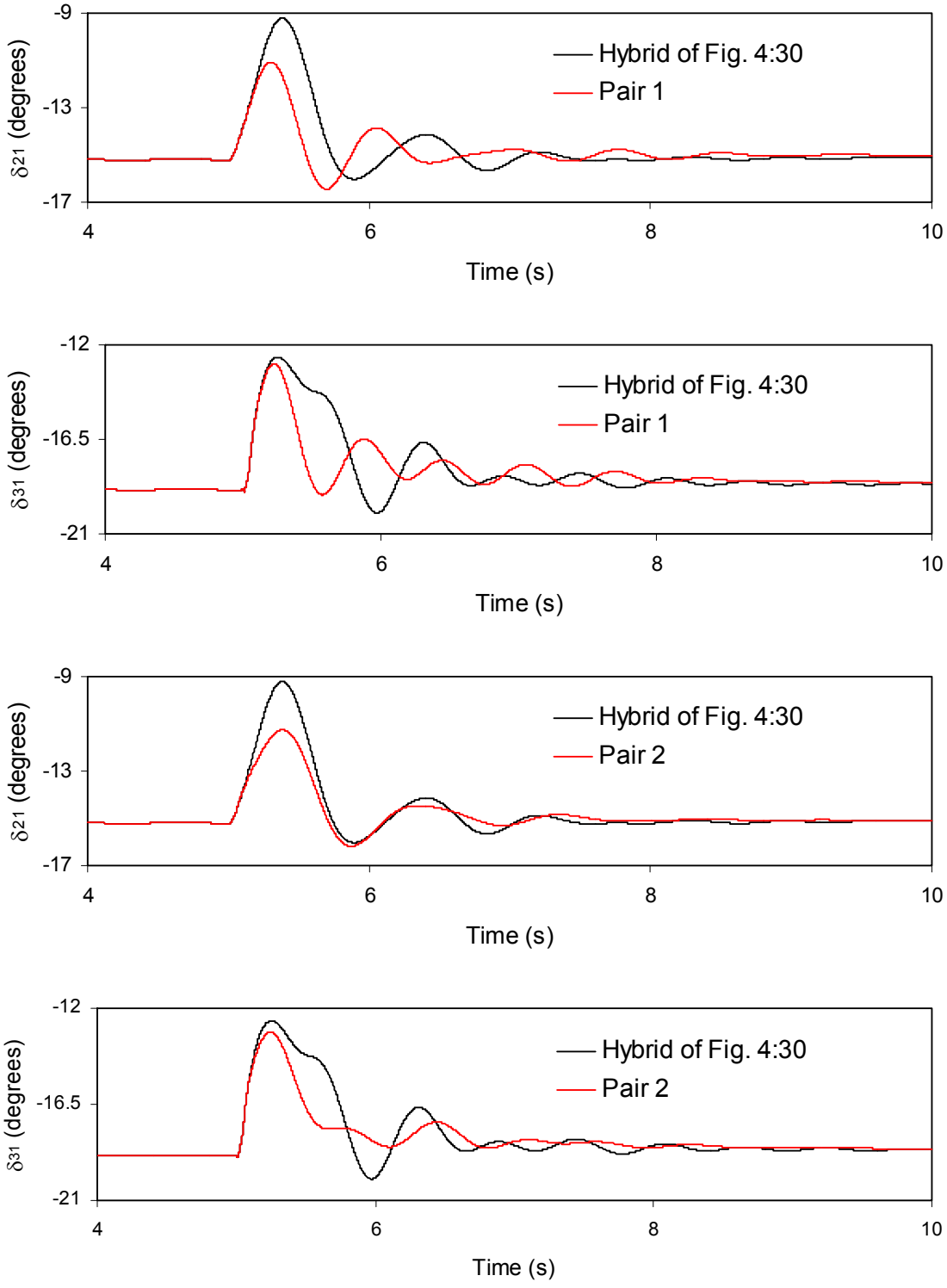

Figure 4.32: Generator load angles, measured with respect to generator 1 load angle, during and after clearing a three-cycle, three-phase fault at bus 4 (case study IV at a different loading profile, dual-channel supplemental controllers).

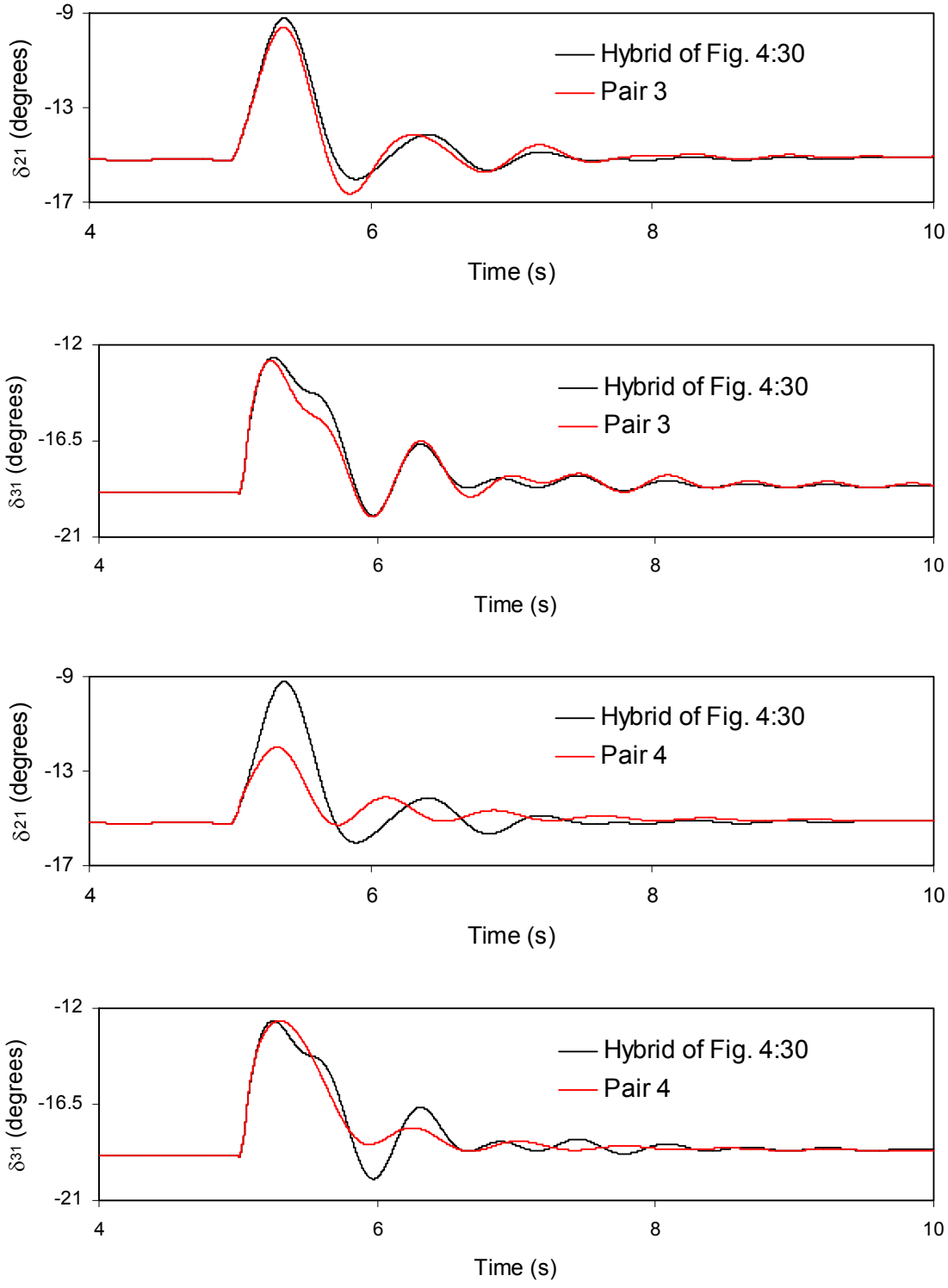

Figure 4.32: Continued.

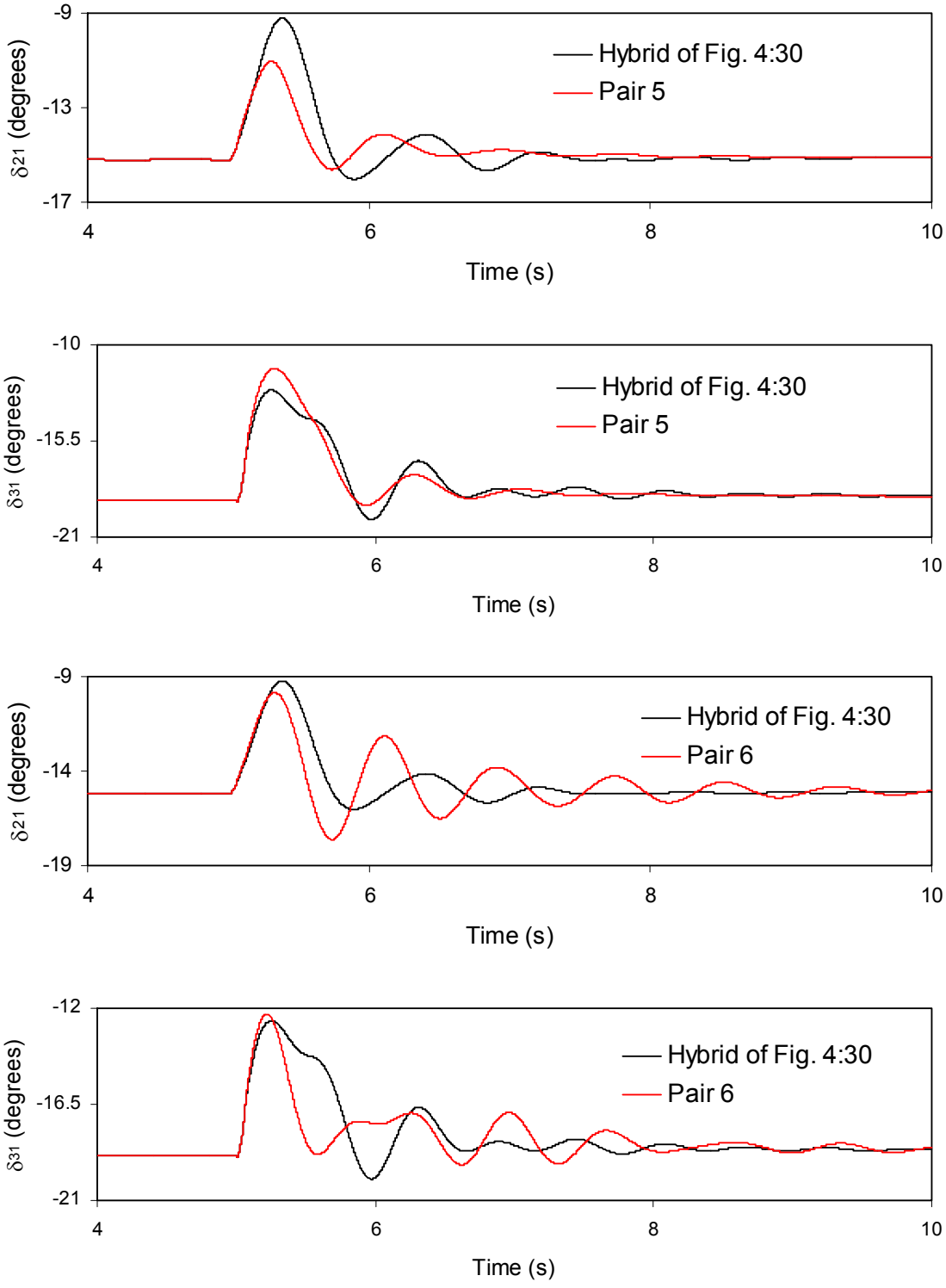

Figure 4.32: Continued.

Figure 4.33 illustrates the three-phase voltages, $V_{X\text{-}Y}$, across the hybrid single-phase-TCSC compensation scheme (installed in L_1) of Figure 3.5 during and after clearing the three-phase fault of Figure 4.32 with pair 2. The system phase imbalance during the disturbance is clearly noticeable especially in phase C.

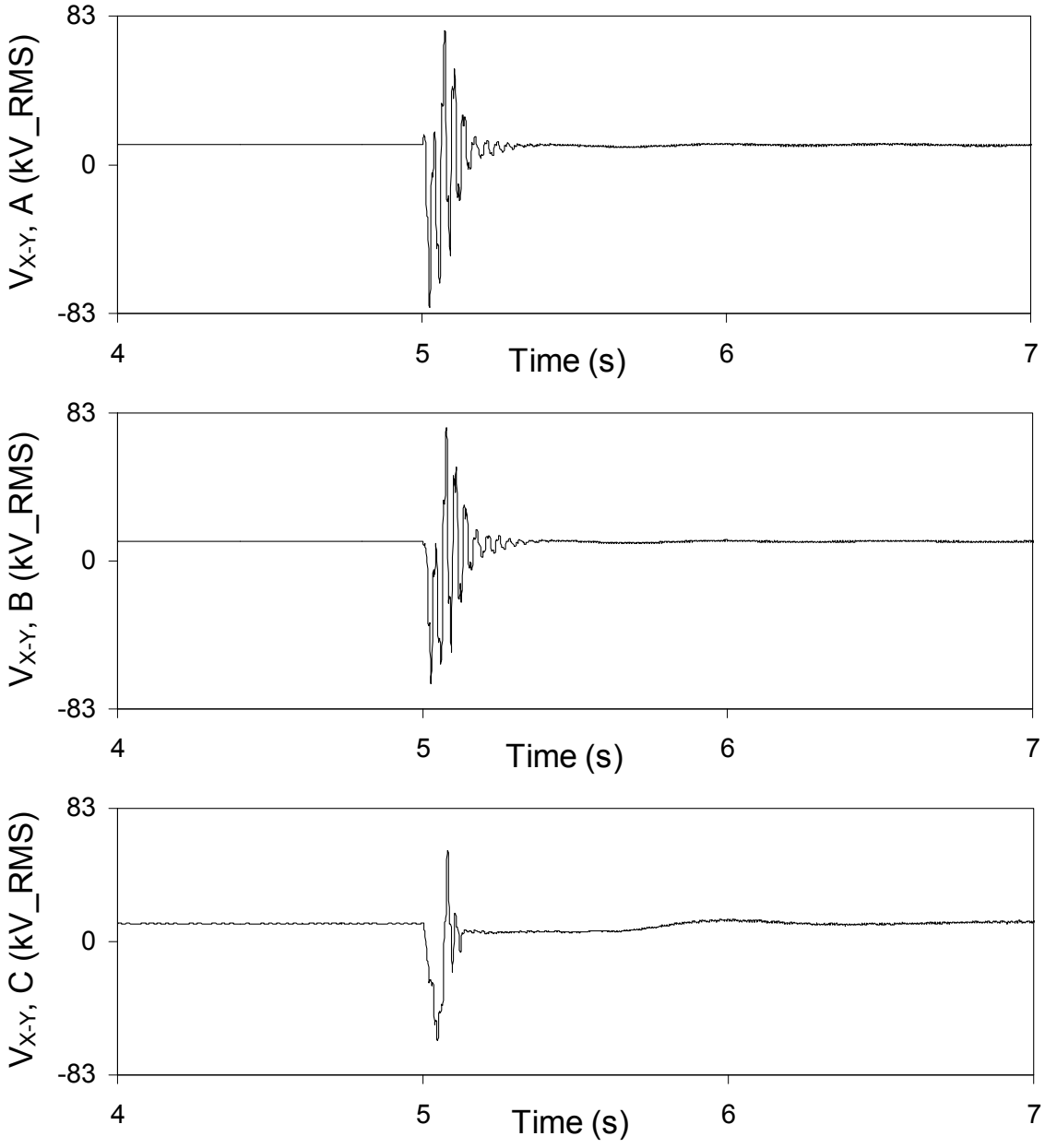

Figure 4.33: Phase voltages, $V_{X\text{-}Y}$ across the hybrid single-phase-TCSC of Fig. 3.5 during and after clearing a three-cycle, three-phase fault at bus 4 (case study IV at a different loading profile, dual-channel supplemental controllers, pair 2, scheme in L_1).

4.7 Case Study V: The Hybrid Single-Phase-TCSC Compensation Scheme is Installed in Lines L_1 and L_3

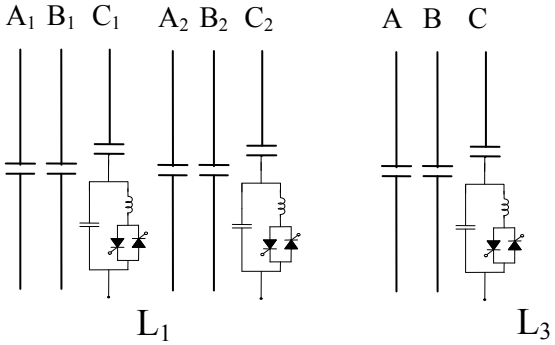

Figure 4.34: Case study V: the hybrid single-phase-TCSC compensation scheme is installed in lines L_1 and L_3.

In this case study, the hybrid single-phase-TCSC compensation scheme is installed in the uncompensated line, L_3, for the purpose of system dynamic reinforcement. As it can be seen from Figure 2.6, line L_3 is the direct interconnection between G_1 and G_2. Controlling the real power flow of this line would have a direct impact on the oscillations between these two generators.

The system pre-fault load flow for this case is shown in Figure 4.35 where it is assumed that the degree of compensation of L_1 and L_3 is 50% and that each single-phase-TCSC provides 50% of the total capacitive compensation. The disturbance is a three-cycle, three-phase fault at bus 4. The final results of the time-domain simulation studies (controller tuning) are compared with Case study III and are shown in Figure 4.36. This figure illustrates the generator load angles, measured with respect to generator 1 load angle, during and after fault clearing. The transfer functions of the TCSC supplemental controllers with the stabilizing signal δ_{21} are given in Table 4.7.

As the result of the series compensation of L_3, the phase angles between buses 1 and 2 as well as between buses 1 and 3 are reduced and the real power transmitted between buses 1 and 2 is increased (from 569 MW, Fig. 2.6 to 724 MW, Fig. 4.35). The reductions in these phase angles are directly reflected into reductions in the initial values of the relative generator load angles δ_{21} and δ_{31} as it is shown in Figure 4.36. The figure also shows that the hybrid single-phase TCSC supplemental controllers provide very effective damping to system oscillations.

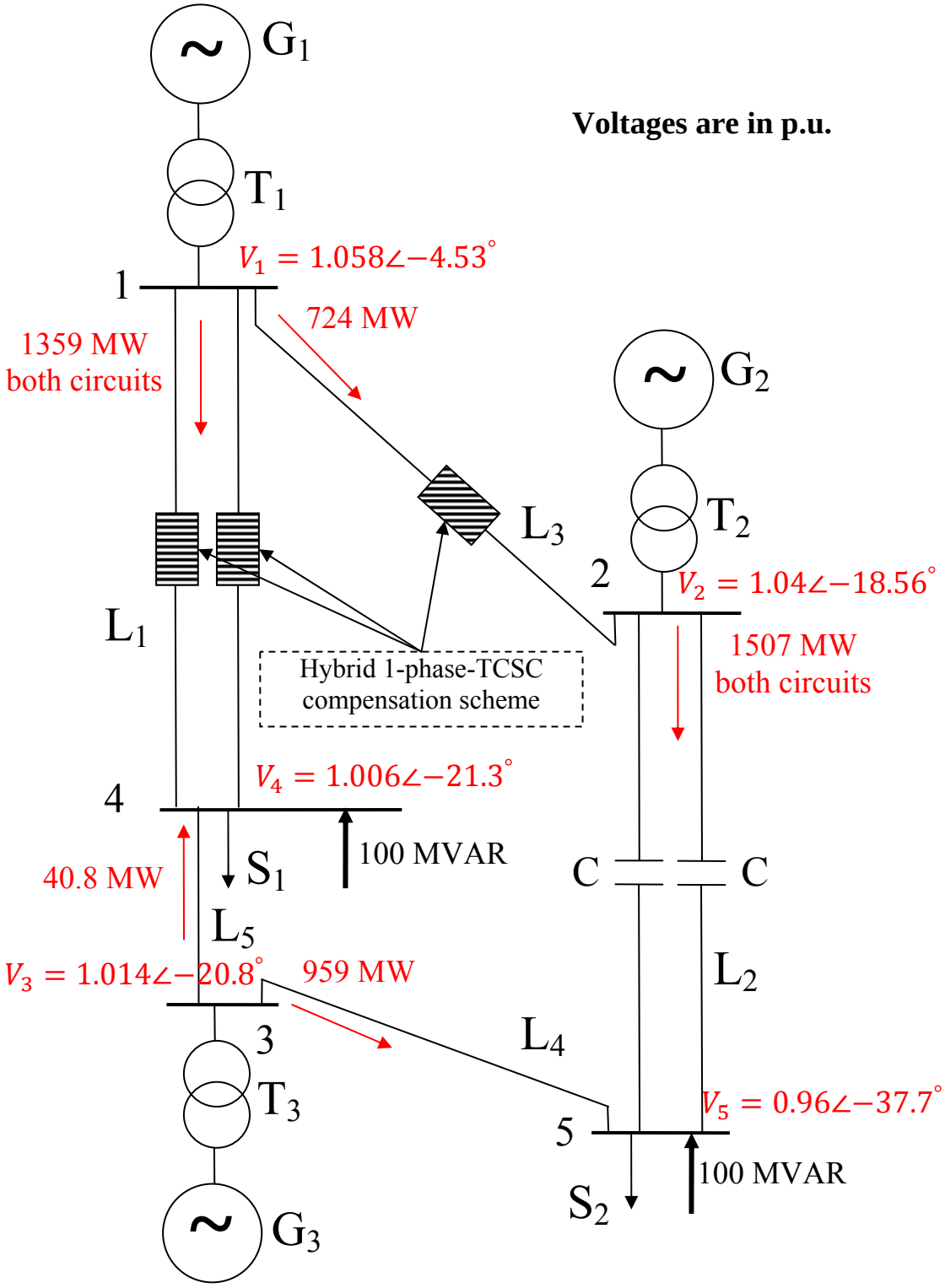

Figure 4.35: Power flow results of bus voltages and line real power flows of the system under study for case study V.

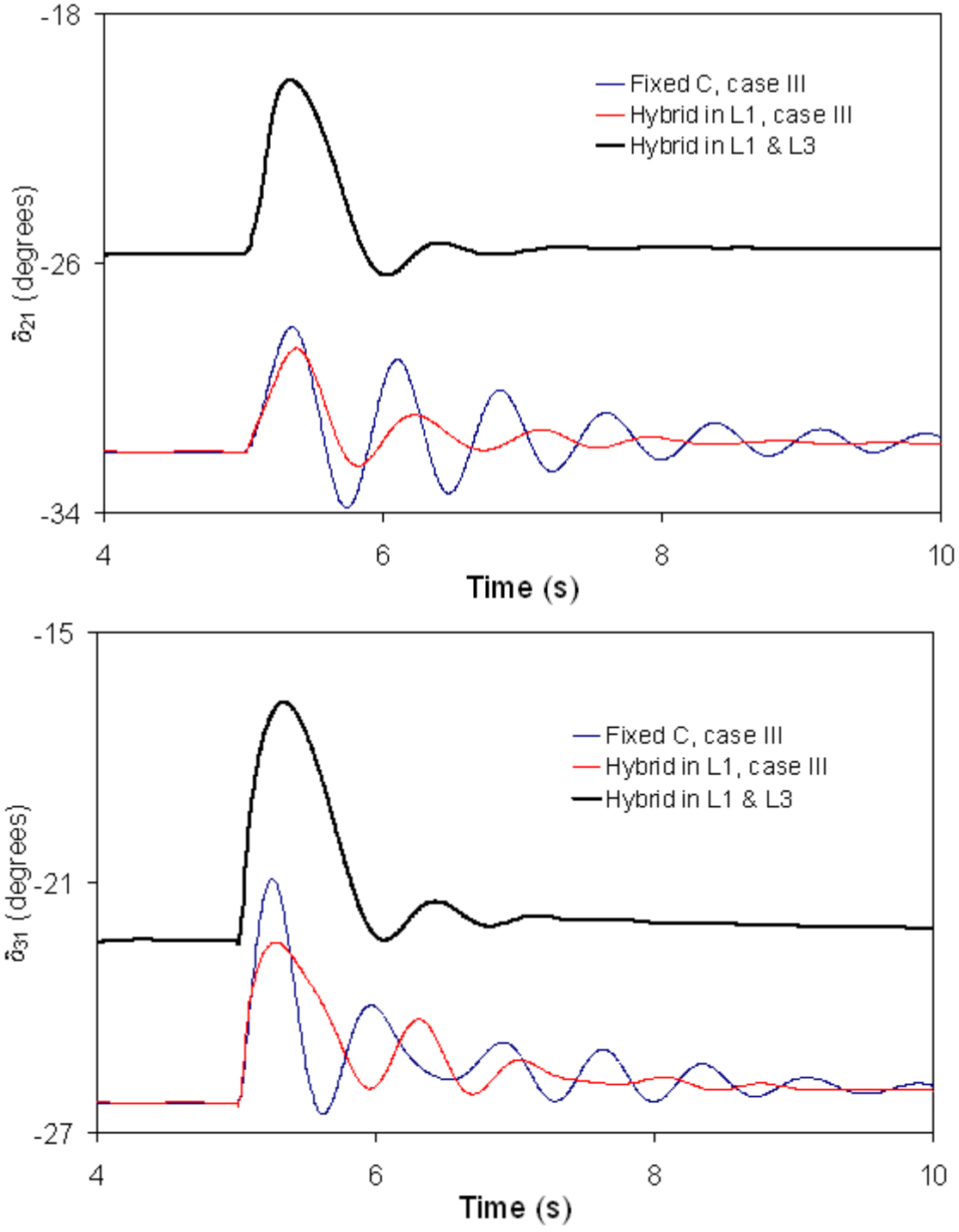

Figure 4.36: Generator load angles, measured with respect to generator 1 load angle, during and after clearing a three-cycle, three-phase fault at bus 4 (case study V, stabilizing signals: δ_{21}).

Table 4.7: Transfer functions of the TCSC supplemental controllers with the stabilizing signal δ_{21} (case V).

Each TCSC in L_1	TCSC in L_3
$G(s) = 0.3 \frac{10}{(s+10)} \frac{3s}{(3s+1)}$	$G(s) = 0.4 \frac{10}{(s+10)} \frac{2s}{(2s+1)}$

4.8 Summary

In this chapter, the effectiveness of the hybrid single-phase-TCSC compensation scheme in damping power system oscillations resulting from clearing system faults is investigated through several case studies of time-domain simulations. In this context, the effects of the number and locations of the schemes installed in the system, the TCSC supplemental controller structures and their stabilizing signals as well as the system load profiles on damping power system oscillations are explored. The main conclusions drawn from the results of these studies are presented in the next chapter.

Chapter 5

SUMMARY AND CONCLUSIONS

5.1 Summary

Oscillations of active power in power transmission systems may arise in corridors between generating areas as a result of poor damping of the interconnection, particularly during heavy power transfer. Such oscillations can be excited by a number of reasons such as line faults, switching of lines or a sudden change of generator output. The presence of active power oscillations acts to limit the power transmission capacity of interconnections between areas or transmission regions.

As a result of the Flexible AC Transmission Systems (FACTS) initiative, considerable effort has been spent in the last two decades on the development of power electronic-based power flow controllers. The potential benefits of these FACTS controllers are now widely recognized by the power system engineering and the transmission and distribution communities. The TCSC has shown to be an attractive and very effective controller for power flow control and system oscillations damping. This thesis reports the results of the investigations that were carried out to explore the effectiveness of the hybrid single-phase-TCSC compensation scheme in damping power system oscillations in multi-machine power systems.

A brief review of the benefits of series compensation of transmission lines is presented in Chapter 1. The inability of series capacitors in providing adequate damping to power system oscillations as well as their contribution to the subsynchronous resonance phenomenon are also discussed in this chapter.

In Chapter 2, the system used in the studies conducted in this thesis is introduced and the mathematical models of its components are presented. The results of digital time-domain simulations of a case study for the system with only fixed capacitance compensation during a three-phase fault are also presented in this chapter.

In Chapter 3, comprehensive descriptions of the TCSC, its three modes of operation and the analysis of its net reactance are presented. The phase imbalanced hybrid single-phase-TCSC

compensation scheme and its modeling in the ElectroMagnetic Transient Program (EMTP-RV) are also presented.

In Chapter 4, several case studies investigating the effects of the location of the hybrid single-phase-TCSC compensation scheme, the degree of compensation provided by the scheme, the TCSC supplemental controller structure, the stabilizing signal as well as the loading profile on the damping of power system oscillations are documented. These studies are intended to demonstrate the effectiveness of the proposed scheme in damping power system oscillations resulting from clearing system faults.

5.2 Conclusions

The studies conducted in this thesis yield the following conclusions for the system under study:

1. The series capacitor compensated system is first swing stable for three-phase faults, but the post-contingency oscillations are not well damped.
2. Although the system has two natural modes of oscillation, generators 2 and 3 tend to oscillate at a single frequency (approximately 1.4 Hz).
3. The hybrid single-phase-TCSC compensation scheme has shown to be, in general, very effective in damping power system oscillations at different loading profiles.
4. Increasing the proportion of the single-phase-TCSC to the fixed capacitor of its phase results in improving the damping of system oscillations. Increasing the proportion of the hybrid single-phase-TCSC compensation scheme to the total fixed capacitor compensation (i.e. installing the scheme in more transmission line circuits replacing fixed capacitor compensation) enhances significantly the damping of system oscillations. Choosing the values of such two proportion options can be considered as an optimization task between dynamic stability improvements and economical and reliability advantages of fixed series capacitors.
5. The performance of the TCSC supplemental controller when the deviation of generator 2 load angle, with respect to generator 1 load angle, is used as the stabilizing signal is better than when the deviations in the generator speeds or the transmission line real power flows are utilized.

6. In the majority of the case studies, adequate power system oscillation damping is obtained with proportional-type TCSC supplemental controllers.
7. With the hybrid single-phase-TCSC compensation scheme installed in all circuits of lines L_1 and L_2, the best performance of the TCSC supplemental controllers is obtained when the deviation of generator 2 load angle, with respect to generator 1 load angle, is used as the stabilizing signal for all controllers.
8. A dual-channel TCSC supplemental controller is more effective in damping power system oscillations than a single-channel controller. In this regard, the best two signals are found out to be the deviation of generator 2 load angle, with respect to generator 1 load angle and the real power flow in line L_1.
9. Overall, the best damping of the relative load angle responses are achieved when the hybrid single-phase-TCSC is installed in line L_3 as well as in the two circuits of line L_1.
10. The reduction of the generator first swings depends on the proportion of the hybrid single-phase-TCSC compensation scheme to the total fixed capacitor compensation in the system. It is observed, however, that in one case there is a slight increase in the first swing of one generator. It should be emphasized here that the main task of the supplemental controller of the hybrid single-phase-TCSC compensation scheme is to damp power system oscillations in the "already stable" system under study. For transient stability control of marginally stable power systems, different TCSC control methodologies are usually used.

As is the case with all research, many venues were not fully explored and many new questions came to light as a result of this research project. It is believed, however, that some key questions regarding the use of the hybrid single-phase-TCSC compensation scheme in damping power system oscillations in multi-machine power systems have been answered. It is hoped that this thesis will be of value to anyone working to improve the damping performance of the scheme in other similar systems.

REFERENCES

[1] P.M. Anderson, *Subsynchronous resonance in power systems,* New York, IEEE Press, 1990.

[2] P.M. Anderson and R.G. Farmer, *Series Compensation of Power Systems*, PBLSH!, 1996.

[3] R. Billinton, M. Fotuhi-Firuzabad and S.O. Faried, "Power System Reliability Enhancement using a Thyristor Controlled Series Capacitor," IEEE Transactions on Power Systems, Vol. 14, No. 1, February 1999, pp. 369-374.

[4] J.L. Batho, J.E. Hardy and N. Tolmunen, "Series Capacitor Installations in the B.C. Hydro 500 kV System," IEEE Transactions on Power Apparatus and Systems, Vol. PAS-96, No. 6, November/December 1977, pp. 1767.1776.

[5] "Increased Power Transmission Capacity on 500 kV Grid by Installation and Refurbishing of Series Capacitors," ABB online web site, [http://www05.abb.com/global/scot/scot221.nsf/veritydisplay/7f8d670d8379cc50c1256fda003b4d0a/$File/McLeese%20A02-0159E.pdf].

[6] D.N. Kosterev, C.W. Taylor, W.A. Mittelstadt, "Model Validation for the August 10, 1996 WSCC System Outage," IEEE Transactions on Power Systems, Vol. 14, No. 3, August 1999, pp. 967-979.

[7] R. Witzmann, Damping of Interarea Oscillations in Large Interconnected Power Systems," Proceedings of the International Conference on Power Systems Transients (IPST01), Rio de Janeiro, Brazil, June 24-28, 2001, paper No. 197.

[8] Y.H. Song and A.T. Johns, *Flexible AC Transmission Systems (FACTS)*, London, Institution of Electrical Engineers, 1999.

[9] N.G. Hingorani and L. Gyugyi, *Understanding FACTS: Concepts and Technology of Flexible AC Transmission Systems,* New York, IEEE Press, 2000.

[10] C. Gama, "Brazilian North-South Interconnection Control-Application and Operating Experience with a TCSC," Proceedings of the 1999 IEEE PES Summer meeting, Edmonton, Alberta, Canada, July 18-22, 1999, Vol. 2, pp. 1103-1108.

[11] C. Gama and L. Angquist, "Commissioning and Operative Experience of TCSC for Damping Power Oscillation in the Brazilian North-South Interconnection," CIGRE, Session 2000, Paris, France, paper No. 14-104.

[12] H.A. Othman and L. Angquist, "Analytical Modeling of Thyristor-Controlled Series Capacitors for SSR Studies," IEEE Transactions on Power Systems, Vol. 11, No. 1, February 1996, pp. 119-127.

[13] B.K. Perkins and M.R. Iravani, "Dynamic Modeling of a TCSC with Application to SSR Analysis," IEEE Transactions on Power Systems, Vol. 12, No. 4, pp. 1619-1625, 1997.

[14] R.J. Piwko, C.W. Wegner, S.J. Kinney and J.D. Eden, "Subsynchronous Resonance Performance Tests of the Slatt Thyristor-Controlled Series Capacitor," IEEE Transactions on Power Delivery, Vol. 11, No. 2, April 1996, pp. 1112-1119.

[15] W. Zhu, R. Spee, R.R. Mohler, G.C. Alexander, W.A. Mittelstadt and D. Maratukulam, "An EMTP Study of SSR Mitigation Using the Thyristor- Controlled Series Capacitor," IEEE Transactions on Power Delivery, Vol. 10, No. 3, July 1995, pp. 1479-1485.

[16] Naoto Kakimoto and Anan Phongphanphanee, "Subsynchronous Resonance Damping Control of Thyristor-Controlled Series Capacitor," IEEE Transactions on Power Delivery, Vol. 18, No. 3, July 2003, pp. 1051-1059.

[17] R. Rajaraman, I. Dobson, R. H. Lasseter, and Y. Shern, "Computing the Damping of Subsynchronous Oscillations due to a Thyristor Controlled Series Capacitor," IEEE Transactions on Power Delivery, Vol. 11, No. 2, April 1996, pp. 1120–1127.

[18] P. Mattavelli, A.M. Stankovic`, and G.C. Verghese, "SSR Analysis with Dynamic Phasor Model of Thyristor-Controlled Series Capacitor," IEEE Transactions on Power Systems, Vol. 14, No. 1, February 1999, pp. 200–208.

[19] Alireza Daneshpooy and A.M. Gole, "Frequency Response of the Thyristor Controlled Series Capacitor," IEEE Transactions on Power Delivery, Vol. 16, No. 1, January 2001, pp. 53-58.

[20] J.F. Hauer, W.A. Mittelstadt, R.J. Piwko, B.L. Damsky, J.D. Eden, "Modulation and SSR Tests Performed on the BPA 500 kV Thyristor Controlled Series Capacitor Unit at Slatt Substation," IEEE Transactions on Power Systems, Vol. 11, No. 2. May 1996, pp. 801-806.

[21] P.S. Dolan, J.R. Smith and W.A. Mittelstadt, "A Study of TCSC Optimal Damping Control Parameters for Different Operating Conditions," IEEE Transactions on Power Systems, Vol. 10, No. 4, November 1995, pp. 1972-1978.

[22] J. Urbanek, R.J. Piwko, E.V. Larsen, B.L. Damsky, B.C. Furumasu and W. Mittlestadt, "Thyristor Controlled Series Compensation Prototype Installation at the Slatt 500 kV Substation," IEEE Transactions on Power Delivery, Vol. 8, No. 3, July 1993, pp. 1460-1469.

[23] S. Nyati, C.A. Wegner, R.W. Delmerico, R.J. Piwko, D.H. Baker and A. Edris, "Effectiveness of Thyristor Controlled Series Capacitor in Enhancing Power System Dynamics: An Analog Simulator Study," IEEE Transactions on Power Delivery, Vol. 9, No. 2, April 1994, pp. 1018-1027.

[24] X. R. Chen, N.C. Pahalawaththa, U.D. Annakkage and C.S. Kumble, "Design of Decentralised output Feedback TCSC Damping Controllers by Using Simulated Annealing," IEE Proceedings, Generation, Transmission and Distribution, Vol. 145, No. 5, September 1998, pp. 553-558.

[25] Y.Y. Hsu and T.S. Luor, "Damping of Power System Oscillations using Adaptive Thyristor-Controlled Series Compensators Tuned by Artificial Neural Networks," IEE Proceedings, Generation, Transmission and Distribution, Vol. 146, No. 2, March 1999, pp. 137-142.

[26] X.X. Zhou and J. Liang, "Nonlinear Adaptive Control of TCSC to Improve the Performance of Power Systems," IEE Proceedings, Generation, Transmission and Distribution, Vol. 146, No. 3, May 1999, pp. 301-305.

[27] P. Kundur, *Power System Stability and Control,* New York, McGraw-Hill, 1994.

[28] Y. Yu, *Electric Power System Dynamics,* New York, Academic Press, 1983.

[29] O.I. Elgerd, *Electrical Energy Systems Theory*, McGraw-Hill, 1971.

[30] EMTP-RV website: www.emtp.com.

[31] A. Daneshpooy and A.M. Gole," Frequency Response of the Thyristor Controlled Series Capacitor," IEEE Transactions on Power Delivery, Vol. 16, No. 1, January 2001, pp. 53-58.

[32] K. Kabiri, S. Henschel and H.W. Dommel, "Resistive Behavior of Thyristor-Controlled Series Capacitors at Subsynchronous Frequencies," IEEE Transactions on Power Delivery, Vol. 19, No. 1, January 2004, pp. 374-379.

[33] R.M. Mathur and R.K. Varma, *Thyristor-Based FACTS Controllers for Electrical Transmission Systems,* Piscataway, NJ, IEEE, 2002.

[34] H. Xie and L. Ängquist, "Synchronous Voltage Reversal control of TCSC – impact on SSR conditions," Proceedings of the Nordic Workshop on Power and Industrial Electronics (NORPIE), 2004.

[35] Lennart Ängquist, "Synchronous Voltage Reversal Control of Thyristor Controlled Series Capacitor," Royal Institute of Technology, TRITA-ETS-2002-07, ISSN 1650-674X.

[36] L. Angquist and C. Gama, "Damping Algorithm based on Phasor Estimation," Proceedings of the IEEE Power Engineering Society Winter Meeting, Columbus, Ohio, January 28 – February 1, 2001, Vol. 3, pp. 1160-1165.

[37] D. Rai, G. Ramakrishna, S.O. Faried and A. Edris," Enhancement of Power System Dynamics Using a Phase Imbalanced Series Compensation Scheme," IEEE Transactions on Power Systems, Vol. 25, No. 2, May 2010, pp. 966-974.

[38] D. Rai, S.O. Faried, G. Ramakrishna, and A. Edris, "Hybrid Series Compensation Scheme Capable of Damping Subsynchronous Resonance," IET Generation, Transmission and Distribution, Vol. 4, No. 3, March 2010, pp. 456-466.

[39] A.M. Gole, S. Filizadeh, R.W. Menzies, and P.L. Wilson, "Optimization-enabled Electromagnetic Transient Simulation," IEEE Transactions on Power Delivery, Vol. 20, No. 1, January 2005, pp. 512–518.

[40] A.M. Gole, S. Filizadeh, and P.L. Wilson, "Inclusion of Robustness into Design using Optimization-enabled Transient Simulation," IEEE Transactions on Power Delivery, Vol. 20, No. 3, July 2005, pp. 1991–1997.

[41] R. Grünbaum and Jacques Pernot, "Thyristor Controlled Series Compensation: A State of the Art Approach for Optimization of Transmission over Power Links, ABB online web site:
[http://www05.abb.com/global/scot/scot221.nsf/veritydisplay/d578889d05b3ba01c1256fda003b4cff/$File/SEE_FIILE2001_TCSC.pdf].

[42] N. Yang, Q. Liu and J. McCalley, "TCSC Controller Design for Interarea Oscillations," IEEE Transactions on Power Systems, Vol. 13, No. 4, November 1998, pp. 1304-1309.

[43] X. Chen, N. Pahalawaththa, U. Annakkage and C. Kumbe, "Output Feedback TCSC Controllers to Improve Damping of Meshed Multi-Machine Power Systems," IEE Proceedings, Generation, Transmission and Distribution, Vol. 44, No. 3, May 1997, pp. 243-248.

[44] J. Machowski, S. Robak and J. Bialek, "Damping of Power Swings by Optimal Control of Series Compensators," Proceedings of the 10th International Conference on Power System Automation and Control *PSAC'97*, Bled, Slovenia, October 1-3, 1997, pp. 39-44.

[45] J.F. Hauer, M.K. Donnelly, W.A. Mittelstadt, W. Litzenberger and D.J. Maratukulam, "Information Functions and Architecture for Networked Monitoring of Wide Area Power System Dynamics: Experience with the Evolving Western System Dynamic Information Network," Proceedings of the Sixth Symposium of Specialists on Electric Operational and Expansion Planning (VI SEPOPE), Bahia, Brazil, May 24-29, 1998.

[46] B. Bhargava and A. Salazar, "Use of Synchronized Phasor Measurement System for Monitoring Power System Stability and System Dynamics in Real-Time," Proceedings of the 2008 IEEE PES GM, Pittsburgh, PA, July 20 – 24, 2008, pp. 1-8.

[47] H. Ni, G.T. Heydt and L. Mili, "Power System Stability Agents using Robust Wide Area Control, "IEEE Transactions on Power Systems, Vol. 17, No. 4, November 2002, pp. 1123-1131.

[48] X. Xie, J. Xiao, C. Lu and Y. Han, "Wide-Area Stability Control for Damping Interarea Oscillations of Interconnected Power Systems," IEE Proceedings, Generation, Transmission and Distribution, Vol. 153, No. 5, September 2006, pp. 507-514.

[49] C.W. Taylor, D.E. Erickson, K.E. Martin, R.E. Wilson and V. Venkatasubramanian," WACS-Wide-Area Stability and Voltage Control System: R&D and Online Demonstration," Proceedings of IEEE, Vol. 93, No. 5, May 2005, pp. 892-906.

[50] X. Zhou and J. Liang, "Overview of Control Schemes for TCSC to Enhance the Stability of Power Systems," IEE Proceedings, Generation, Transmission and Distribution, Vol. 146, No. 2, March 1999, pp. 125-130.

APPENDIX A

DATA OF THE SYSTEM UNDER STUDY

A.1 Synchronous Generators

Table A.1: Synchronous generator data.

	G_1	G_2	G_3
Rating, MVA	2400	1000	1100
Rated voltage, kV	26	26	26
Armature resistance, r_a, p.u.	0	0.0045	0.0045
Leakage reactance, x_l, p.u.	0.13	0.14	0.12
Direct-axis synchronous reactance, x_d, p.u.	1.79	1.65	1.54
Quadrature-axis synchronous reactance, x_q, p.u.	1.71	1.59	1.5
Direct-axis transient reactance, x'_d, p.u.	0.169	0.25	0.23
Quadrature-axis transient reactance, x'_q, p.u.	0.228	0.46	0.42
Direct-axis subtransient reactance, x''_d, p.u.	0.135	0.2	0.18
Quadrature-axis subtransient reactance, x''_q, p.u.	0.2	0.2	0.18
Direct-axis transient open-circuit time constant, T'_{do}, s	4.3	4.5	3.7
Quadrature-axis transient open-circuit time constant, T'_{qo}, s	0.85	0.55	0.43
Direct-axis subtransient open-circuit time constant, T''_{do}, s	0.032	0.04	0.04
Quadrature-axis subtransient open-circuit time constant, T''_{qo}, s	0.05	0.09	0.06
Zero-sequence reactance, x_o, p.u.	0.13	0.14	0.12
Inertia constant, H, s	7	3.7	3.12

A.2 Transformers

Table A.2: Transformer data.

	T_1	T_2	T_3
Rating, MVA	2400	1000	1100
Rated voltage, kV	26/500	26/500	26/500
Resistance, r_T , p.u.	0	0	0
Leakage reactance, x_T , p.u.	0.1	0.1	0.1

A.3 Transmission Lines

All transmission lines have the same series impedance and shunt admittance per unit length.

$$Z_{T.L.series} = 0.01864 + j\,0.3728\ \Omega / km$$

$$Y_{T.L.shunt} = j\,4.4739\ \mu S / km$$

Transmission voltage = 500 kV

A.4 System Loads

$$S_1 = 1400 + j\,200\ \ MVA$$

$$S_2 = 2400 + j\,300\ \ MVA$$

A.5 Excitation System

Table A.3: Excitation system data.

K_A = 2	K_E = 1.0
K_{FE} = 0.03	T_A = 0.04 s
T_{FE} = 1.0 s	T_E = 0.01s
Lim_max = 4.75 p.u.	*Lim_min* = -4.75 p.u.

APPENDIX B

SINGLE-PHASE TCSC DATA FOR CASE STUDY I

Table B: TCSC data.

$K_p = 0.5$	$K_I = 5$
$C_{TCSC} = 72.63\ \mu F$	$L_{TCSC} = 15.50\ mH$

APPENDIX C

ADDITIONAL CASE STUDY:

THE HYBRID SINGLE-PHASE-TCSC COMPENSATION SCHEME IS INSTALLED IN BOTH CIRCUITS OF LINE L_2

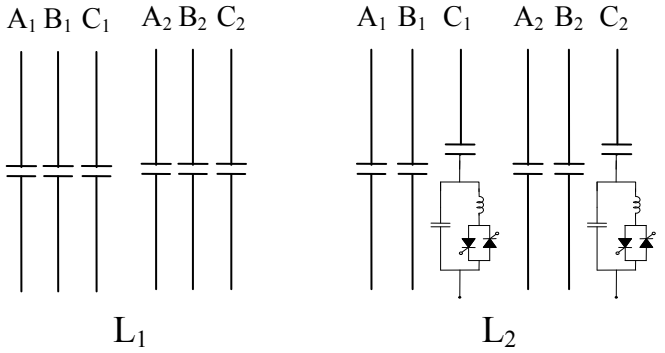

Figure C.1: The hybrid single-phase TCSC compensation scheme is installed in both circuits of line L_2.

Each TCSC provides 50% of the total capacitive compensation and the stabilizing signal is δ_{21} for both controllers. The generator load angles and speeds, measured with respect to generator 1 load angle and speed, and the transmission line real power flow responses during and after clearing a three-cycle, three-phase fault at bus 5 are illustrated in Figures C.2 to C.4 for the case when the TCSC supplemental controllers are of a proportional type with a transfer function:

$$G_{P-\delta 21}(s) = -0.5\frac{10}{(s+10)}\frac{s}{(s+1)} \qquad \text{(C.1)}$$

The comparison between Figures C.2 and 4.12 as well as between Figures C.3 and 4.13 shows that, installing the hybrid single-phase-TCSC compensation scheme in the second circuit of L_2 improves the system damping near steady state, especially for δ_{21} and ω_{21}. The comparison also shows insignificant change in the damping of the system oscillations during the first cycle.

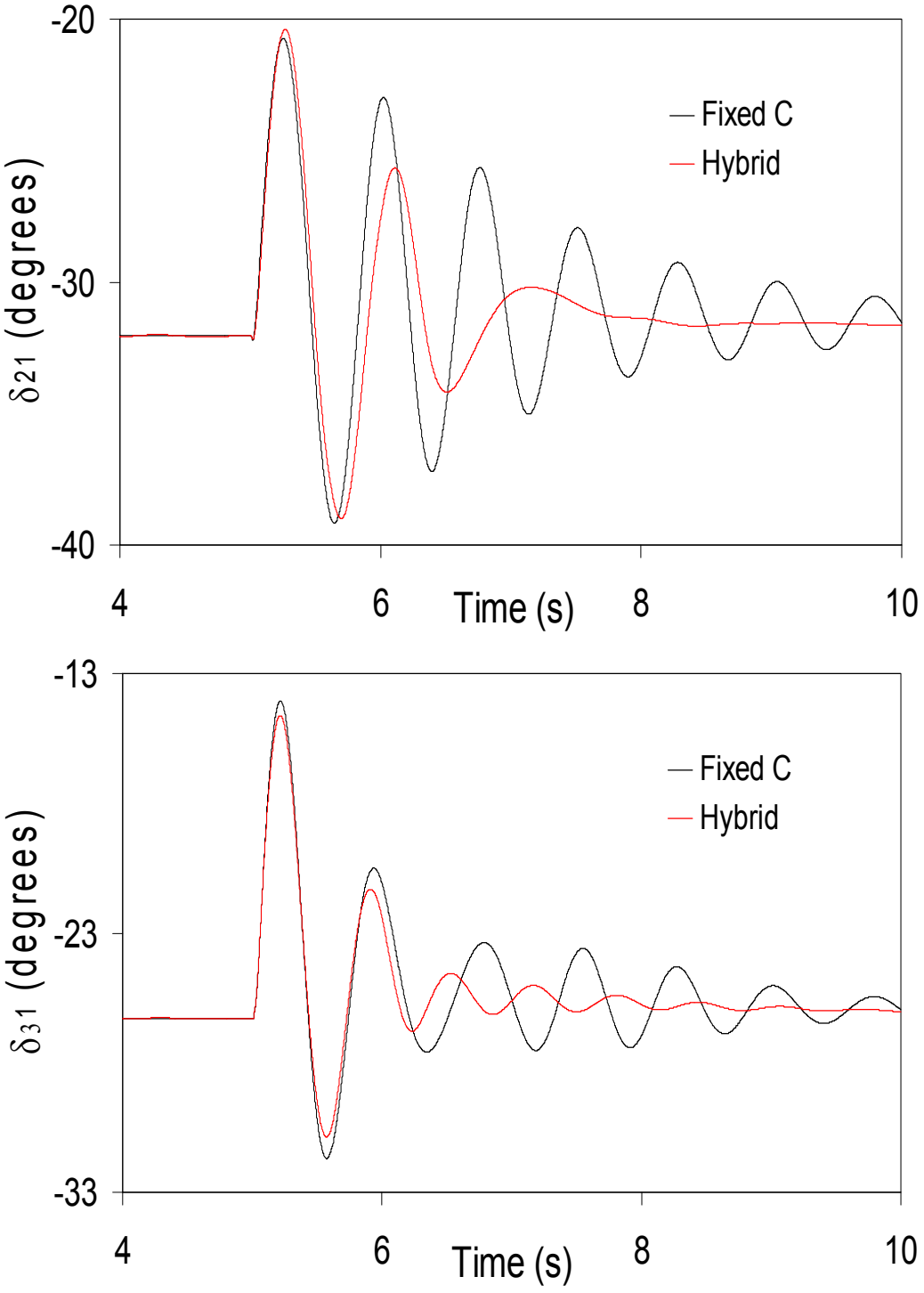

Figure C.2: Generator load angles, measured with respect to generator 1 load angle, during and after clearing a three-cycle, three-phase fault at bus 5 (stabilizing signal, δ_{21}).

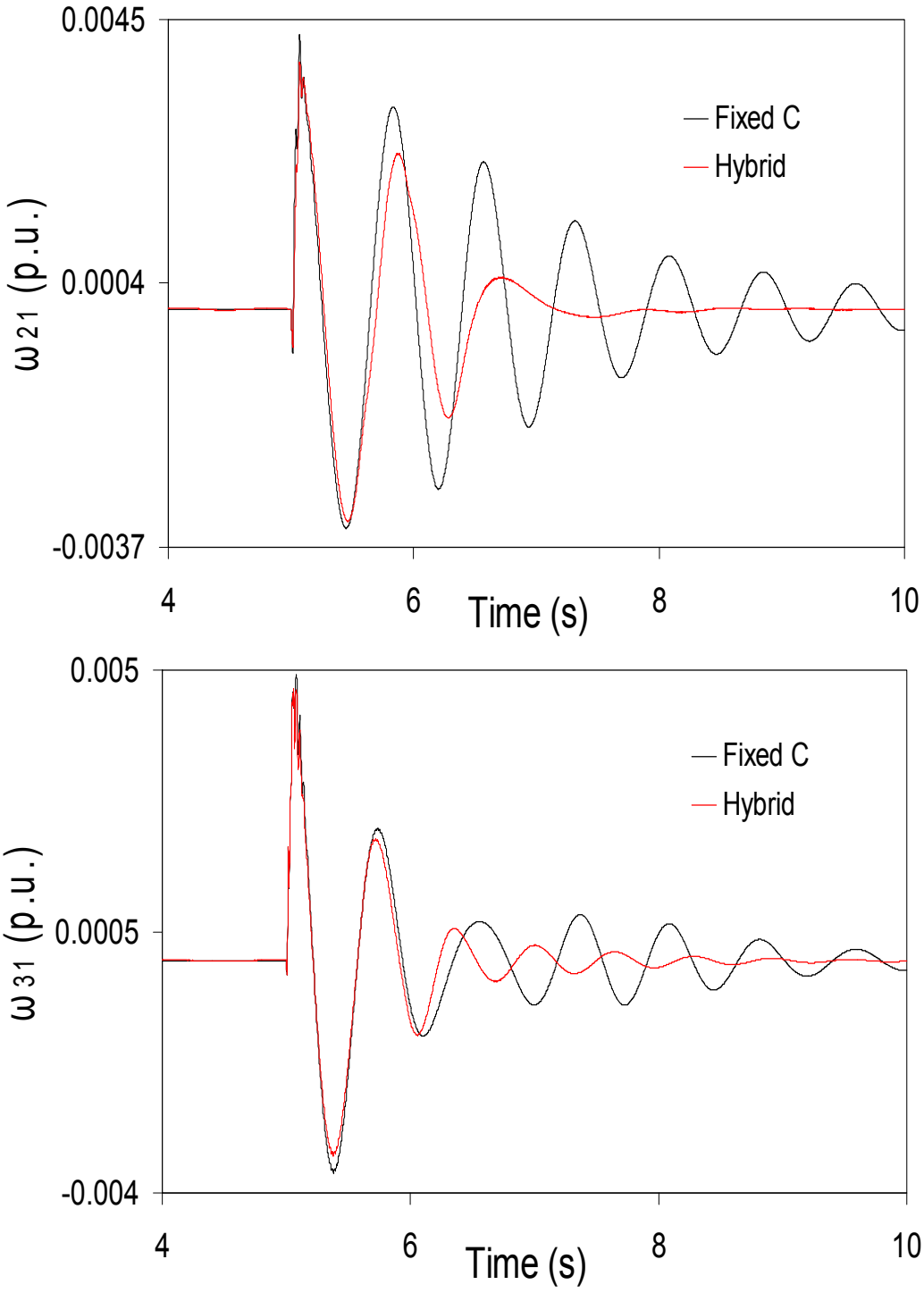

Figure C.3: Generator speeds, measured with respect to generator 1 speed, during and after clearing a three-cycle, three-phase fault at bus 5 (stabilizing signal, δ_{21}).

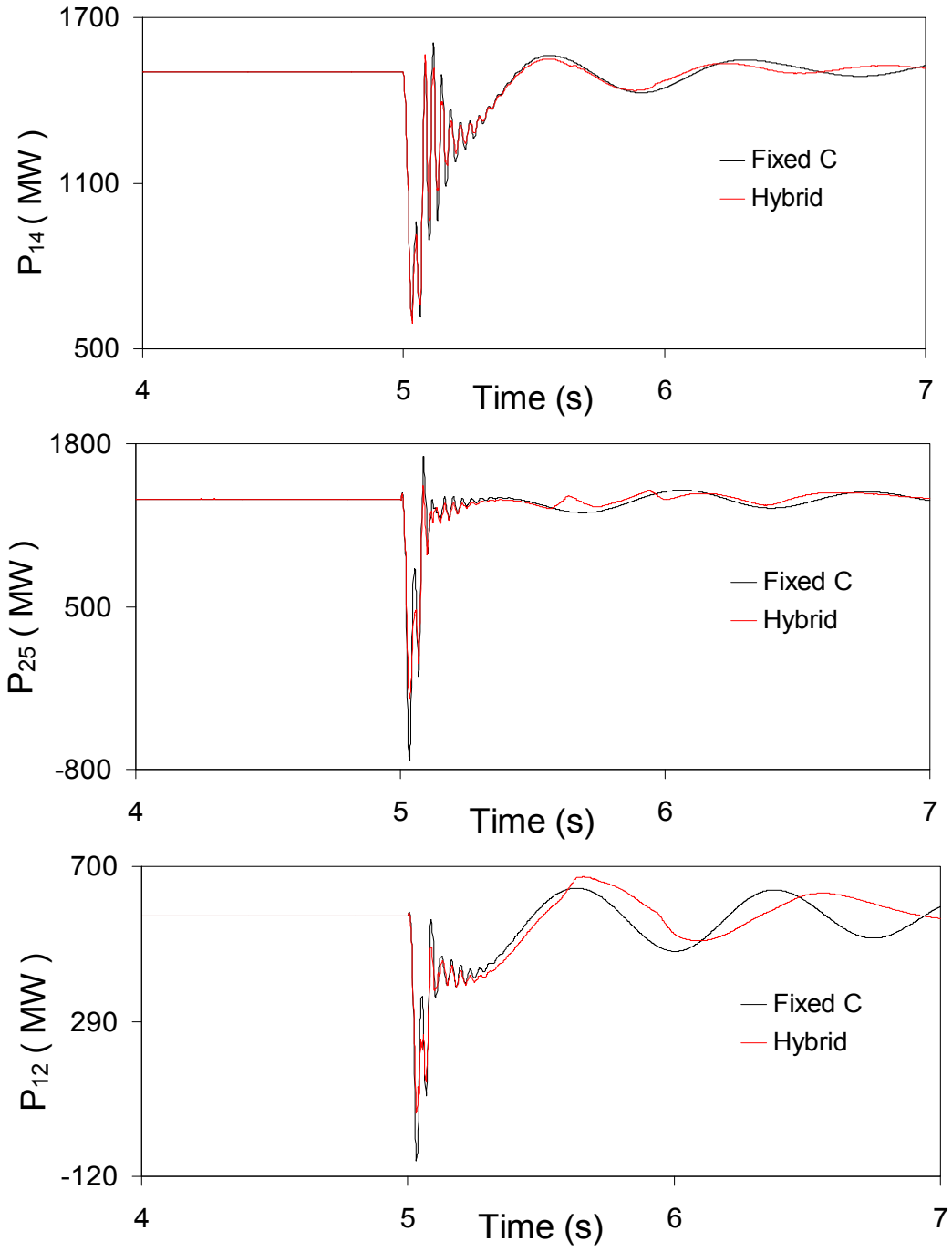

Figure C.4: Transmission line real power flows during and after clearing a three-cycle, three-phase fault at bus 5 (stabilizing signal, δ_{21}).

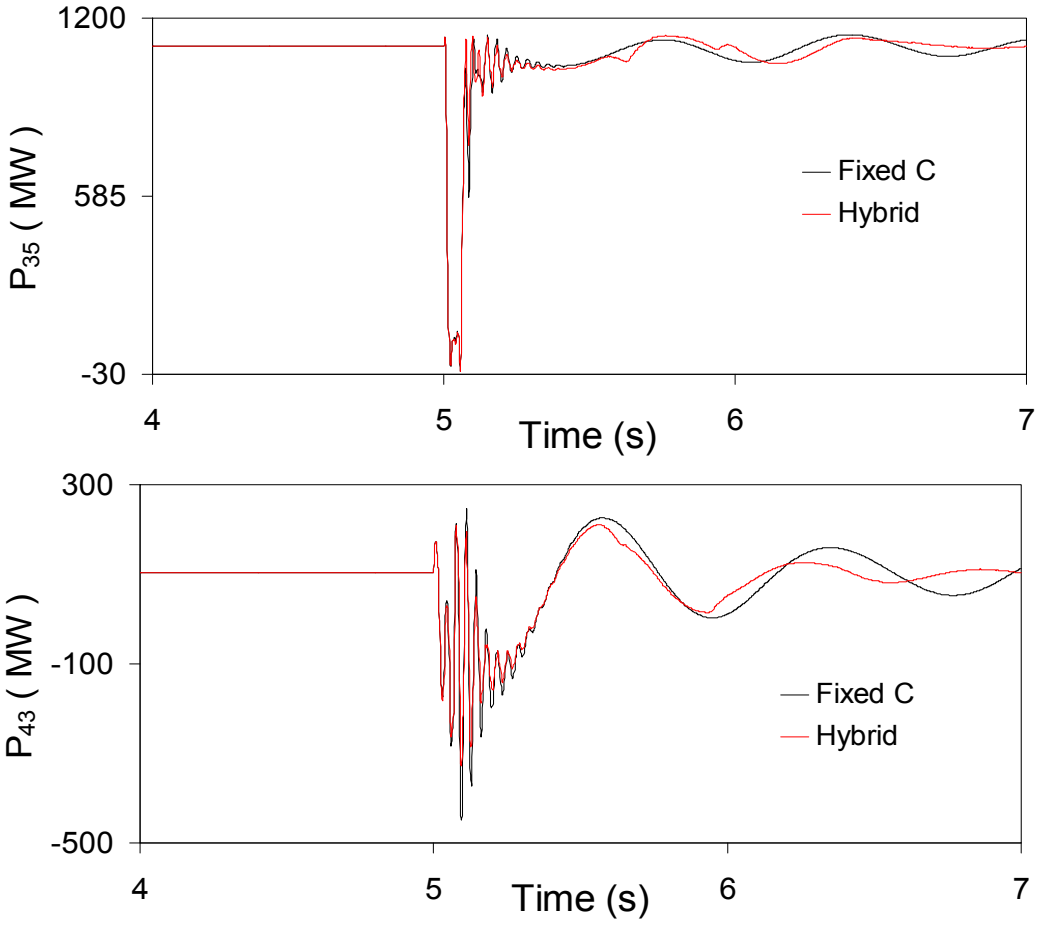

Figure C.4: Continued.